

**UCSF**

**UC San Francisco Electronic Theses and Dissertations**

**Title**

Epigenetic maintenance of neural stem cell positional identity in the ventricular-subventricular zone

**Permalink**

<https://escholarship.org/uc/item/6cp6z8n8>

**Author**

Mansky, Ben E.

**Publication Date**

2020

Peer reviewed|Thesis/dissertation

Epigenetic maintenance of neural stem cell positional identity in the  
ventricular-subventricular zone

by  
Ben Mansky

DISSERTATION

Submitted in partial satisfaction of the requirements for degree of  
DOCTOR OF PHILOSOPHY

in

Neuroscience

in the

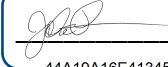
GRADUATE DIVISION

of the

UNIVERSITY OF CALIFORNIA, SAN FRANCISCO

Approved:

DocuSigned by:



44A19A16E413450...

John Rubenstein

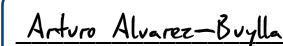
Chair

DocuSigned by:



DocuSigned by: 428...

Daniel Lim



DocuSigned by: 492...

Arturo Alvarez-Buylla



DocuSigned by: 251AC7A581B94CA...

Bassem Al-Sady

Committee Members

Copyright 2020  
by  
Ben Mansky

## Acknowledgments

Science is not just the work of individuals – it is an act of community. This dissertation would not exist without the support of many, many people.

To my research advisors, Daniel Lim and Arturo Alvarez-Buylla, thank you for providing an incredible environment for learning and growth, for always challenging me to think more deeply, more creatively. To each of my labs, your collaborative spirit, your generous feedback, and your new ways of looking at the many problems that arise during a PhD have all been essential. I'd especially like to thank Ryan Delgado for helping to guide the early stages of my research, and for taking the time to train and advise me. I'd also like to thank Stephanie Redmond, Marcos Nascimento, and Arantxa Cebrián-Silla for building a warm and welcoming space to do science. Thanks also to my thesis committee, John Rubenstein and Bassem Al-Sady, for your guidance throughout the PhD process.

A key part of my time at UCSF has been the support and friendship of my cohort. Michael, Selin, Frances, Match, Leah, Trisha, Hannah – sharing the ups and downs of graduate school with you all has been an honor and a privilege. I also owe a lot to the people and organizations who have helped me grow as a communicator, an advocate, and a person. I want to thank the team at Carry the One Radio, Fog at Bay, the Interprofessional Diversity and Equity Alliance, the Graduate and Postdoc Queer Alliance, the Science and Health Education Partnership, the UCSF Photoclub, Liz Watkins, Liz Silva, D'Anne Duncan, LaMisha Hill and so many others.

I would not have become a scientist without the support of my family. To my parents, thank you for cultivating my curiosity and encouraging me to be true to myself. To my brothers, thank you for showing me the beauty and satisfaction to be found in learning. To Tiff, thank you for keeping me grounded, for inspiring me to work harder and do better. I am who I am because of each of you. None of this would have been possible without you.

## Contributions to Presented Work

The work described below was designed and completed with the supervision of Dr. Daniel Lim and Dr. Arturo Alvarez-Buylla.

Chapter 2 is a manuscript published in the April 03 issue of *Science* with authors Ryan N. Delgado, Ben Mansky, Sajad H. Ahanger, Changqing Lu, Rebecca E. Andersen, Yali Dou, Arturo Alvarez-Buylla, and Daniel A. Lim. I designed and performed experiments, analyzed data, and co-wrote the manuscript.

Delgado, R. N., Mansky, B., Ahanger, S. H., Lu, C., Andersen, R. E., Dou, Y., Alvarez-Buylla, A., Lim, D. A. (2020). Maintenance of neural stem cell positional identity by mixed-lineage leukemia 1. *Science*. <https://doi.org/10.1126/science.aba5960>

Parts of Chapter 3 are from a manuscript in preparation with authors Stephanie A. Redmond, Ben Mansky, Arantxa Cebrián-Silla, Marcos Assis Nascimento, and Arturo Alvarez-Buylla. I conceptualized the project and carried out single-cell analysis with Stephanie A. Redmond and Marcos Assis Nascimento. Arantxa Cebrián-Silla performed RNAScope and IHC. Research was supervised by Arturo Alvarez-Buylla, and all authors co-wrote the manuscript.

# Epigenetic maintenance of neural stem cell positional identity in the ventricular-subventricular zone

By  
Ben Mansky

## Abstract

The mammalian brain contains complex regional structures that emerge from heterogeneous populations of neural stem cells (NSCs) during development. Through the process of embryogenesis, NSCs gain positional identities as a result of morphogen signaling, organizing them into distinct lineage-restricted domains. These domains persist from the embryo into the ventricular-subventricular zone (V-SVZ), a postnatal stem cell niche lining the lateral walls of the lateral ventricles. Yet, how NSCs maintain these identities as the brain expands is not known. Here I show that ventral NSCs can maintain region-specific gene expression independently of morphogen Sonic hedgehog (Shh), which initially confers ventral identity. Instead, ventral identity is preserved by chromatin modifier *Mixed lineage leukemia 1* (*MLL1*), which functions as part of an epigenetic memory system. Interfering with MLL1 activity causes a persistent loss of ventral identity, leading NSCs to produce neurons resembling those of dorsal origin. To gain more insight into the differences between NSCs in the V-SVZ, we conducted single-cell and single-nucleus RNA sequencing of the niche. We find that positional identity is a strong driver of both NSC and neuroblast heterogeneity in the V-SVZ, allowing us to identify novel markers of the dorsal and ventral NSC lineages. A subset of region-specific genes is maintained from NSCs through the intermediate progenitor stage and into neuroblasts, giving insight into the extent and timing of NSC lineage commitment. Together, these findings help explain how NSCs in the developing and postnatal brain remember the positional information necessary to produce the brain's characteristic anatomical complexity.

## Table of Contents

<b>Chapter 1: Introduction</b> .....	1
<i>Stem cell patterning and fate determination</i> .....	1
<i>The origins of neural stem cell heterogeneity</i> .....	1
<i>The importance of positional identity in the V-SVZ</i> .....	4
<i>Maintenance of neural stem cell identity in the V-SVZ</i> .....	5
<i>Epigenetic maintenance of cell fate</i> .....	7
<i>Polycomb and Trithorax play a role in maintaining positional identity</i> .....	9
<i>Overview</i> .....	10
<b>Chapter 2: Maintenance of neural stem cell positional identity by MLL1</b> .....	11
Summary .....	11
Introduction .....	11
<i>MLL1, not Shh, maintains NKX2-1 expression in NSCs in vivo</i> .....	12
<i>MLL1<sup>-/-</sup> NSCs adopt a dorsal-like transcriptional profile</i> .....	13
<i>Ventral NSC transcriptional identity requires continuous MLL1 function</i> .....	15
<i>Transient MLL1 inhibition alters developmental fate of ventral NSCs</i> .....	17
<i>Outlook</i> .....	19
Materials and Methods.....	20
<b>Chapter 3: ScRNA-seq shows heterogeneous lineage commitment of V-SVZ NSCs</b> .....	46
Introduction .....	46
<i>The biological importance of stem cell diversity</i> .....	46
<i>Heterogeneity in the V-SVZ</i> .....	46
<i>ScRNA-seq and V-SVZ lineage commitment</i> .....	47
Results.....	48
<i>Generation of the whole-cell sequencing dataset</i> .....	48

<i>Generation of the single-nucleus sequencing dataset</i> .....	50
<i>B cell clusters correspond to regionally distinct domains</i> .....	52
<i>A cell heterogeneity is linked to regional identity</i> .....	54
<i>Specific markers define dorsal/ventral neurogenic lineages</i> .....	56
Discussion .....	57
Materials and Methods.....	58
<b>Chapter 4: Discussion and Concluding Remarks</b> .....	<b>73</b>
<i>Overview</i> .....	73
<i>How does MLL1 maintain positional identity?</i> .....	73
<i>What distinguishes B cell populations from one another?</i> .....	75
<i>Cellular memory systems and NSC identity</i> .....	77
<b>References</b> .....	<b>78</b>



**List of Figures**

Figure 1.1 .....2  
Figure 1.2 .....5  
Figure 2.1 .....29  
Figure 2.2 .....30  
Figure 2.3 .....31  
Figure 2.4 .....32  
Figure 2.5 .....34  
Figure 2.6 .....36  
Figure 2.7 .....37  
Figure 2.8 .....39  
Figure 2.9 .....40  
Figure 2.10 .....41  
Figure 2.11 .....43  
Figure 2.12 .....45  
Figure 3.1 .....63  
Figure 3.2 .....65  
Figure 3.3 .....66  
Figure 3.4 .....68  
Figure 3.5 .....70  
Figure 3.6 .....71

# Chapter 1: Introduction

## *Stem cell patterning and fate determination*

Higher-order organisms have intricate body plans and organ systems that emerge over the course of development in a highly regulated, stereotyped fashion. It takes a wide range of cell types to compose a functional organism, all of which are originally generated from stem cells. In the earliest stages of development, stem cells have the capacity to generate any other kind of cell the body needs. As development proceeds, secreted morphogen signals diffuse across the embryo. Stem cells receive different morphogen doses based on their physical location in the tissue. The specific dose of morphogen a stem cell receives will trigger programs of gene expression that define its positional identity, restricting its ability to produce particular cell types and beginning the process of lineage commitment (Hillman et al. 1972, Ashe & Briscoe 2006).

The cross-repression of region-specific transcription factors creates highly specific regional domains with distinct borders (Wolpert 1969, Briscoe & Small 2015). As each domain expands and differentiates, it will produce a set repertoire of mature cell types within the tissue, giving rise to the organism's body plan. If the behavior of these genes is disrupted, the identities and fates of the affected stem cells will change, undergoing a homeotic shift and generating the wrong region of an organism (Nusslein-Volhard 1980, Akam 1987). Stem cell patterning is an essential component in the development of all organ systems and is particularly important in the brain, which requires the generation of a diverse array of neuronal and glial cell types to assemble neural circuits.

## *The origins of neural stem cell heterogeneity*

In the developing central nervous system (CNS), morphogen gradients pattern neural stem cells (NSCs) based on their location in the neural tube (Fig. 1.1A). These NSCs are the

primary progenitors of the nervous system, specialized glial cells capable of generating intermediate progenitors that will give rise to the neurons and glia that compose the brain and spinal cord. NSCs line the walls of the ventricles, and their divisions drive the expansion of the telencephalon (Kriegstein & Alvarez-Buylla 2009). The dose and combination of morphogens that NSCs receive induce patterns of gene expression in different areas of the developing CNS, establishing regional heterogeneity and restricting the types of neurons and glia each population of NSCs can produce (Shimamura et al. 1997, Xu 2004).

One such morphogen is the ventralizing factor Sonic hedgehog (Shh), which is initially secreted from the notochord during embryonic development. Shh signaling triggers the formation of the floor plate and additional Shh secretion from the ventral domain of the neural tube (Britto et al. 2002, Martí & Bovolenta 2002).

At the same time, dorsalizing bone morphogenetic proteins (BMPs) and Wnt proteins are secreted from the dorsal ectoderm (Bier & De Robertis 2015, Mulligan & Cheyette 2012).

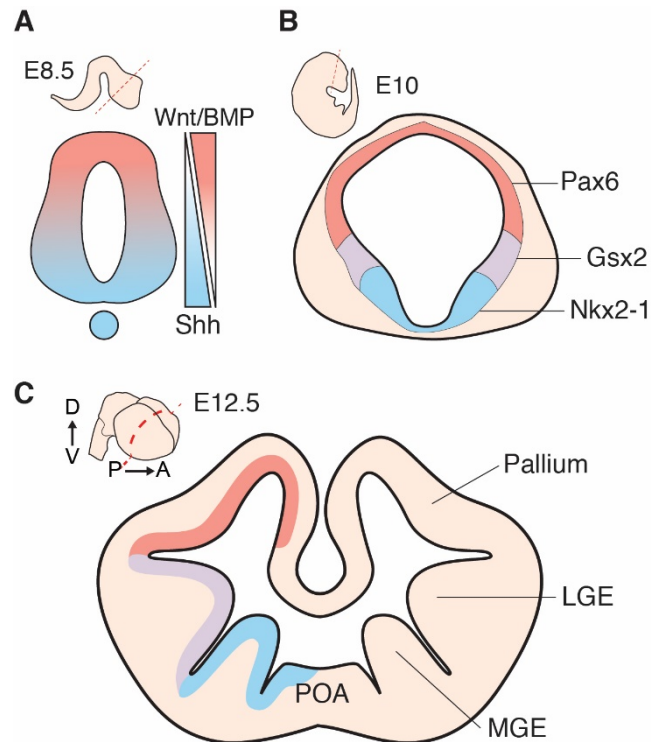


Fig. 1.1. Morphogen gradients establish distinct NSC domains during embryogenesis.

(A) Schematic of the embryonic day 8.5 (E8.5) mouse neural tube in coronal section. Blue indicates dose of Shh, red indicates dose of Wnt/BMP. (B) Schematic of the E10 telencephalon in coronal section. Regional expression domains are marked by genes such as Nkx2-1 (blue), Gsx2 (lavender), and Pax6 (red). (C) Schematic of the E12.5 mouse brain in coronal section, with the Nkx2-1 domain in blue, Gsx2 domain in lavender, and Pax6 domain in red. Embryonic structures are labeled, including the pallium, lateral ganglionic eminence (LGE), medial ganglionic eminence (MGE), and preoptic area (POA). D, dorsal; V, ventral; P, posterior; A, anterior.

Together, the varying levels of morphogen signal induce region-specific gene expression in the neural tube and expanding telencephalon, giving rise to positionally distinct NSC domains (B).

In the embryonic telencephalon, the ventricular stem cell layer is divided into pallial and subpallial compartments, each containing transcriptionally distinct populations of NSCs (Flames et al. 2007). NSCs in the pallium generate the majority of excitatory neurons in the cortex, while the subpallium produces nearly all the cortex's inhibitory interneurons and several important subcortical cell types. Different cortical and subcortical interneuron subtypes are generated by distinct groups of NSCs spatially segregated into three ganglionic eminences and the septum. The medial, caudal, and lateral ganglionic eminences (MGE, CGE, LGE) each express sets of genes that are essential to their regional identity, initially established by morphogen signaling in development (Wonders & Anderson 2006) (Fig. 1.1C). For example, the MGE expresses ventral marker *Nkx2-1*, which is induced by Shh signaling around embryonic day 9 (E9). In mice that lack *Nkx2-1*, the MGE fails to form. Instead, the NSCs that would normally make up the MGE undergo a shift to a more dorsal identity, leading to a reduction in cortical interneurons and an expansion of the LGE and striatum (Sussel et al. 1999).

The regulation of stem cell identity is not only spatial, but also temporal. While regional identity is usually maintained for a long period of time, stem cell pools shift the types of cells they produce as an organ matures. NSCs in the mammalian brain first produce neurons, and then subsequently switch to produce glia as development proceeds (Miller & Gauthier 2007, Okano & Temple 2009). As the cell types that are generated change, regional distinctions remain. For example, when cortical interneuron production begins in the E11 MGE, NSCs largely produce somatostatin-expressing cells, but by E15, the majority of cells produced in the MGE are parvalbumin-expressing chandelier cells, a specific superficial interneuron subtype not produced by neighboring regions (Hu et al. 2017, Sultan et al. 2018). Regional information is preserved even after NSCs switch to producing glia; astrocytes display hallmarks of regional identity based on the domains where they are originally born (Hochstim et al. 2008). Altogether,

the positional identity of NSCs is remarkably persistent throughout the process of embryonic development – and beyond.

### *The importance of positional identity in the V-SVZ*

In the postnatal mouse, key aspects of NSC positional identity are retained in the ventricular-subventricular zone (V-SVZ), an adult stem cell niche that occupies the lateral walls of the lateral ventricles (Doetsch et al. 1999, Merkle et al. 2006, Young et al. 2007, Delgado & Lim 2015) (Fig. 1.2A). The V-SVZ produces interneurons for the olfactory bulb (OB) and remains active throughout the life of the mouse. NSCs in the V-SVZ, also called B cells, continue to express markers of positional identity that directly correspond to their developmental regions of origin, holding onto patterns of gene expression from the embryo even as the brain grows (Fuentelba et al. 2015, Lim & Alvarez-Buylla 2016). Region-specific gene expression in NSCs informs the transcriptional profiles of their progeny: intermediate progenitors, or C cells, and the young neuroblasts, or A cells, they produce. The neuroblasts migrate in chains along the rostral migratory stream (RMS) to the OB, where they integrate into local circuits and complete their differentiation into fully mature neurons (Alvarez-Buylla & García-Verdugo 2002).

The positional identities of NSCs are essential to guide the set of cell types each can produce. At least 8 morphologically distinct OB interneuron subtypes come from the V-SVZ. Once they reach the OB, these subtypes contribute to distinct circuits and exhibit distinct electrical properties from one another (Lledo et al. 2008, Merkle et al. 2014, Nagayama et al. 2014). Within these morphological divisions, OB interneuron types can be further subdivided based on their expression of proteins like tyrosine hydroxylase (TH), calretinin (CalR), or calbindin (CalB) (Kosaka & Kosaka 2010, Iseppe et al. 2016, Bonzano et al. 2016). Based on the subdomain of the V-SVZ where an NSC resides, it will have the capacity to produce a subset of these cell types, the most common of which are granule cells (GCs) and periglomerular cells (PGCs). One of the clearest distinctions is between the dorsal and ventral

domains of the V-SVZ; dorsal NSCs produce superficial GCs and TH+ PGCs while ventral NSCs produce deep GCs and calbindin+ PGCs (Merkle et al. 2007, Obernier et al. 2014) (Fig. 1.2B).

Although there are obvious distinctions between the developmental fates of NSCs in different V-SVZ regions, it is not entirely clear how stem cells are able to hold onto their positional identities over the course of development. The

brain increases in size and anatomical complexity by orders of magnitude, yet sharp borders continue to delineate region-specific gene expression in V-SVZ domains. Are morphogens still responsible for positional identity in the postnatal niche, or is another mechanism at play?

### *Maintenance of neural stem cell heterogeneity in the V-SVZ*

When it comes to long-term maintenance of transcriptional programs, the assumption in the field has been that constant reinforcement by morphogen signaling is required not only to establish, but also to maintain NSC positional identity. Previous work has shown that morphogens including Shh and Wnt are partially responsible for ensuring proper proliferation

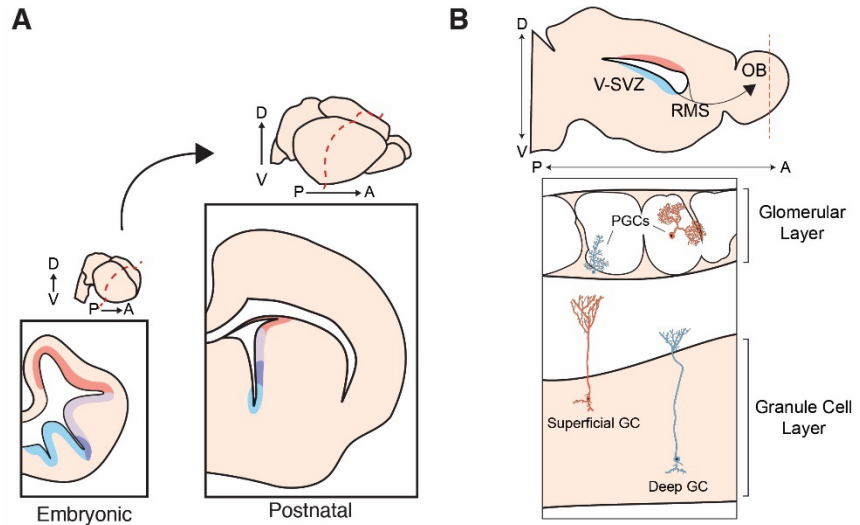


Fig. 1.2. Positional identity persists in the V-SVZ and affects NSC developmental potential.

(A) Embryonic patterns of gene expression are preserved in the postnatal ventricular-subventricular zone (V-SVZ). Shown here are the following domains: Nkx2-1 (blue), Nkx6-2 (dark purple), Gsx2 (lavender), and Pax6 (red). (B) Sagittal schematic showing the path newborn neurons take from the SVZ along the rostral migratory stream (RMS) to the olfactory bulb (OB). Coronal section of the OB, showing the types of periglomerular cells (PGCs) and granule cells (GCs) produced by dorsal and ventral NSCs in the V-SVZ. Dorsal is represented in red, and ventral in blue. D, dorsal; V, ventral; P, posterior; A, anterior.

and lineage progression in the V-SVZ (Balordi & Fishell 2007, Azim et al. 2014), but evidence for maintenance of regional identity is less clear. Ihrie et al. (2011) described a reduction in proliferation and a shift toward dorsal fates among V-SVZ NSCs following the tamoxifen-induced removal of *Shh* from all Shh-expressing cells, suggesting that Shh signaling remains important to maintain identity in at least a subset of NSCs in the niche.

However, there is some evidence that the regional identity of NSCs may be maintained independently of the initializing morphogen even as early as the latter stages of embryogenesis. Shh expression is reduced following the embryonic deletion of ventral-lineage genes *Lhx6* and *Lhx8*, but ventral marker *Nkx2-1* is only lost at the dorsal margin of the MGE. In fact, deleting *Shh* from the inhibitory lineage using *Dlx1/2-Cre* leaves *Nkx2-1* expression largely intact in the MGE around E11.5, despite losses in downstream effectors of the Shh pathway (Flandin et al. 2011), suggesting that different subdomains may have different requirements for morphogen signaling to maintain aspects of their identity, and that it may vary based on the developmental stage of the animal.

In the postnatal V-SVZ, there is compelling evidence for morphogen-independent maintenance of positional identity. Dorsal and ventral NSCs continue to express markers of their respective regions of origin as they divide, including dorsal genes like *Pax6* and ventral genes like *Nkx2-1*. When dorsal and ventral NSCs are removed from the V-SVZ, they still retain expression of regional genes. Delgado et al. (2016) found that dorsal and ventral NSCs dissected from the postnatal mouse brain and propagated in culture retain key positional markers even over multiple rounds of cell division. When pushed to differentiate *in vitro*, ventral NSC cultures generate CalB<sup>+</sup> neuroblasts, while dorsal cultures do not, in line with their *in vivo* developmental potential. The ability of proliferative regional V-SVZ cultures to maintain expression of genes like *Nkx2-1* suggests that positional identity is encoded heritably across cell division.

V-SVZ NSCs' ability to hold onto positional information also seems to be a cell-intrinsic phenomenon. When ventral NSCs are dissected from the V-SVZ and grafted into the dorsal V-SVZ (i.e. heterotopically), they still produce neuron subtypes characteristic of a ventral origin. Similarly, dorsal NSCs produce dorsal-lineage neurons even after heterotopic transplantation into the ventral V-SVZ (Merkle et al. 2007). Even after mixing "out-of-region" and "host-region" NSCs 1:10 prior to transplantation, heterotopically grafted cells generated neurons corresponding with their original birthplace in the V-SVZ. Altogether, these results show that positional identity of NSCs is cell-intrinsic and inherited across cellular generations, suggesting the activity of an epigenetic mechanism.

#### *Epigenetic maintenance of cell fate*

NSCs in the V-SVZ retain signatures of positional identity even when they are actively dividing outside of their niche of origin, both in culture and after heterotopic graft into an *in vivo* context. To propagate regional patterns of gene expression without extrinsic signals to maintain them, NSCs must pass the information down to their daughter cells. Given that nearly all cells in an organism share the same genetic code, this must take the form of inherited regulatory information – i.e., epigenetic.

Here I use "epigenetic" to describe any phenomenon that 1) modifies a cell's transcriptional state without altering the genetic sequence and 2) is heritable at the cellular level, passed from one cell to its progeny over cell division. Epigenetic regulation may maintain gene repression or activation, tune expression levels, or hold genes in a poised state. Forms of epigenetic regulation are essential to maintain gene expression programs over time, serving as a long term cellular "memory" that self-perpetuates independent of signals in the environment. Most forms of gene regulation do not change the DNA sequence (e.g. transcription factor binding, enhancer activity) but are not persistent through mitosis, providing a limited set of



known mechanisms that may explain the apparent cell-intrinsic propagation of NSC regional identity in the V-SVZ.

Epigenetic phenomena can be mediated through activity of transcription factors (TFs), changes in the structure of chromatin, or some combination of the two. Individual TFs may directly activate their own promoters or use a downstream network of TF expression to self-maintain after their initial establishment by an external signal like a morphogen. Over subsequent cell division, inherited TFs in the cytoplasm of daughter cells or TFs that remain complexed to the chromatin through mitosis can re-initiate their own expression (Crews & Pearson 2009, Raccaud & Suter 2018, Leyva-Díaz & Hobert 2019). However, all of this is predicated on the accessibility of the loci these TFs regulate, which highlights the importance of chromatin in epigenetic regulation of gene expression.

Chromatin is the complex polymer of DNA wrapped around histones, proteins which condense and organize the genome within the nucleus. Based on the physical conformation of chromatin and its location in the nucleus, sites on the DNA may be more or less accessible to TFs, rendering genes in a given span of the genome more or less likely to be expressed (Hübner et al. 2013, Mattout et al. 2015, van Steensel & Belmont 2017). Residues on the N-terminal tails of histone subunits can be covalently modified, and particular modifications correlate with different chromatin states. For example, when the 4<sup>th</sup> lysine on histone subunit H3's tail (H3K4) is modified with a trimethyl group (me<sub>3</sub>), the genetic locus complexed to that histone is more likely to be expressed. (Kouzarides 2007, Schuettengruber et al. 2007). While chromatin state can be perpetuated across cellular generations, there is not strong evidence that histone modifications themselves are heritable. A more likely explanation is that chromatin-modifying proteins are able to mediate the re-establishment of the chromatin state from a parent cell in its progeny (Huang et al. 2013, Moazed 2011). When it comes to cellular memory in development, polycomb and trithorax are well-described to maintain regional patterns of gene expression.

### *Polycomb and Trithorax play a role in maintaining positional identity*

Polycomb and trithorax were identified in *Drosophila melanogaster* after the observation that mutations in these genes caused homeotic shifts, leading to dysregulation of body plan development. Follow-up investigation showed that polycomb group (PcG) and trithorax group (TrxG) proteins maintain, but do not establish the repression and activation, respectively, of genes essential for *Drosophila* morphogenesis (Lewis 1978, Sedkov et al. 1994). By working in opposition to one another, PcG and TrxG preserve the finely tuned patterns of gene expression the body requires to form properly (Scheuttengruber et al. 2011). They accomplish this through the assembly of large chromatin-modifying complexes that bind to response elements in the *Drosophila* genome, alter chromatin accessibility, and deposit histone marks (Gould 1997, Mahmoudi & Verrijzer 2001, Steffen & Ringrose 2014). Each group of proteins is associated with a particular set of histone marks – PcG with “repressive mark” H3K27me3 and TrxG with “active mark” H3K4me3, most often (Cao & Zhang 2004, Papp & Muller 2006). While polycomb and trithorax response elements have been identified in the *Drosophila* genome, no such binding sites have been found in mammals (Ringrose & Paro 2007). As a result, the mechanisms of mammalian PcG and TrxG homologs have been more difficult to identify.

As in *Drosophila*, PcG and TrxG homologs regulate developmental patterning genes in mammalian cells. Polycomb repressive complex 1 (PRC1) and 2 (PRC2) have both been found to regulate the expression of homeobox-containing (*Hox*) genes, which guide the formation of the body plan (Mallo & Alonso 2013, Schoenfelder et al. 2015). Mutations in trithorax homolog *Mixed lineage-leukemia 1 (Mll1)* alter the expression of multiple *Hox* genes, perturbing borders of their expression domains and causing homeotic shifts in developing animal's body plan (Yu et al. 1995, Hanson et al. 1999, Terranova et al. 2006). *Mll1* maintains, but does not establish *Hox* gene expression, indicating that positional identity may be converted to an epigenetic “memory” after it is initially conferred by external signals (Yu et al. 1998). Yet, how *Mll1* accomplishes this

is not clear. MLL1 protein is nearly 4000 amino acids long and is cleaved and reassembled after translation. WDR5 mediates its binding to chromatin, where it complexes with Ash2L, RbBP5, and DPY-30. Once bound, its SET domain allows it to catalyze H3K4 mono-, di-, and tri-methylation (Patel et al. 2009, Cosgrove & Patel 2010, Cao et al. 2014). Still, how MLL1's methyltransferase function relates to its ability to maintain gene expression over cell division is unknown.

In NSCs of the postnatal V-SVZ, *Mll1* deletion disrupts expression of proneural homeobox gene *Dlx2*, leading to a buildup of immature neuroblasts and a significant reduction in the size of the OB (Lim et al. 2009). *Mll1*'s importance in the V-SVZ introduces the possibility that it may have a role in maintaining the long-term gene expression programs that define NSC positional identity. However, it is unclear if TrxG proteins maintain regional transcription in NSCs as they do in the development of the body plan – regional transcription essential to generate the remarkable structures and circuits of the mammalian brain.

### *Overview*

In this thesis, I propose a model in which heterogeneous positional identities are established in development, then epigenetically maintained for long periods of time across cell division and cell-type transitions, generating the diversity of cell types required for a functional brain. I have found that morphogen-independent epigenetic mechanisms can take over maintenance of NSC positional identity after it is established in embryogenesis, detailed in Chapter 2. In Chapter 3, I describe how NSC regional heterogeneity persists both within the postnatal stem cell niche and through the neurogenic lineage as a kind of cellular memory. In all, this work may change our understanding of how NSCs can reliably produce an organ as intricate as the mammalian brain.

## Chapter 2: Maintenance of neural stem cell positional identity by Mixed-lineage leukemia 1

### Summary

Neural stem cells (NSCs) in the developing and postnatal brain have distinct positional identities that dictate the types of neurons they generate. Although morphogens initially establish NSC positional identity in the neural tube, it is unclear how such regional differences are maintained as the forebrain grows much larger and more anatomically complex. We found that the maintenance of NSC positional identity in the murine brain requires a *mixed-lineage leukemia 1 (Mll1)*-dependent epigenetic memory system. After establishment by sonic hedgehog, ventral NSC identity became independent of this morphogen. Even transient MLL1 inhibition caused a durable loss of ventral identity, resulting in the generation of neurons with the characteristics of dorsal NSCs *in vivo*. Thus, spatial information provided by morphogens can be transitioned to epigenetic mechanisms that maintain regionally distinct developmental programs in the forebrain.

### Introduction

Early in embryonic development, morphogens provide positional information to NSCs, inducing the expression of region-specific transcription factors (Ericson et al. 1997, Fuccillo et al. 2006, Sur & Rubenstein 2005). The morphogen sonic hedgehog (Shh) drives ventral NSC identity across the neural tube, including the telencephalon, where it induces the expression of ventral transcription factors such as *NK homeobox 2 (Nkx2-1)* (Ericson et al. 1995). NSCs of the postnatal ventricular-subventricular zone (V-SVZ) also have distinct positional identities along the dorsal-ventral axis (Merkle et al. 2007) and arise from embryonic NSCs before embryonic day 13.5 (E13.5) (Fuentelba et al. 2015, Merkle et al. 2004). V-SVZ NSCs maintain the positional information of their embryonic precursors, including the expression of region-specific

transcription factors, throughout adulthood (Fuentelba et al. 2015), making them a well-suited model system in which to study the mechanisms underlying long-term maintenance of positional identity. In particular, embryonic NSCs in the ventrally located medial ganglionic eminence (MGE) express *Nkx2-1* and give rise to the population of *Nkx2-1+* NSCs in the postnatal ventral V-SVZ (Delgado & Lim 2015, Young et al. 2007) (Fig. 2.1A).

### *Mll1, not Shh, maintains NKX2-1 expression in NSCs in vivo*

Although it has been hypothesized that ongoing morphogen signaling is required to maintain the positional identity of NSCs (Fuccillo et al 2006, Ihrie et al. 2011), other studies have suggested that NSC positional identity is maintained in a cell-autonomous fashion (Merkle et al. 2007). Around E8.0, Shh signaling induces the expression of *Nkx2-1* in the ventral neural tube (Shimamura et al. 1995), and deletion of *Shh* at ~E10 reduces *Nkx2-1* expression in the dorsal aspect of the E12.5 MGE (Xu et al. 2005). To determine whether ongoing SHH signaling was required to maintain *Nkx2-1* expression in V-SVZ NSCs, we used the *Nkx2-1-Cre* driver to delete conditional alleles of the SHH receptor *Smoothened* (*Smo<sup>F</sup>*) and followed the fate of recombined cells with a tdTomato transgenic Cre reporter (Ai14). Although deletion of *Smo* at ~E8.25 has been shown to abolish the initiation of *Nkx2-1* expression in ventral NSCs (Fuccillo et al. 2004), the majority ( $99.7 \pm 0.45\%$ ,  $n = 3$  animals) of tdTomato+ cells in the postnatal V-SVZ of *Nkx2-1-Cre; Smo<sup>F/F</sup>; Ai14* mutant mice remained NKX2-1+ (Fig. 2.1, B and C), as did *Nkx2-1-Cre; Smo<sup>F/+</sup>* controls ( $99.2 \pm 0.01\%$ ,  $n = 3$  animals,  $P = 0.10$ ). These data indicate that once *Nkx2-1* is expressed, canonical SHH signaling is no longer required to maintain the *Nkx2-1+* population of ventral V-SVZ precursors, and instead they are maintained by another mechanism.

*Mixed-lineage leukemia 1 (Mll1)* is the mammalian homolog of the *Drosophila* gene *trithorax*, and these genes are required to maintain—but not induce—the proper regional expression of *Hox* cluster genes that determine the anterior-posterior body plan during early

embryogenesis (Geisler & Paro 2015, Schuettengruber et al. 2007, Yu et al. 1995). The vertebrate telencephalon develops from the most anterior aspect of the neural tube, and telencephalic NSCs remain regionally distinct throughout development and into postnatal life (Young et al. 2007, Alvarez-Buylla et al. 2008, Delgado & Lim 2017). To investigate whether *Mll1* is required to maintain *Nkx2-1* in ventral NSCs through embryonic and postnatal development, we used the *Nkx2-1-Cre* driver to delete conditional alleles of *Mll1* (*Mll1<sup>F</sup>*) (Jude et al. 2007). *Nkx2-1-Cre;Mll1<sup>F/F</sup>;Ai14* animals were born at expected Mendelian frequencies but died by postnatal day 13 (P13). *Nkx2-1-Cre;Mll1<sup>F/F</sup>;Ai14* mutants exhibited a progressive loss of NKX2-1 in tdTomato+ cells as compared with *Nkx2-1-Cre;Mll1<sup>F/+</sup>* controls beginning at E15.5 and reached an 80% reduction by P10 (Fig. 2.1, D and E, and Fig. 2.2A)—the decrease occurring in a posterior-to-anterior gradient over this developmental period (Fig. 2.2, B and C). In *Nkx2-1-Cre;Mll1<sup>F/F</sup>;Ai14* mutants, the expression of the cell cycle marker Ki67 in tdTomato+ cells was not different from that in controls (Fig. 2.2, D and E), indicating that changes in NSC proliferation do not account for the decrease in NKX2-1+/tdTomato+ cells. Mice with germline null mutation of *Mll1* at E10 had normal expression of NKX2-1 in ventral NSCs (Fig. 2.2F), indicating that *Mll1* is not required for the initial expression of *Nkx2-1*. Thus, *Mll1* is required for the maintenance, but not the initial induction, of *Nkx2-1 in vivo*.

#### *Mll1<sup>-/-</sup>* NSCs adopt a dorsal-like transcriptional profile

To further investigate the mechanisms that maintain NSC positional identity, we used postnatal V-SVZ NSC cultures that maintain their positional identity through serial passage in vitro (Merkle et al. 2007, Delgado et al. 2016) (Fig. 2.3A). Dorsally derived NSC cultures had higher expression of transcription factors found in the dorsal V-SVZ in vivo—e.g., *paired box 6* (*Pax6*), *empty spiracles homeobox 1* (*Emx1*), and *GS homeobox 2* (*Gsx2*)—and ventral NSC cultures were enriched for factors such as *Nkx2-1*, *ventral anterior homeobox 1* (*Vax1*), and *NK2 homeobox 3* (*Nkx2-3*) (Fig. 2.3A and data S1). Ventral NSCs expressed *Shh* as well as

*patched 1 (Ptch1)* and *GLI-kruppel family member GLI1 (Gli1)* (Fig. 2.3A), two genes that are downstream transcriptional readouts of Shh signaling. While the addition of *Smo* pharmacological inhibitors cyclopamine or vismodegib reduced *Gli1* and *Ptch1* mRNA levels, the expression of *Nkx2-1* remained unchanged, as assessed by quantitative polymerase chain reaction (qPCR) (Fig. 2.3B) and immunocytochemistry (Fig. 2.4, A and B). Sequestration of Shh ligand by the 5E1 antibody resulted in decreased expression of *Ptch1* and *Gli1* but did not affect *Nkx2-1* expression (Fig. 2.4, C to E). We also genetically disrupted Shh signaling by deriving ventral V-SVZ cultures from *Smo<sup>FF</sup>* mice carrying the *UBC-Cre-ERT2* transgene (Ruzankina et al. 2007) and adding 4-hydroxytamoxifen (4-OHT) to induce recombination. RNA sequencing (RNA-seq) analysis of *Smo*-deleted cultures identified 59 differentially expressed genes (27 down-regulated, 32 up-regulated) as compared with *UBC-CreERT2;Smo<sup>F/+</sup>* controls (Fig. 2.3C, Fig. 2.4F, and data S2). With *Smo* deletion, *Smo*, *Gli1*, and *Ptch1* were all significantly down-regulated, but the expression of *Nkx2-1*, *Vax1*, and *Nkx2-3* remained unchanged. Thus, neither pharmacological nor genetic disruption of SHH signaling reduces the expression of transcriptional markers of ventral V-SVZ NSCs.

To study *Mll1* deletion in ventral V-SVZ NSCs, we derived cultures from *UBC-CreERT2;Mll1<sup>FF</sup>* mice. After 4-OHT-induced deletion of *Mll1* (Fig. 2.4G), we performed RNA-seq, identifying 272 differentially expressed genes (81 down-regulated, 191 up-regulated) as compared with *UBC-CreERT2;Mll1<sup>F/+</sup>* controls (Fig. 2.3D and data S3). Genes down-regulated in *Mll1*-deleted cultures were almost entirely distinct from those down-regulated in *Smo*-deleted cultures (Fig. 2.4H). Whereas neither *Gli1* nor *Ptch1* was decreased by *Mll1*-deletion (Fig. 2.4I), the expression of ventral genes including *Nkx2-1*, *Vax1*, and *Nkx2-3* was down-regulated (Fig. 2.3D and Fig. 2.4J). Similar to the progressive loss of NKX2-1 observed in vivo (Fig. 2.1E), the proportion of NKX2-1+ cells in *Mll1*-deleted cultures decreased with serial passage (Fig. 2.3, E and F) without differences in cell proliferation, as measured by incorporation of the thymidine analog 5-ethynyl-2'-deoxyuridine (Fig. 2.4K) or cell death (Fig. 2.4L). Shh pathway inhibition did

not increase the rate or magnitude of *Nkx2-1* loss after *Mll1*-deletion (Fig. 2.5, A to D), indicating that the gradual nature of *Nkx2-1* loss was not due to persistent Shh signaling. Instead, inhibition of cell proliferation with either mitomycin C or colchicine (Fig. 2.5, E and F) attenuated *Nkx2-1* loss in *Mll1*-deleted cells over time (Fig. 2.5, G to I), suggesting that the progressive loss of *Nkx2-1* relates to serial cell division. In *Mll1*-deleted ventral NSCs, we also observed increased levels of dorsally enriched genes including *limb and CNS expressed 1 (Lix1)* as well as bone morphogenetic protein (BMP) pathway genes such as *bone morphogenetic protein 2 (Bmp2)*, *SMAD family member 9 (Smad9)*, and *inhibitor of DNA binding 3 (Id3)* (Fig. 2.3D and data S3). BMP signaling has multiple developmental functions including the dorsalization of the telencephalon (Bond et al. 2012), leading to the expression of the dorsal marker *Msx1* (Furuta et al. 1997), which was also up-regulated in *Mll1*-deleted NSCs (Fig. 2.3D). However, inhibition of BMP signaling with LDN-193189 (Cuny et al. 2008, Chambers et al. 2012) in *Mll1*-deleted cells did not prevent the loss of *Nkx2-1* expression (Fig. 2.5, J to M), suggesting that the loss of this aspect of ventral identity is not secondary to increased BMP signaling. Together, these results indicate that, in addition to losing the expression of ventral markers, ventral NSCs also gain some transcriptional characteristics of dorsal NSCs after the deletion of *Mll1*.

#### *Ventral NSC transcriptional identity requires continuous MLL1 function*

MM-401 is a small-molecule drug that specifically blocks MLL1 function and is reversible upon drug removal (Cao et al. 2014) (hereafter referred to as washout). Deletion of *Mll1* inhibits neurogenesis from V-SVZ NSCs (Lim et al. 2009), and consistent with these prior results, the presence of MM-401 in ventral V-SVZ cultures abolished the production of new neurons in culture (Fig. 2.6A). After MM-401 washout, NSCs produce the same number of new neurons as control-treated cells (Fig. 2.6B and Fig. 2.7A) with no difference in cell death or proliferation (Fig. 2.7, B and C).



Although transient MLL1 inhibition did not impair the ability of V-SVZ NSCs to differentiate into neurons in vitro, we considered the possibility that NSC positional identity might have been durably affected. Consistent with *Mll1* deletion in ventral NSCs (Figs. 2.1, D and E, and 2.3, D to F), including those from adult mice (Fig. 2.7, D and E), the presence of MM-401 reduced the proportion of NKX2-1+ cells as compared with control-treated cultures (Fig. 2.6C), without changes to the expression levels of *Gli1* and *Ptch1* (Fig. 2.7C). Even after 10 days of MM-401 washout (five serial passages), the expression of *Nkx2-1* did not recover (Fig. 2.6D and Fig. 2.7, F and G). Similarly, transient inhibition of MLL1 in ventral NSCs from adult (P60) mice also resulted in stable loss of *Nkx2-1* expression (Fig. 2.7, D and H), suggesting that MLL1 activity is required for NSC positional identity throughout life. In addition to *Nkx2-1*, ~28% of the genes down-regulated in the presence of MM-401 remained down-regulated after drug washout, as revealed by RNA-seq (data S4 and S5). Among the genes that were down-regulated in the presence of MM-401, *Nkx2-1* was the most down-regulated after washout of MM-401 (Fig. 2.7G). Although it has been suggested that NKX2-1 protein can autoregulate its own expression (Das et al. 2011, Oguchi & Kimura 1998) (Fig. 2.8A), in ventral NSCs in vivo, active transcription of the *Nkx2-1* locus did not require NKX2-1 protein (Fig. 2.8, B to D). Thus, continuous MLL1 function is required for the transcriptional memory of markers of ventral identity in proliferating NSC cultures.

MLL1 can regulate chromatin via its methyltransferase domain, recruitment of acetyltransferases, and antagonism of polycomb repressive factors (Schuettengruber et al. 2017, Ernst et al. 2001, Milne et al. 2002, Dou et al. 2006, Patel et al. 2009, De Guzman et al. 2006, Cosgrove & Patel 2010). We therefore performed genome-wide analysis of modifications related to histone methylation (H3K4me3 and H3K4me1), acetylation (H3K27ac), and polycomb factor repression (H3K27me3) using Cleavage Under Targets and Release Using Nuclease (CUT&RUN) (Skene & Henikoff 2017). In ventral V-SVZ cultures, H3K4me1, a mark associated with transcriptional enhancers, and H3K27ac, a mark associated with active enhancers and

promoters, were the most commonly decreased chromatin marks during MM-401 treatment (Fig. 2.9A). These changes corresponded to the differential gene expression observed with this ongoing inhibition of MLL1 activity (fig. 2.10A). Ten days after MM-401 washout, the genome-wide landscape of NSCs remained enriched for changes of H3K4me1 and H3K27ac levels (Fig. 2.9A). Fifty-three percent of loci with decreased H3K4me1 and 51% of loci with decreased H3K27ac under MLL1 inhibition remained decreased after MM-401 washout (Fig. 2.10B). This “stable” loss of H3K4me1 at putative enhancer sequences correlated significantly with stably down-regulated gene expression (Fig. 2.10C). Within gene bodies, the stable loss of H3K27ac also corresponded to stably down-regulated gene expression (Fig. 2.10D). Focusing on genes that remained down-regulated after MM-401 washout, we found that decreases in H3K4me1 and/or H3K27ac enrichment were the most common chromatin changes (Fig. 2.9B).

At the *Nkx2-1* locus, MLL1 protein was enriched near the transcriptional start site, as indicated by chromatin immunoprecipitation (ChIP) analysis (Fig. 4C). Treatment with MM-401 resulted in a small but statistically significant decrease (18.8%,  $P_{adj} = 0.009$ ) in H3K4me3 enrichment across the *Nkx2-1* gene body (Fig. 2.9D, left, and fig. 2.10D). However, this decrease in H3K4me3 was transient as there was no difference in H3K4me3 enrichment detected after the washout of MM-401 (Fig. 2.9D, right, and Fig. 2.10D). In contrast, we observed a durable loss of H3K27ac enrichment across the *Nkx2-1* gene body both during MM-401 treatment (Fig. 2.9E, left, and Fig. 2.10E) and after washout of the inhibitor (Fig. 2.9E, right, and Fig. 2.10E). Together, these results indicate that transient MLL1 inhibition leads to persistent changes to the chromatin landscape that relate to stable differential gene expression.

#### *Transient MLL1 inhibition alters developmental fate of ventral NSCs*

To investigate whether transient inhibition of MLL1 activity affected the developmental potential of ventral NSCs, we studied the fate of their daughter cells after transplantation back to the V-SVZ. Throughout life, the V-SVZ produces new neurons for the olfactory bulb, and NSC

positional identity underlies which olfactory bulb neuronal subtypes are generated (Merkle et al. 2007). In vivo, dorsal NSCs generate superficial granule cells, whereas ventral NSCs generate deep granule cells (Merkle et al. 2007, Young et al. 2007), and such differences in developmental potential are maintained in vitro even after transplantation to ectopic V-SVZ locations (Merkle et al. 2007) (e.g., ventral NSCs still generate deep granule cells when grafted to the dorsal V-SVZ). Thus, deep and superficial granule cells are distinct neuronal subtypes that arise from different populations of NSCs with distinct positional identities related to their location in the walls of the V-SVZ.

We treated ventral NSC cultures with MM-401 or vehicle control for 10 days, after which the cells were cultured under washout conditions for 4 days before transplantation to the V-SVZ of adult mice (Fig. 2.11A). MM-401-washout and control NSCs were labeled with either tdTomato or green fluorescent protein (GFP) and mixed together in equal numbers before being cotransplanted into the V-SVZ. In experiments performed in parallel, consistent with previous findings (Merkle et al. 2007), control NSCs from the dorsal V-SVZ generated granule cell neurons more superficial than those generated from ventral V-SVZ NSCs (Fig. 2.11B). Four weeks post-transplantation, the number of olfactory bulb neurons derived from MM-401-washout and control NSCs was similar (Fig. 2.12A), again indicating that transient MLL1 inhibition does not impair the ability of NSCs to differentiate into neurons (Fig. 2.6, A and B). Furthermore, graft-derived neurons had normal morphologies and were dispersed throughout the olfactory bulb (Fig. 2.11, C and D, and Fig. 2.12, B and C). However, instead of producing deep granule cells, MM-401-washout ventral NSCs produced granule cells whose location was similar to those born from dorsal NSC controls (Fig. 2.11B).

MM-401-washout cells also generated a greater number of periglomerular cells (Fig. 2.11E), an olfactory bulb neuron subtype preferentially born from the anterior V-SVZ (Merkle et al. 2007). Thus, after transient MLL1 inhibition, the normal developmental potential of ventral V-

SVZ NSCs is altered, producing neuronal subtypes more typical of an anterior-dorsal NSC identity (Fig. 2.11F).

### *Outlook*

Our results support a model in which MLL1 functions as part of a transcriptional memory system in telencephalic NSCs, retaining key aspects of NSC positional identity that underlie the generation of proper neuronal diversity. After ventral NSC identity is established by SHH in the early forebrain, MLL1 is required to maintain this positional information (Fig. 2.11G). As key aspects of ventral NSC identity are not lost by inhibition of SHH signaling, we propose that the maintenance of regional differences in NSCs during telencephalic development can become independent of the morphogen gradients that initially pattern the neural tube. MLL1 can remain localized to target genes through mitosis, allowing for the rapid reestablishment of transcription after cell cycle exit (Blobel et al. 2009, Bina et al. 2013). In ventral NSCs, MLL1 may be targeted to loci by SHH-induced transcription factors, with MLL1 remaining localized over serial cell divisions, resulting in persistent chromatin-state changes even after SHH withdrawal.

The mechanism(s) by which chromatin regulators maintain specific patterns of gene expression over serial cell division remain poorly understood. We found persistent, genome-wide changes in H3K4me1 and H3K27ac after transient inhibition of MLL1 (Fig. 2.9A). MM-401 blocks the interaction between MLL1 and WD repeat-containing protein 5 (WDR5), which disrupts the localization of MLL1 to chromatin (Lim et al. 2009). A lack of proper MLL1 localization may lead to both the local loss of H3K4me1, which is one of the histone modifications catalyzed by MLL1 (Patel et al. 2009), and loss of H3K27ac, which is catalyzed by CREB (cAMP response element-binding protein) binding protein (CBP), a histone acetyltransferase that interacts directly with MLL1 (De Guzman et al. 2006, Cosgrove & Patel 2010). Whereas many loci exhibited persistent changes of H3K4me1 and H3K27ac after MM-401 washout, losses of H3K4me3 enrichment were relatively few and mostly transient,

suggesting that other histone methyltransferases can compensate for loss of MLL1 activity. Rather than acting solely through its methyltransferase function, localized MLL1 protein may serve as a genomic “bookmark” for the reestablishment of gene expression after mitosis (Blobel et al. 2009, Bina et al. 2013).

This model provides an alternative understanding of how the boundaries for populations of regionally distinct NSCs are maintained as the cells continue to proliferate—expanding the germinal zones by many orders of magnitude—and while the brain undergoes complex morphological changes. Our finding that MLL1 plays a role in the positional identity of NSCs may inform future methods for producing specific neuronal subtypes from NSCs in vitro for clinical or research purposes or provide additional insights into the neurodevelopmental defects of Wiedemann-Steiner syndrome, which is caused by mutations in *MLL1* (Jones et al. 2012).

## Materials and Methods

### *Animals*

Wildtype (C57bl/6J), *Nkx2-1-Cre* (RRID:IMSR\_JAX:008661) (Xu et al. 2008), *UBC-CreERT2* (RRID:IMSR\_JAX:007001) (Ruzankina et al. 2007), *Nkx2-1<sup>CreER</sup>* (RRID:IMSR\_JAX:014552) (Taniguchi et al. 2011), *Smo<sup>F/F</sup>* (RRID:IMSR\_JAX:004526) (Long et al. 2001), mT/mG (RRID:IMSR\_JAX:007676) (Muzumdar et al. 2007), UBI-GFP (RRID:IMSR\_JAX:004353) (Schaefer et al. 2001), and Ai14 (RRID:IMSR\_JAX:007914) (Madisen et al. 2010) mice were obtained from Jackson Laboratory and maintained locally in the University of California, San Francisco animal facility. *Mll1<sup>F/F</sup>* (Jude et al. 2007) mice were generated by Dr. Patricia Ernst. *Mll1* “deleted” mice were generated by crossing *Mll1<sup>F/F</sup>* mice with *Ella-Cre* (Lasko et al. 1996) mice to drive germline recombination of *Mll1*, and then crossing the resulting F1 progeny. Cre+, heterozygous (F/+) littermates were used as controls for all experiments using Cre-mediated deletion. Embryonic day 0.5 was estimated to be at 12:00 pm on the day that vaginal plugs were observed. To induce Cre activity in *Nkx2-1<sup>CreER;Ai14</sup>*

timed pregnant dams, 5mg of tamoxifen (Sigma) per 30g body weight were administered via oral gavage at E17.5. All protocols and procedures followed the guidelines of the Laboratory Animal Resource Center at the University of California, San Francisco and were conducted with IACUC approval (AN175389-02B and AN180518-01B).

#### *Tissue preparation and immunohistochemistry*

Brains were fixed as previously described (Delgado & Lim 2015). For immunohistochemistry, 12- $\mu$ m frozen sections were used with the following antibodies: rabbit anti-NKX2-1 (1:400, Santa Cruz Biotechnology, Cat# sc-13040, RRID:AB\_793532), mouse anti-Mll1 (1:500, MilliporeSigma, Cat# 05-764, RRID: AB\_309976), rat anti-Ki67 (1:500, eBioscience, Cat# 14-5698-82, RRID: AB\_10854564), rabbit anti-dsRed (1:500, Takara Bio Clontech, Cat# 632496, RRID: AB\_10013483), goat anti-tdTomato (1:500, SICGEN, Cat# AB8181-200, RRID:AB\_2722750), chicken anti-GFP (1:1000, Aves, Cat# GFP-1020, RRID:AB\_10000240). Staining was performed as previously described (Delgado & Lim 2015). Alexa-Fluor secondary antibodies (Invitrogen) and DAPI (Sigma) nuclear counterstain were used.

#### *Cell culture and immunocytochemistry*

Regional monolayer SVZ cultures were derived from postnatal day 7 and adult (2 month-old) mice pups as previously described (Delgado et al. 2016). Dissections from multiple littermates of both sexes were pooled into single biological samples. In brief, following microdissection of the dorsal and ventral SVZ, cells were dissociated in 2.5% trypsin and plated in 48-well plates (Corning) at  $\sim 30000$  cells/cm<sup>2</sup> in media containing DMEM/F12 + Glutamax (Invitrogen), N2 (Invitrogen), 5% FBS (Hyclone), 20ng/ml EGF (Peprotech), 20ng/ml bFGF (Peprotech), and 35ug/ml bovine pituitary extract (Invitrogen), hereafter referred to as proliferation media. Cultures were split 1:2 once they reached 90% confluence and passaged 3-8 times for experiments. To differentiate cells, cultures were switched to differentiation media

containing DMEM/F12 + Glutamax, N2 (Invitrogen), 2% FBS (Hyclone), and 35ug/ml bovine pituitary extract. For pharmacological Shh pathway inhibition, 5  $\mu$ M Cyclopamine (Enzo Chemical) or 100nM Vismodegib (Selleckchem) were added to culture media. Both drugs were resuspended in DMSO and added to proliferation media so that DMSO (Sigma) comprised 1% of media by volume. Proliferation media with 1% DMSO was used as vehicle control. For sequestration of SHH by antibody binding, 5E1 (DSHB, Cat# 5E1, RRID:AB\_528466) was added to proliferation media at 10ug/mL for 48 hours. For BMP pathway inhibition, 500 nM LDN-193189 (Selleckchem) was added to culture media, also dissolved in 1% DMSO, used as vehicle control.

For cell cycle inhibition by mitomycin C, cells were dosed with 10  $\mu$ g/mL mitomycin C (Sigma-Aldrich) in culture media for 2.5 hours, then maintained in proliferation media. For inhibition by colchicine, cells received 0.5  $\mu$ g/mL colchicine (Sigma-Aldrich) dissolved in 1% DMSO in culture media and were re-dosed every 3 days. 1% DMSO was used as vehicle control. For conditional deletion using the *UBC-Cre<sup>ER</sup>* driver, 4-hydroxytamoxifen (4-OHT) (Sigma) dissolved in 1% EtOH (Sigma) was added to culture media at 100nM for 2 passages and then replaced with normal proliferation media. For deletion with Cre-expressing adenovirus, *Mll1<sup>F/+</sup>* and *Mll1<sup>F/F</sup>* cells received 1  $\mu$ L Adeno;Cre virus ( $1.45 \times 10^{13}$  pfu/mL) per 50,000 cells suspended in culture media 4-6 hours after passage. Media was changed after 24 hours of virus incubation. For MM-401 experiments, dissociated cultures were generated as described above and then switched to media containing 25 $\mu$ M MM-401 (in 1% DMSO) or vehicle control (1% DMSO) 24 hours after plating. Cultures were passaged for 10 days in MM-401 media or vehicle control before replacing with normal proliferation media. 5-Ethynyl-2'-deoxyuridine (EdU) labeling was performed using Click-iT EdU imaging kit (Invitrogen). To label cells in S-phase, 10  $\mu$ M EdU was added to culture media for 2 hours prior to fixing cells. Cells were fixed and stained as previously described (20). Cultures were labeled with the following antibodies: rabbit anti-NKX2-1 (1:400, 1:400, Santa Cruz Biotechnology, Cat# sc-13040, RRID:AB\_793532), mouse

anti-Mll1 (1:500, MilliporeSigma, 1:500, MilliporeSigma, Cat# 05-764, RRID: AB\_309976), mouse anti-Tuj1 (1:1000, Covance, Cat# MMS-435P, RRID:AB\_2313773), rabbit anti-Casp3 (Cell Signaling Technology Cat# 9661, RRID:AB\_2341188).

### *Microscopy and quantification*

For quantification of *Nkx2-1*-lineage labeled cells through development, at least two sections per anterior-posterior level per animal were analyzed. Coronal sections were binned into anterior, middle, or posterior groups based on anatomical landmarks. In embryonic animals anterior-posterior bins correspond to schematized coronal sections in figures 2N (anterior), 3M (middle), and 4N (posterior) from Flames et al. (2007).

Postnatally, sections anterior to where the ventral tip of the lateral ventricles curve medially were considered anterior, while those anterior to the foramina of Monro were considered middle, and sections at the level of the third ventricle were considered posterior. For *in vitro* image analysis, at least three non-overlapping fields of view were analyzed.

Quantification was performed blinded to genotype or treatment. Imaging was performed using a DMI4000 B epifluorescent microscope and DFC345 FX camera with 10X or 20X objectives, a Leica TCS SP5 X confocal microscope with 20X objective, and a Keyence BZ-X710. Image processing was performed in Fiji (Schindelin et al. 2012) and Adobe photoshop (Adobe).

Measurements of olfactory neuron location were made as previously described (Delgado & Lim 2015). Statistical analysis using two-tailed student's t-test was performed in Figs. 2.1C, 2.1E, 2.2E, 2.4C, 2.4D, 2.4L, 2.5D, 2.5G, 2.5L, 2.7A, 2.7B, 2.7C, 2.7E, and 2.7H. Statistical analysis using two-tailed ratio paired t-test was performed in Figs. 2.4B, 2.4F, 2.6B, 2.7A. Statistical analysis using two-way ANOVA with Tukey's multiple comparison test was performed in Fig. 2.5C, 2.5H, 2.5I and 2.5L. Statistical analysis using one-way ANOVA with Tukey's multiple comparison test was performed in Fig. 2.3F. Data from each biological replicate shown in each



figure panel along with mean  $\pm$  standard deviation. NS= non significant ( $P>0.05$ ), \* ( $P<0.05$ ), \*\*( $P<0.01$ ), \*\*\* ( $P<0.001$ ).

### *qRT-PCR and RNA-Sequencing*

Total RNA was isolated from cultured cells using TRIzol (Invitrogen) and purified using Direct-zol (Zymo) kit. cDNA synthesis was performed using Transcriptor First Strand cDNA synthesis kit (Roche). qPCR was performed using SYBR green (Roche) on a LightCycler 480 II (Roche). Relative gene expression was calculated using the delta-delta CT method using *ribosomal protein lateral stalk subunit P0 (Rplp0)* as a housekeeping gene. Strand-specific poly(A) selected cDNA libraries were generated using TruSeq Stranded mRNA kit (Illumina). Paired-end, 50bp sequencing of libraries was performed on a HiSeq 4000 (Illumina). Reads were pseudoaligned to Gencode GRCm38.6 transcriptome using Kallisto (Bray et al. 2016) with 100 bootstrap samples. Gene-level differential expression analysis was performed with Sleuth (Pimentel et al. 2017) using the transformation function =  $\text{function}(x) \log_2(x + 0.5)$  convert b value output from Sleuth into log<sub>2</sub> fold-change. Genes that surpassed a threshold of  $qval < 0.1$  and log<sub>2</sub> fold-change (“b” column in data tables) value  $> 0.5$  were considered differentially expressed. Statistical analysis of qRT-PCR data using two-tailed student’s t-test was performed in Figs. 2.3B, 2.4C, 2.4G, 2.5M. Data from each biological replicate shown in each figure panel along with mean  $\pm$  standard deviation, except for *Ptch1* levels in Fig. 2.3B which are shown in technical triplicate. NS= non significant ( $P>0.05$ ), \* ( $P<0.05$ ), \*\*( $P<0.01$ ), \*\*\* ( $P<0.001$ ).

### *CUT&RUN*

We used a modified version of the CUT&RUN (Skene & Henikoff 2017) protocol in which nuclei were isolated from 100,000 cells from the ventral portion of the ventricular-subventricular zone (V-SVZ). Briefly, cells were resuspended in 500  $\mu$ L ice cold Nuclei Isolation Buffer (NIB)

(10 mM HEPES-KOH, Ph 7.9, 10 mM KCl, 0.1% NP40, 0.5 mM Spermidine and 1X Halt protease inhibitor cocktail) and incubated for 10 min in ice. The nuclear pellet was collected by centrifuging at 600xg for 3 min at 4<sup>0</sup>C and again washed with 500  $\mu$ L NIB. Nuclei were collected by centrifugation at 600xg for 3 min and resuspended in 100  $\mu$ L of NIB. Successful nuclei isolation was confirmed by visual inspection under a phase contrast microscope. Next, 10  $\mu$ L Concanavalin A lectin beads (Bio-Mag Plus) washed and resuspended in Binding Buffer (BiB) (20 mM HEPES-KOH, pH 7.9, 10 mM KCl, 1 mM CaCl<sub>2</sub> and 1 mM MnCl<sub>2</sub>) were added to each sample and mixed for 10 min at room temperature. Nuclei bound Concanavalin A beads were pulled by placing the tubes on a magnetic stand to remove the supernatant. Bead bound nuclei were incubated overnight on a rotator at 4<sup>0</sup>C in 50  $\mu$ L Blocking Buffer (BlocB) (Wash buffer containing 2mM EDTA) containing antibodies (1:100 dilution) for the following histone marks: H3K27me3 (Cell Signaling Technologies, Cat# 9733, RRID:AB\_2616029), H3K27me4 (Cell Signaling Technologies, Cat# 9751, RRID:AB\_2616028), H3K4me1 (Cell Signaling Technologies, Cat# 5326, RRID:AB\_10695148) and H3K27ac (Cell Signaling Technologies, Cat# 8173, RRID:AB\_10949503).

An IgG control was run in parallel for all experiments (1:100, Cell Signaling Technologies, Cat# 2729, RRID:AB\_1031062). Next day, samples were briefly spun and placed on magnetic stand to clear off the liquid. Samples were washed twice with 1mL Wash Buffer (WaB) (20 mM HEPES-KOH, pH 7.5, 150 mM NaCl, 0.1% BSA, 0.5 mM Spermidine and 1X Halt protease inhibitor cocktail). At the end of two washing steps, Concanavalin A bound nuclei were resuspended in 50  $\mu$ L of WaB and gently mixed. To each tube, 2.5  $\mu$ L of pA-MNase (diluted 1:10 in WaB from 140  $\mu$ g/mL stock) kindly provided by Henikoff lab (Fred Hutchison Cancer Research Center) was added and rotated for 1 hour at 4<sup>0</sup>C. Samples were briefly spun and placed on magnetic stand to remove the liquid. Samples were washed twice with 1mL WaB. At the end of two washing steps, Concanavalin A bound nuclei were resuspended in 100  $\mu$ L of WaB and gently mixed. The tubes were placed in pre-chilled metal blocks sitting in ice. While

gently vortexing, 2  $\mu$ L of 100 mM  $\text{CaCl}_2$  was added to initiate MNase digestion and returned to pre-chilled metal blocks. Digestion was carried out for 30 min and stopped by adding 100  $\mu$ L of 2XSTOP (200 mM NaCl, 20 mM EDTA, 4 mM EGTA, 50  $\mu$ g/mL RNaseA, 40  $\mu$ g/mL Glycogen and 10 pg/mL of heterologous DNA) while gently vortexing. To release pA-MNase cleaved fragments, samples were incubated at 37°C for 15 min. DNA was extracted from total fraction (soluble + insoluble) using Phenol: Chloroform extraction method.

### *Chromatin Analysis*

CUT&RUN libraries were sequenced for either 100 or 150 cycles on an Illumina HiSeq 4000 or Novaseq 6000 in paired-end mode. Primers and reads with quality scores <30 were filtered using BBDuk (BBMap – Bushnell B. – [sourceforge.net/projects/bbmap/](https://sourceforge.net/projects/bbmap/)). Filtered reads were then aligned to the UCSC mm10 genome using bowtie2 (Langmead et al. 2012) with the following parameters. Differential enrichment analysis between treatment and control conditions was performed in biological duplicate using DiffReps (negative binomial test) (Shen et al. 2013) in “block” mode and differentially enriched loci that intersected with peaks called by MACS2 (Zhang et al. 2008) were retained for downstream analysis. Differentially enriched peaks within 10kb of each other were collapsed to a single “locus” using bedtools function merge and intersections between datasets was performed using the intersect function (Quinlan et al. 2010). Putative enhancer-gene pairings were obtained from ENCODE website (<http://chromosome.sdsc.edu/mouse/download.html>) and those pairings found in “Cortex” and “E14.5 brain” samples were used for intersectional analysis. Odds ratios of differentially enriched chromatin loci and differentially expressed genes were calculated using the GeneOverlap R package (Li Shen and Mount Sinai (2019). GeneOverlap: Test and visualize gene overlaps. R package version 1.20.0. <http://shenlab-sinai.github.io/shenlab-sinai/>)

### *Chromatin Immunoprecipitation (ChIP)*

Chromatin analysis of the *Nkx2-1* locus was performed using ChIP-qPCR (qChIP). Chromatin was isolated as previously described (27) and antibodies for MLL1 (1ug, Bethyl #A300-37A, Cat# A300-374A, RRID:AB\_345243) or IgG (1ug, Cell Signaling Technologies, Cat# 2729, RRID:AB\_1031062) were used for immunoprecipitation. Quantification of immunoprecipitation was performed by qPCR using primers tiling the *Nkx2-1* locus and SYBR Green (Roche) on a LightCycler 480 II (Roche). Fold enrichment to input was performed using the delta-delta-ct method.

### *V-SVZ NSC Transplantation*

To control for the variation related to stereotactic injection, control- and MM-401-treated NSCs were labeled with either GFP or tdTomato, mixed at a 1:1 ratio, and co-injected into the same host mouse V-SVZ. Prior to transplantation, NSCs were cultured with proliferative media containing either 25 $\mu$ M MM-401 or vehicle control (DMSO) for ten days and then washed out with normal proliferation media for four days. Using a 5 $\mu$ L glass micropipette (Drummond Scientific) and a stereotactic rig, we injected ~60,000 cells (30,000 cells from each treatment condition) resuspended in 500nl of DMEM into the SVZ ( $x= 0.5$ ,  $y= 0.850$ ,  $z= -2.15$ ) of an adult (P60-90) CD-1 mouse with  $x$  and  $y$  coordinates zeroed at bregma, and  $z$  coordinate zeroed at the brain surface. We performed two separate rounds of transplantation using cultures derived from mT/mG and UBI-GFP mice, which ubiquitously express tdTomato and GFP, respectively. In the first round, tdTomato+ cells were treated with MM-401, and GFP+ cells were treated with vehicle control. In the second round, we reversed the cell-labeling and treatment conditions (tdTomato+ cells were treated with vehicle control, and GFP+ cells were treated with vehicle control). We also performed a third round of transplants using cultures derived from Ai14 tdTomato reporter mice that were either virally transduced with pSicoR-GFP (Ventura et al. 2004) lentivirus to label them with GFP, or incubated with Cre Recombinase Gesicles (Clontech) to label NSCs with tdTomato. In the third round of transplants, for half of the

transplants, tdTomato+ cells were treated with MM-401, and GFP+ cells were the co-injected control; for the other transplants, tdTomato+ cells were the control population, and GFP+ cells were treated with MM-401.

After 28 days, we euthanized the host mouse, fixed the brain, and analyzed the olfactory bulb by immunohistochemistry. We analyzed 8-14 sections per animal and excluded animals that had fewer than 5 cells per treatment or control condition. For GC layer analysis, 8 animals that received ventral transplants, and 7 animals that received dorsal transplants, met these inclusion criteria (with at least 2 animals per round of transplants). For PGC layer analysis, 7 animals met these inclusion criteria. Statistical analysis of transplanted NSC data using two-tailed student's t-test was performed in Figs. 2.11B, 2.11E. Statistical analysis using two-tailed ratio paired t-test was performed in Fig. 2.12A. Data from each biological replicate shown in each figure panel along with mean  $\pm$  standard deviation.

## Figures

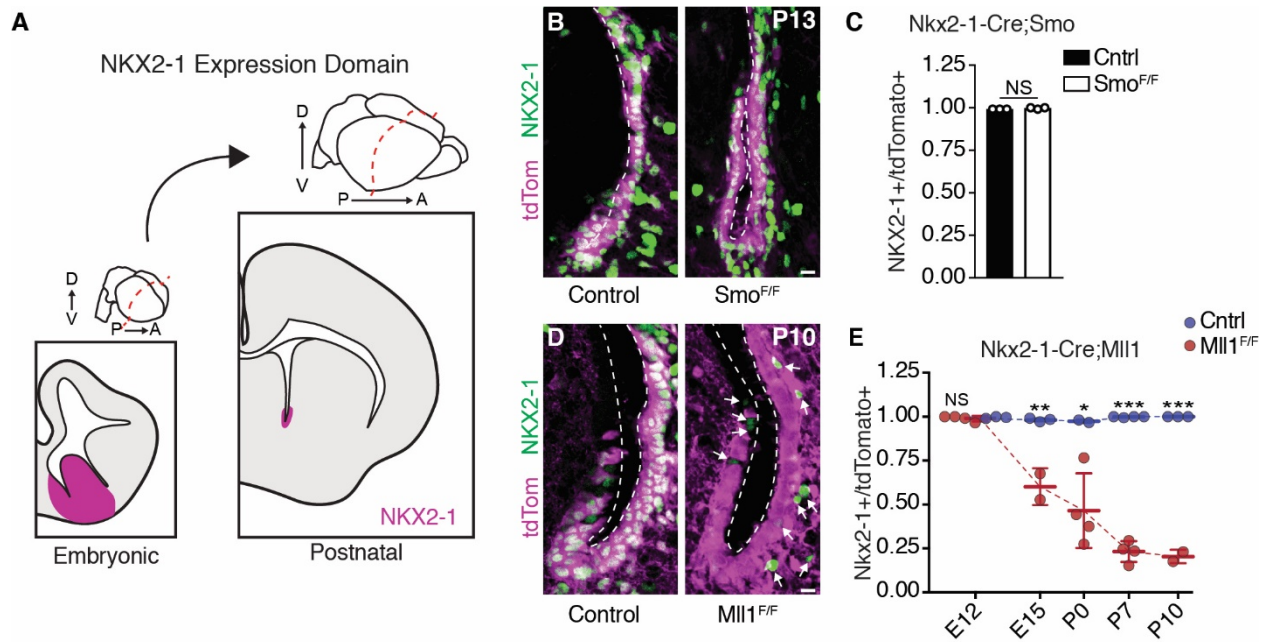


Fig. 2.1. *MII1*, but not SHH signaling, is required to maintain NKX2-1 expression in postnatal V-SVZ.

(A) NKX2-1 expression in the germinal zones of embryonic forebrain and postnatal V-SVZ. NKX2-1 domain shown in magenta. D, dorsal; V, ventral; P, posterior; A, anterior. (B) Representative images of NKX2-1 (green) and tdTomato (magenta) expression in P13 coronal sections from ventral V-SVZ of *Nkx2-1-Cre;Smo<sup>F/+</sup>* and *Nkx2-1-Cre;Smo<sup>F/F</sup>* mice. Ventricular walls are demarcated by a dashed line. (C) Quantification of NKX2-1+;tdTomato+ double-positive V-SVZ cells in *Nkx2-1-Cre;Smo<sup>F/+</sup>* (control) and *Nkx2-1-Cre;Smo<sup>F/F</sup>* animals at P13 (mean ± SD; NS, not significant; two-tailed student's t test). (D) Representative images of NKX2-1 (green) and tdTomato (magenta) expression in ventral V-SVZ of P10 *Nkx2-1-Cre;MII1<sup>F/+</sup>* and *Nkx2-1-Cre;MII1<sup>F/F</sup>* mice. Ventricular walls are demarcated by a dashed line. Arrows indicate tdTomato-;NKX2-1+ cells. (E) Quantification of NKX2-1+;tdTomato+ double-positive V-SVZ cells from *Nkx2-1-Cre;MII1<sup>F/+</sup>* (control) and *Nkx2-1-Cre;MII1<sup>F/F</sup>* mice over the course of development (mean ± SD, \**P* < 0.05, \*\**P* < 0.01, \*\*\**P* < 0.001, two-tailed student's t test). Scale bars, 10 μm [(B) and (D)].

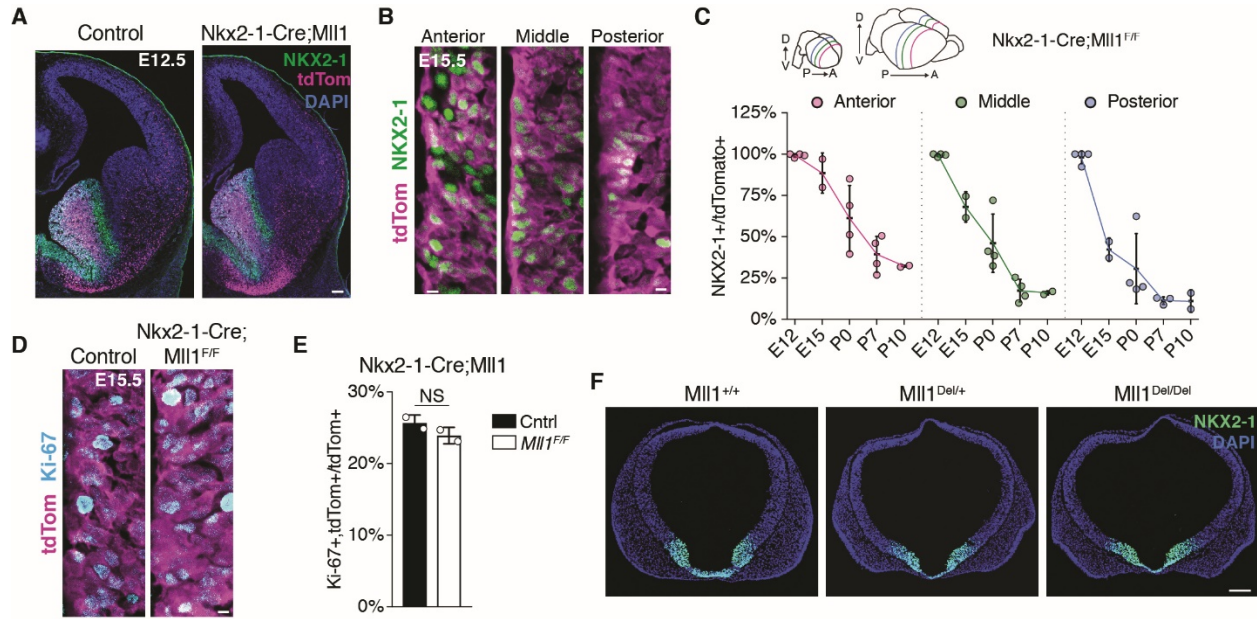


Fig. 2.2. *Mll1* does not establish *Nkx2-1* in the developing brain.

(A) Representative images of NKX2-1 (green) and tdTomato (magenta) expression in E12.5 coronal sections from ventral *Nkx2-1-Cre;Mll1<sup>F/+</sup>* and *Nkx2-1-Cre;Mll1<sup>F/F</sup>* mouse telencephalon. (B) High-magnification coronal images of NKX2-1 (green) and tdTomato (magenta) expression in the lateral ventricular wall of E15.5 *Nkx2-1-Cre;Mll1<sup>F/F</sup>* mice. Left, representative anterior section. Middle, representative mid-telencephalon section. Right, representative posterior section. (C) Quantification of NKX2-1<sup>+</sup>;tdTomato<sup>+</sup> double positive cells in ventral progenitor zone from anterior, middle, and posterior regions of *Nkx2-1-Cre;Mll1<sup>F/F</sup>* mice throughout development (mean  $\pm$  SD, two-way ANOVA with Tukey's multiple comparison test). (D) High-magnification coronal images of Ki-67 (cyan) and tdTomato (magenta) expression in the lateral ventricular wall of E15.5 *Nkx2-1-Cre;Mll1* mice. (E) Quantification of Ki-67<sup>+</sup>; tdTomato<sup>+</sup> germinal zone cells relative to total tdTomato<sup>+</sup> cells in E15.5 *Nkx2-1-Cre;Mll1* mice (mean  $\pm$  SD, NS= not significant, two-tailed student's t-test). (F) Representative images of NKX2-1 (green) expression in E10.0 coronal forebrain sections from *Mll1*-del mice and littermate controls. Scale bars, 100  $\mu$ m (A,F), 10  $\mu$ m (B,D).

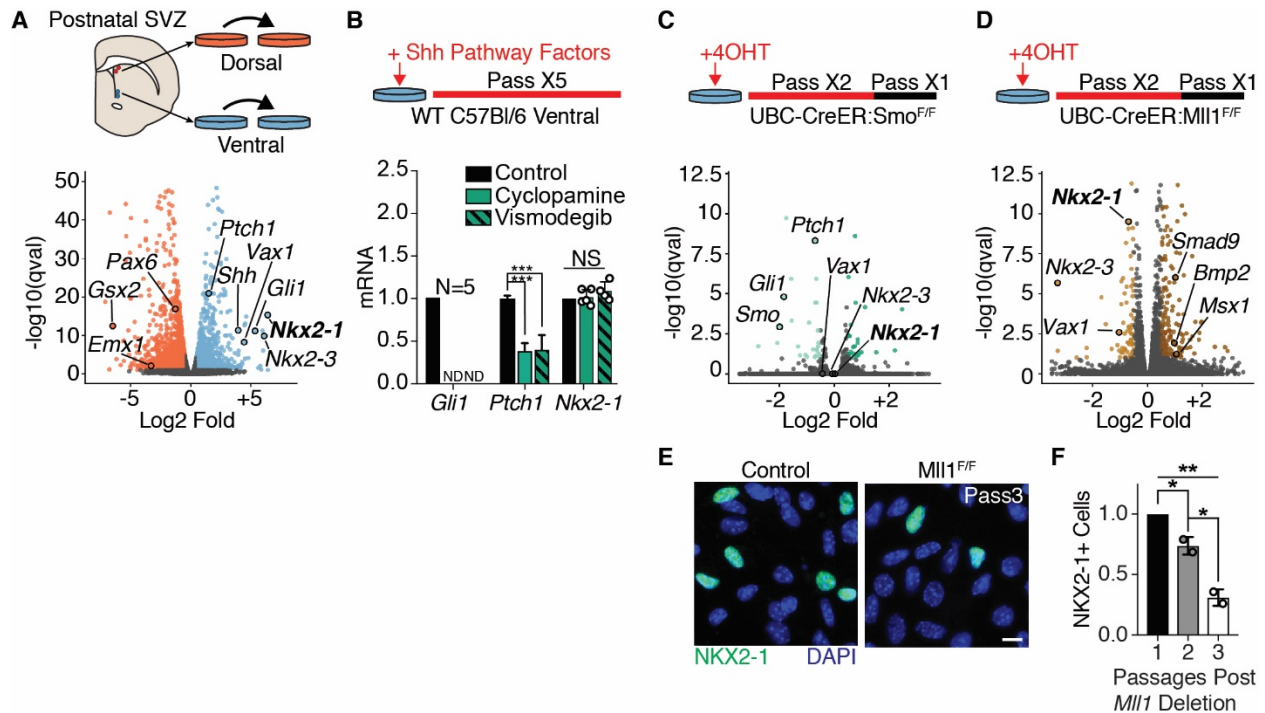


Fig. 2.3. *MII1*-dependent NSC transcriptional identity does not require Shh signaling.

(A) Derivation of region-specific NSC cultures from the dorsal and ventral P7 mouse V-SVZ (top panel). Volcano plot of differential gene expression by RNA-seq in dorsal and ventral NSC cultures. Dorsal-enriched genes, orange; ventral-enriched genes, light blue. (B) Pharmacological Shh pathway inhibition assay timeline (top panel). qPCR from ventral V-SVZ NSC cultures exposed to Shh pathway inhibitors (mean ± SD, \*\*\* $P < 0.001$ , two-tailed student's t test; ND, not detected). *Gli1* and *Nkx2-1* analysis from 4 to 5 biological replicates, *Ptch1* in technical triplicate. (C) Schematic of ubiquitous *Smo* deletion from ventral NSC cultures by 4-OHT administration (top). Volcano plot of differential gene expression by RNA-seq in ventral UBC-CreER;Smo<sup>F/+</sup> and UBC-CreER;Smo<sup>F/F</sup> NSC cultures. Genes up-regulated, dark green; down-regulated, light green; not significantly changed, gray. (D) Schematic of ubiquitous *MII1* deletion from ventral NSC cultures by 4-OHT administration (top). Volcano plot of differential gene expression by RNA-seq in ventral UBC-CreER;MII1<sup>F/+</sup> and UBC-CreER;MII1<sup>F/F</sup> NSC cultures. Genes up-regulated, dark brown; down-regulated, light brown; not significantly changed, gray. (E) Representative image of NKX2-1+ cells in ventral UBC-CreER;MII1<sup>F/+</sup> and UBC-CreER;MII1<sup>F/F</sup> NSC cultures. Scale bar, 10 μm. (F) Quantification of NKX2-1+ cells after in vitro deletion of *MII1* by UBC-CreER relative to baseline at first passage (mean ± SD, \* $P < 0.05$ , \*\* $P < 0.01$ , one-way analysis of variance with Tukey's multiple comparison test).



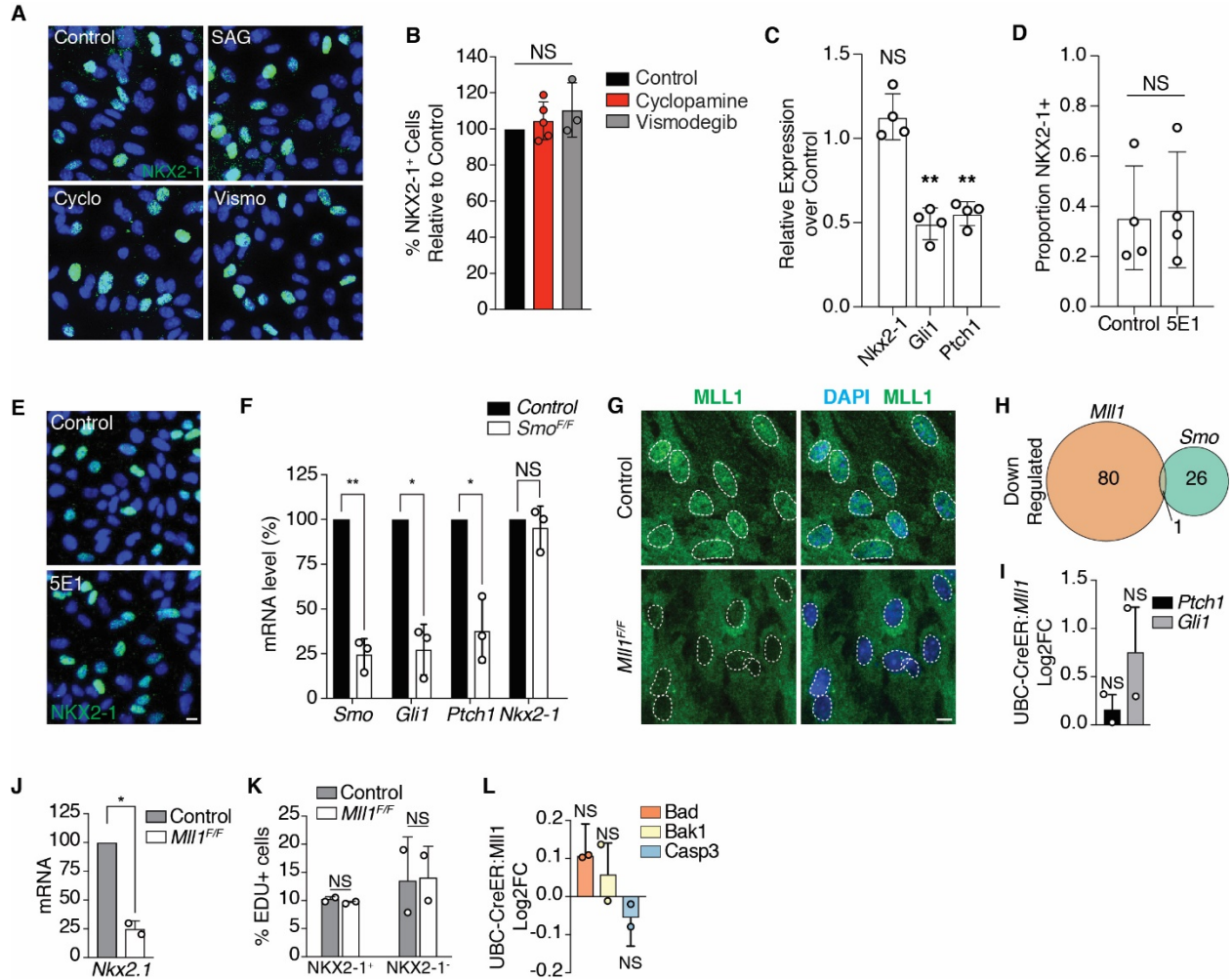


Fig. 2.4. *Nkx2-1* expression is affected by *Mll1* deletion, but not Shh inhibition.

(A) Representative images of NKX2-1 (green) expression in ventral NSC cultures treated with SHH inhibitors. (B) Quantification of NKX2-1<sup>+</sup> cells treated with SHH inhibitors relative to vehicle control (mean ± SD, NS= not significant, two-tailed student's t-test). (C) qPCR from ventral WT NSCs cultured with the SHH-blocking antibody 5E1 (mean ± SD, \*\* p<0.01, NS= not significant, two-tailed one-sample t-test). (D) Quantification of NKX2-1<sup>+</sup> cells in ventral WT NSC cultures following treatment with SHH-blocking antibody 5E1 (mean ± SD, NS= not significant, two-tailed ratio-paired t-test). (E) Representative images of NKX2-1 (green) expression in ventral NSC cultures treated with SHH-blocking antibody 5E1. (F) qRT-PCR from ventral UBC-CreER;*Smo* cultures following *Smo* deletion by 4-OHT (mean ± SD, \* p<0.05, \*\* p<0.01, NS= not significant, two-tailed ratio-paired t-test). (G) Representative images of MLL1 (green) expression in SVZ monolayer cultures derived from control and UBC-CreER;*Mll1*<sup>F/F</sup> mice. Nuclei outlines in dashed white line. (H) Venn diagram comparing down-regulated genes from UBC-CreER;*Mll1*<sup>F/F</sup> and UBC-CreER;*Smo*<sup>F/F</sup> cultures. (I) Differential expression (log<sub>2</sub> fold change ± SE) of SHH-responsive genes in UBC-CreER;*Mll1* deleted NSCs compared to control cultures by RNA-seq.

(J) qPCR of *Nkx2-1* following *in vitro* deletion of *Mll1* by UBC-CreER (mean  $\pm$  SD, \*  $p < .05$ , two-tailed ratio paired t-test). (K) Quantification of EDU incorporation in ventral UBC-CreER:*Mll1* V-SVZ NSC cultures (mean  $\pm$  SD, NS= not significant, two-tailed student's t-test). (L) Differential expression ( $\log_2$  fold change  $\pm$  SE) of pro-apoptotic genes in UBC-CreER:*Mll1* deleted NSCs compared to control cultures by RNA-seq. Scale bars, 10  $\mu$ m (A,E,G).

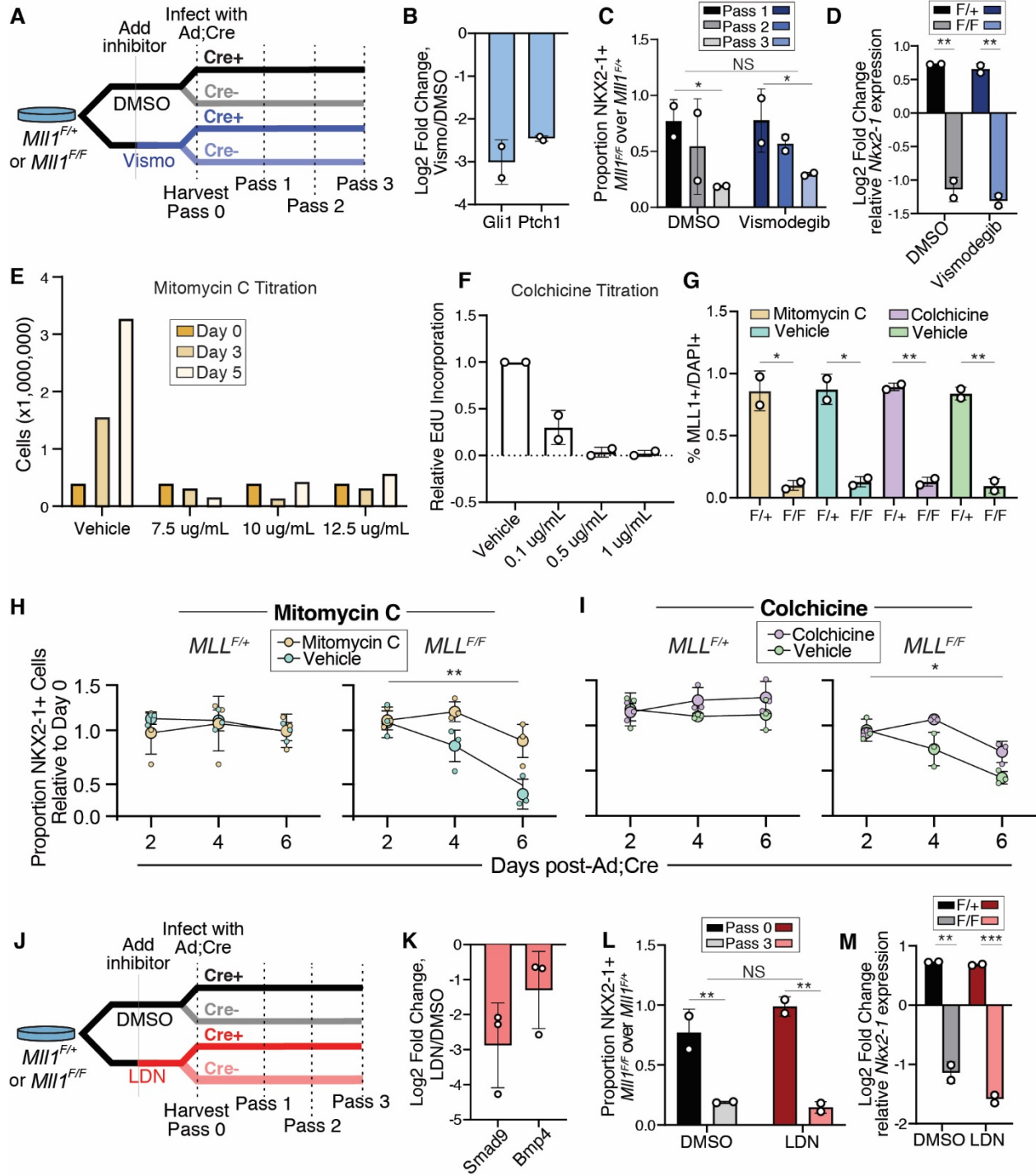


Fig. 2.5. *Mll1*-mediated loss of *Nkx2-1* is morphogen independent and related to cell cycle.

(A) Treatment timeline of *Mll1*<sup>F/+</sup> and *Mll1*<sup>F/F</sup> ventral cultures with Shh pathway inhibitor vismodegib in the presence and absence of Cre. (B) Confirmation of Shh pathway inhibition by qPCR, represented as log<sub>2</sub> fold change in *Gli1* and *Ptch1* under vismodegib treatment relative to vehicle control (mean ± SD). (C) Relative number of NKX2-1<sup>+</sup> cells in *Mll1*<sup>F/F</sup> cultures normalized

to *Mll1<sup>F/+</sup>* cultures over three passages, by ICC (mean  $\pm$  SD, NS=not significant, \*  $p < 0.05$ , two-way ANOVA). (D) Log<sub>2</sub> fold change in expression of *Nkx2-1* by qPCR after addition of Cre, relative to control with no Cre (mean  $\pm$  SD, \*\*  $p < 0.01$ , two-tailed student's t-tests). (E) Cell counts for five days following a single 2.5 hour treatment of different concentrations of mitomycin C. (F) Proportion of EdU incorporating cells following treatment with different concentrations of colchicine. Cells were incubated with EdU for 1 hour (mean  $\pm$  SD). (G) Quantification of MLL1<sup>+</sup> cells by ICC in *Mll1<sup>F</sup>* ventral NSC cultures 3 days after infection with Adeno;Cre, treated with either mitomycin C, colchicine, or their respective vehicle controls (mean  $\pm$  SD, \*  $p < 0.05$ , \*\*  $p < 0.01$ , two-tailed student's t-test). (H) Proportion NKX2-1<sup>+</sup> cells in mitomycin-C-treated control *Mll1<sup>F/+</sup>* (left) and *Mll1<sup>F/F</sup>* cultures (right) following the administration of Adeno;Cre. Proportions are normalized to Day 0 levels. Vehicle controls included for each treatment condition (mean  $\pm$  SD, \*\*  $p < 0.01$ , two-way ANOVA, effect of treatment). (I) Proportion NKX2-1<sup>+</sup> cells in colchicine-treated control *Mll1<sup>F/+</sup>* (left) and *Mll1<sup>F/F</sup>* cultures (right) following the administration of Adeno;Cre. Proportions are normalized to Day 0 levels (mean  $\pm$  SD, \*\*  $p < 0.05$ , two-way ANOVA, effect of treatment). (J) Treatment timeline of ventral *Mll1<sup>F/+</sup>* and *Mll1<sup>F/F</sup>* cultures with pan-BMP pathway inhibitor LDN-193189 in the presence and absence of Cre. (K) Confirmation of BMP pathway inhibition by qPCR, represented as log<sub>2</sub> fold change in *Smad9* and *Bmp4* under LDN treatment relative to vehicle control (mean  $\pm$  SD). (L) Relative number of NKX2-1<sup>+</sup> cells in *Mll1<sup>F/F</sup>* cultures normalized to *Mll1<sup>F/+</sup>* cultures at the time Adeno;Cre was administered and after three passages (mean  $\pm$  SD, \*\*  $p < 0.01$ , two-tailed student's t-tests; NS=not significant, two-way ANOVA, effect of treatment). (M) Log<sub>2</sub> fold change in *Nkx2-1* expression by qPCR after addition of Adeno;Cre, normalized to the Cre- condition (mean  $\pm$  SD, \*\*  $p < 0.01$ , \*\*\*  $p < 0.001$ , two-tailed student's t-test).

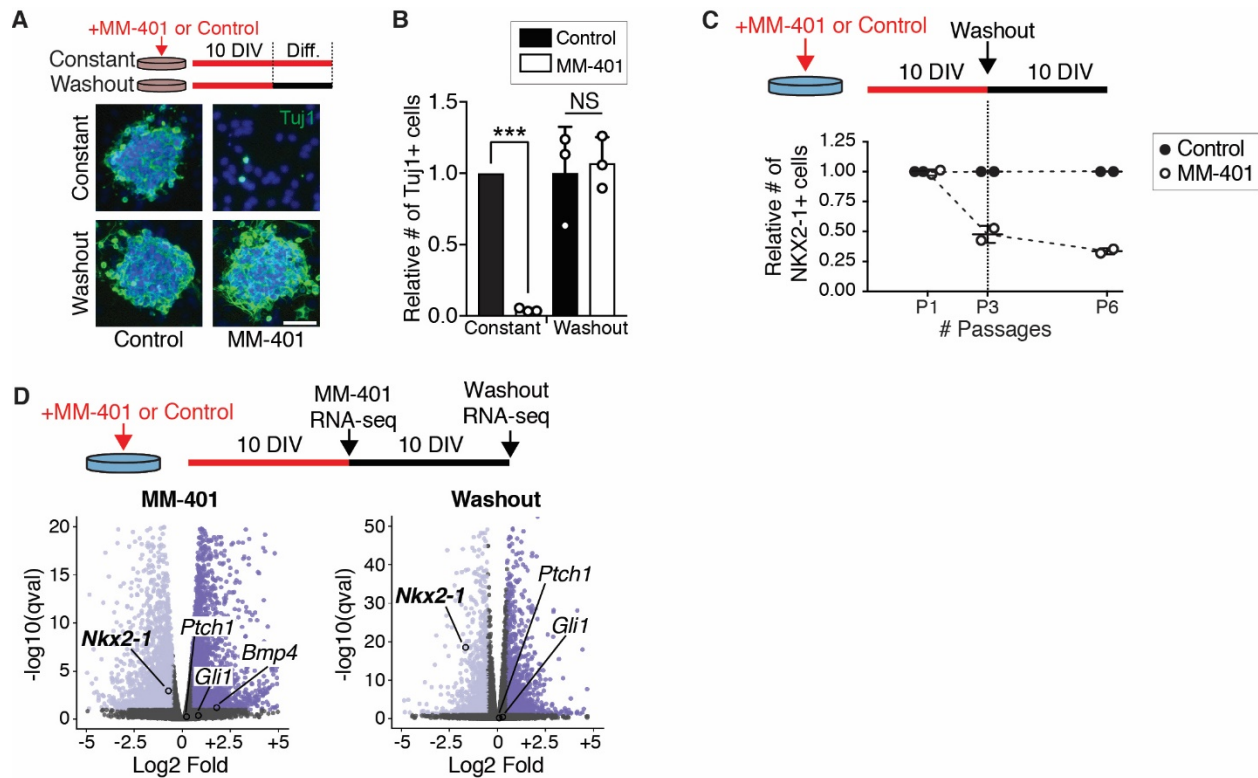


Fig. 2.6. Ventral NSC transcriptional identity requires continuous MLL1 function.

(A) Treatment timeline of V-SVZ NSCs with the MLL1-specific inhibitor MM-401 (or vehicle control) under proliferative conditions for 10 days in vitro (DIV), followed by differentiation (Diff.) with or without drug washout (top). Representative images of Tuj1 (green) and DAPI (4',6-diamidino-2-phenylindole, blue) after differentiation. Scale bar, 50  $\mu$ m. (B) Quantification of Tuj1+ cells after differentiation of MM-401-treated NSCs (mean  $\pm$  SD, \*\*\* $P$  < 0.001, two-tailed student's t test). (C) Treatment timeline of ventral V-SVZ NSCs with MM-401 and subsequent washout under proliferative conditions (top). Quantification of NKX2-1+ cells normalized to control-treated group at each time point. (D) Volcano plot of differential gene expression by RNA-seq in ventral NSCs treated with MM-401 (left) and then after washout (right) under proliferative conditions. Genes up-regulated, dark purple; down-regulated, light purple; not significantly changed, gray.

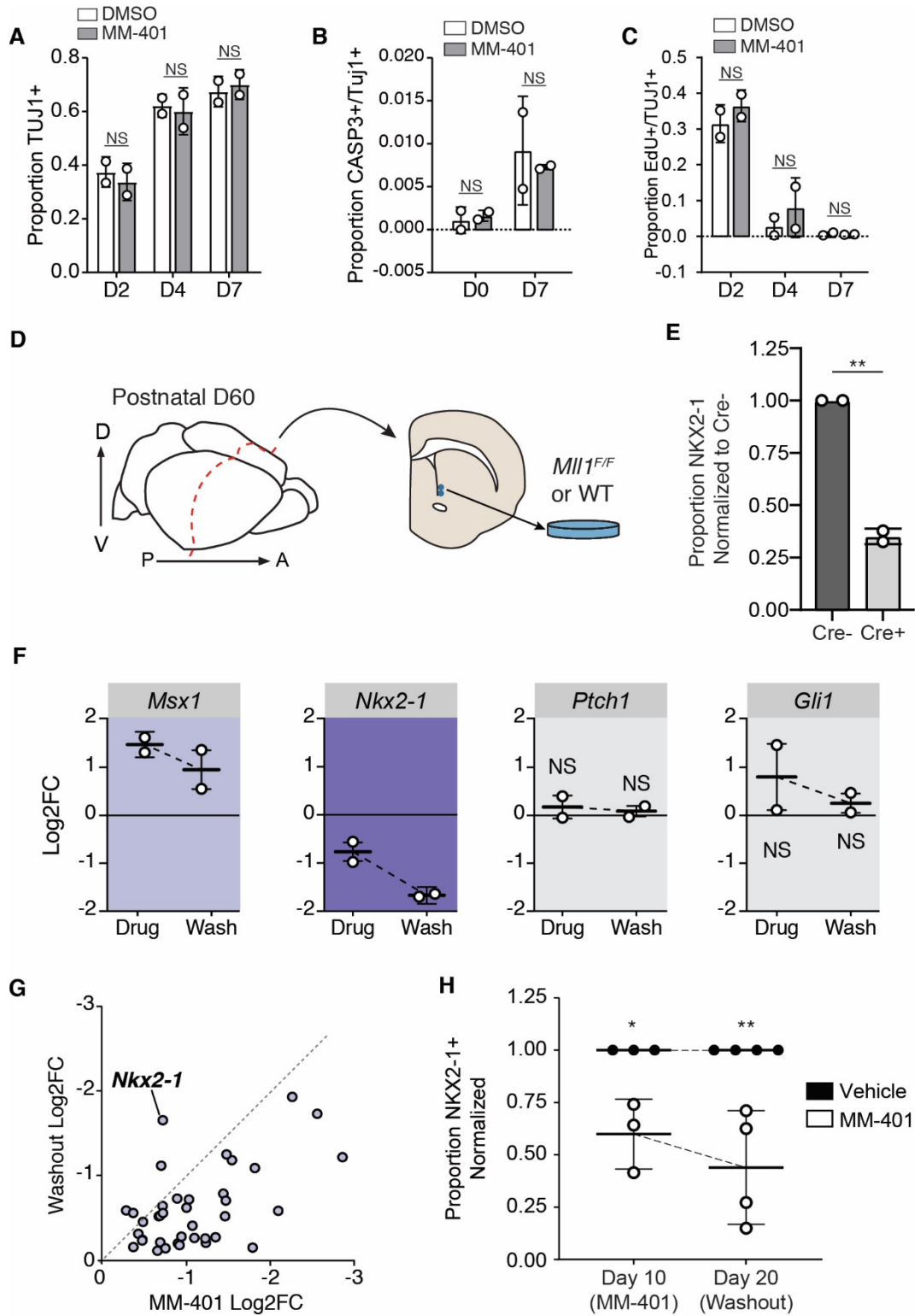


Fig. 2.7. Effects of MM-401 on P7 and P60 cultures.

(A) Quantification of TUJ1<sup>+</sup> cells from MM-401-washout and control ventral NSCs at day (D) 2, 4 and 7 of in vitro differentiation (mean  $\pm$  SD, NS= not significant, two-tailed student's t-tests). (B) Proportion of Edu<sup>+</sup>/TUJ1<sup>+</sup> cells from MM-401-treated and control-treated ventral NSCs at D0, D4 and D7 of in vitro differentiation (mean  $\pm$  SD, two-tailed student's t-tests). (C) Quantification of CASP3<sup>+</sup>/TUJ1<sup>+</sup> cells from MM-401-treated and control-treated ventral NSCs at D0 and D7 of in vitro differentiation (mean  $\pm$  SD, two-tailed student's t-tests). (D) Schematic depicting microdissection of ventral V-SVZ to establish adult NSC cultures from P60 mice. (E) Relative number of NKX2-1<sup>+</sup> cells in ventral adult (P60-derived) *Mll1<sup>F/F</sup>* NSC cultures infected with Adeno;Cre normalized to Cre- cultures, by ICC (mean  $\pm$  SD, \*\* p<0.01, two-tailed student's t-test). (F) Differential expression (log<sub>2</sub> fold change  $\pm$  SE) of select genes in MM-401-treated and MM-401-washout ventral NSCs by RNA-seq. All genes shown are significantly differentially regulated except for those marked with NS (not significant). (G) Scatterplot of genes significantly downregulated in both MM-401-treated and UBC-CreER;*Mll1<sup>F/F</sup>* cultures by RNA-seq. X-axis depicts log<sub>2</sub> fold-change during MM-401 treatment, while Y-axis depicts log<sub>2</sub> fold-change following MM-401-washout. Dashed line depicts where fold change in treatment = fold change in washout. (H) Relative number of NKX2-1<sup>+</sup> cells by ICC in ventral cultures derived from wild type P60 mice, comparing MM-401 treated NSCs normalized to vehicle control after 10 days of treatment and 10 days of washout (mean  $\pm$  SD, \* p<0.05, \*\* p<0.01, two-tailed student's t-test).

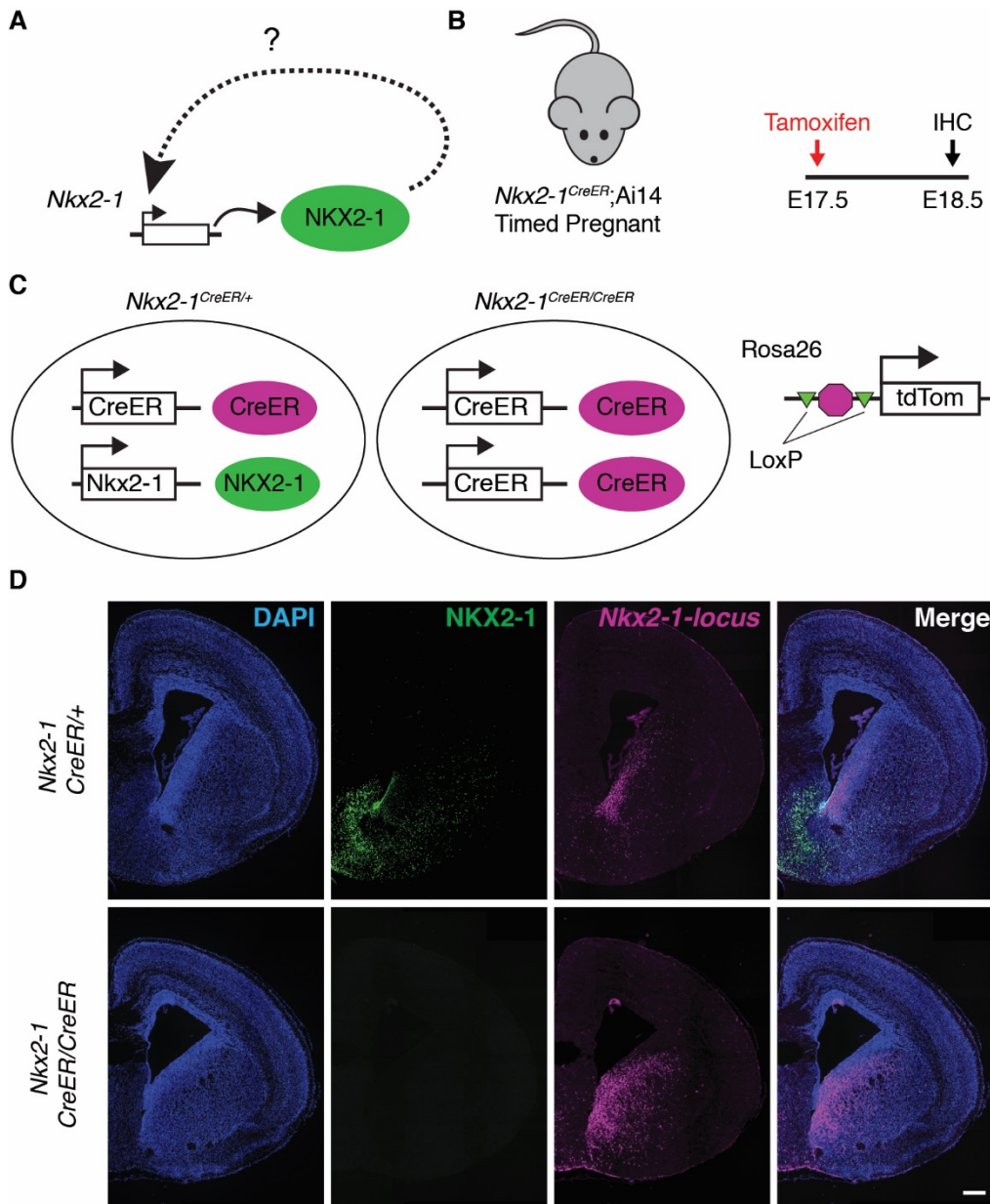


Fig. 2.8. *Nkx2-1* is not maintained through autoregulation.

(A) Schematization of *Nkx2-1* autoregulation hypothesis. *Nkx2-1* locus is depicted generating NKX2-1 protein which then positively regulates the *Nkx2-1* locus. (B) Experimental design used to test *Nkx2-1* autoregulation hypothesis. Timed pregnant dam carrying *Nkx2-1*<sup>CreER</sup>; Ai14 litter is given tamoxifen at E17.5 and then embryos are collected at E18.5. (C) Schematic depicting both alleles of the *Nkx2-1* locus in *Nkx2-1*<sup>CreER/+</sup> and *Nkx2-1*<sup>CreER/CreER</sup> mice including the gene products they produce. (D) Representative images of NKX2-1 and tdTomato expression in E18.5 coronal sections from *Nkx2-1*<sup>CreER/+</sup> and *Nkx2-1*<sup>CreER/CreER</sup> mice that received tamoxifen one day prior (E17.5). Scale bar, 250  $\mu$ m (E).



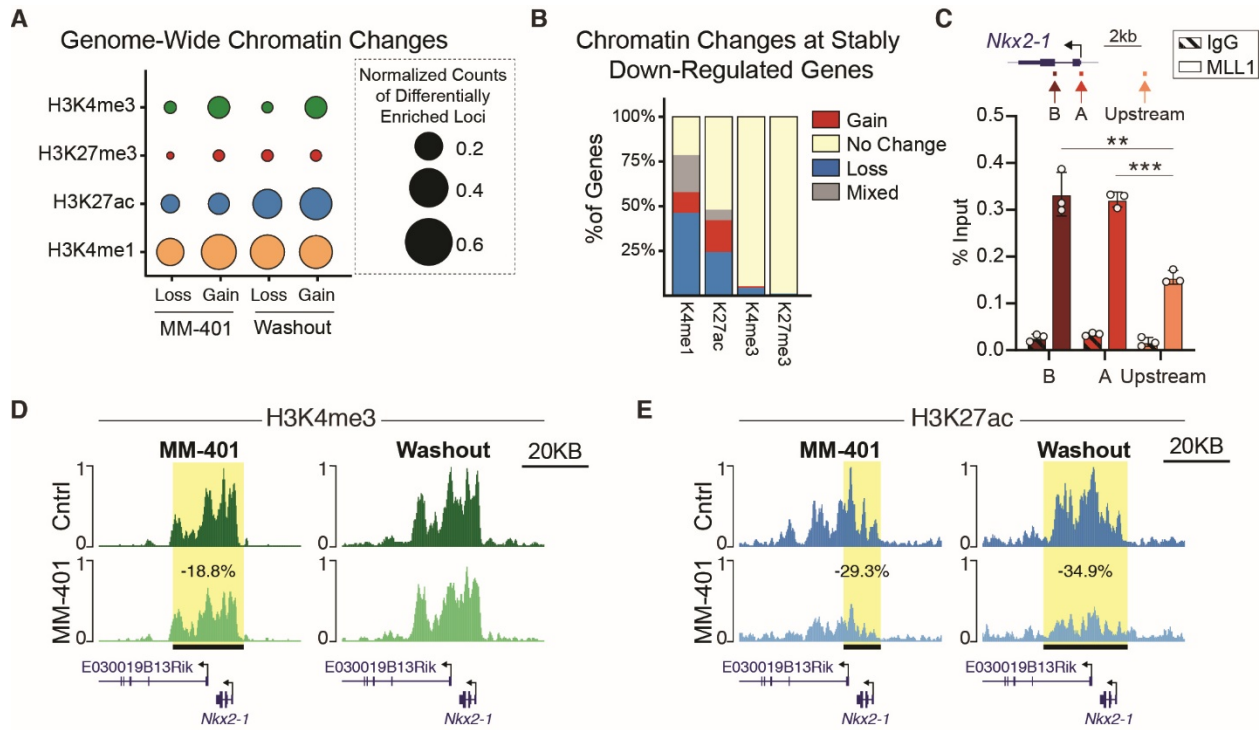


Fig. 2.9. Chromatin state changes to ventral NSCs after transient MLL1 inhibition.

(A) Genome-wide quantification of chromatin changes in MM-401-treated and MM-401-washout ventral NSC cultures. Circle size represents the number of sites that have either a gain or loss of a chromatin mark in the treatment group compared with control, normalized to the size of genome covered by statistically called peaks for that chromatin mark ( $\times 10,000$ ). (B) Quantification of chromatin changes within stably down-regulated genes after MM-401 washout. (C) Locations of qPCR primers at the *Nkx2-1* locus (top). ChIP-qPCR analysis of MLL1 enrichment at *Nkx2-1* (mean  $\pm$  SD,  $**P < 0.01$ ,  $***P < 0.001$ , two-tailed student's t test, in technical triplicate). IgG, immunoglobulin G; kb, kilobases. (D and E) CUT&RUN traces of (D) H3K4me3 and (E) H3K27ac enrichment over the *Nkx2-1* locus in control- and MM-401-treated cultures (left) and after 10 days of washout (right). Horizontal black bar with yellow highlight depicts genomic region with statistically significant differential chromatin enrichment.

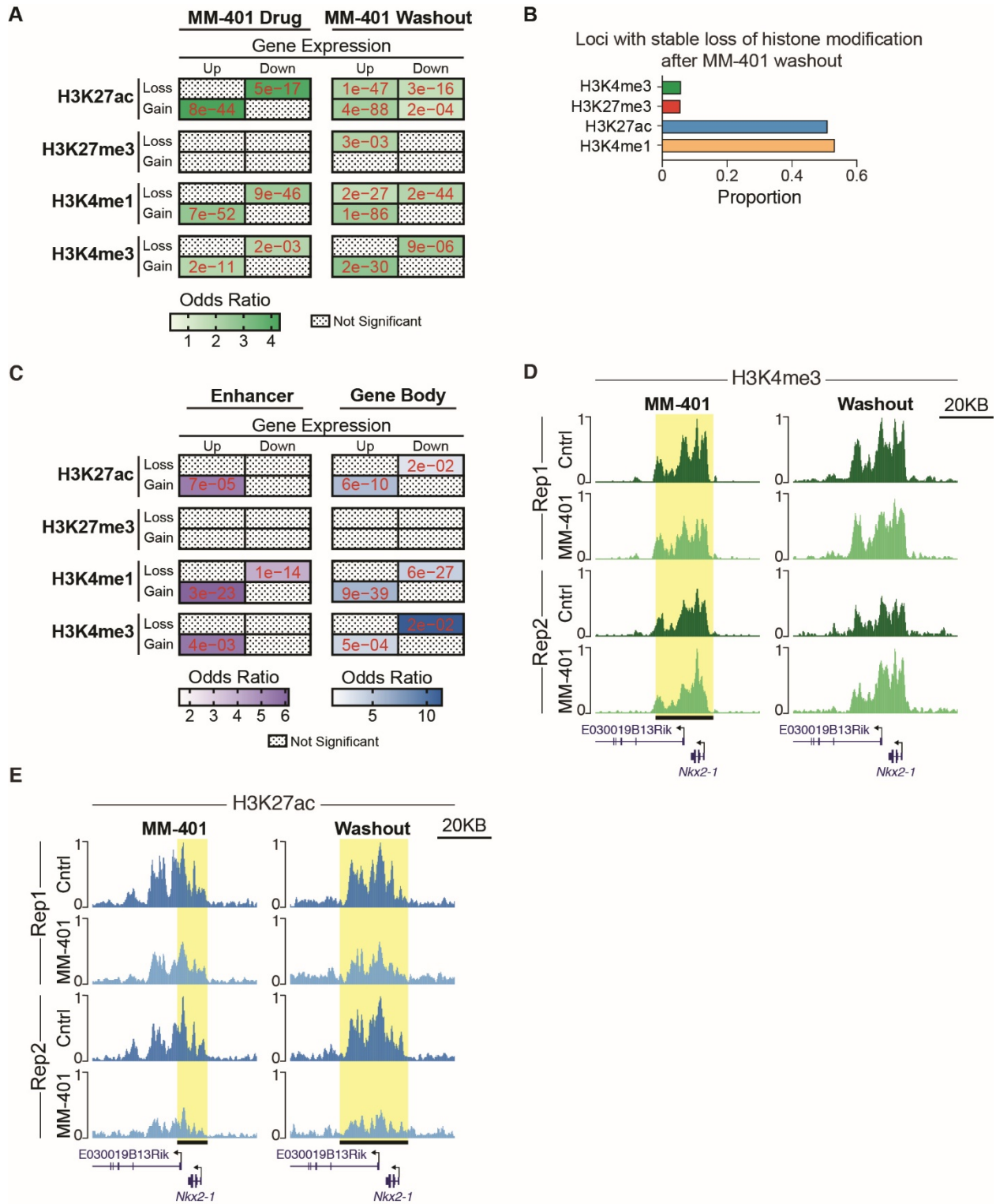


Fig. 2.10. Changes in peak enrichment relate to changes in gene expression.

(A) Heatplot depicting the association of differentially enriched chromatin loci with genes that are differentially expressed in MM-401 treatment and Washout conditions using Fisher's exact

test. Color of cell denotes odd ratio. Red text within box represents multiple hypothesis adjusted p-value (significant =  $p < 0.05$ , NS= not significant). (B) Proportion of differentially enriched loci following 10 days of MM-401 treatment that are still present following 10 days of washout. (C) Heatplots depicting the association between the putative enhancers (left) or gene bodies (right) of stably up- or down-regulated genes with stable chromatin state changes following MM-401 treatment and washout using Fisher's exact test. Color of cell denotes odd ratio from Fisher's exact test and red text within box represents multiple hypothesis adjusted p-value (adjusted p-value  $> 0.05$  are considered not significant). Concordant chromatin changes found in MM-401 treated NSCs that remain in MM-401-Washout conditions are considered "stable". Enhancer-gene pairs were obtained from the ENCODE project. (D and E) Chromatin traces for H3K4me3 (D) and H3K27ac (E) over the *Nkx2-1* locus in Control- and MM-401 treated cultures after 10 days of inhibition (left) and 10 days of inhibition followed by 10 days of washout (showing biological duplicates). Horizontal black bar with yellow highlight depicts genomic region with statistically significant differential chromatin enrichment.

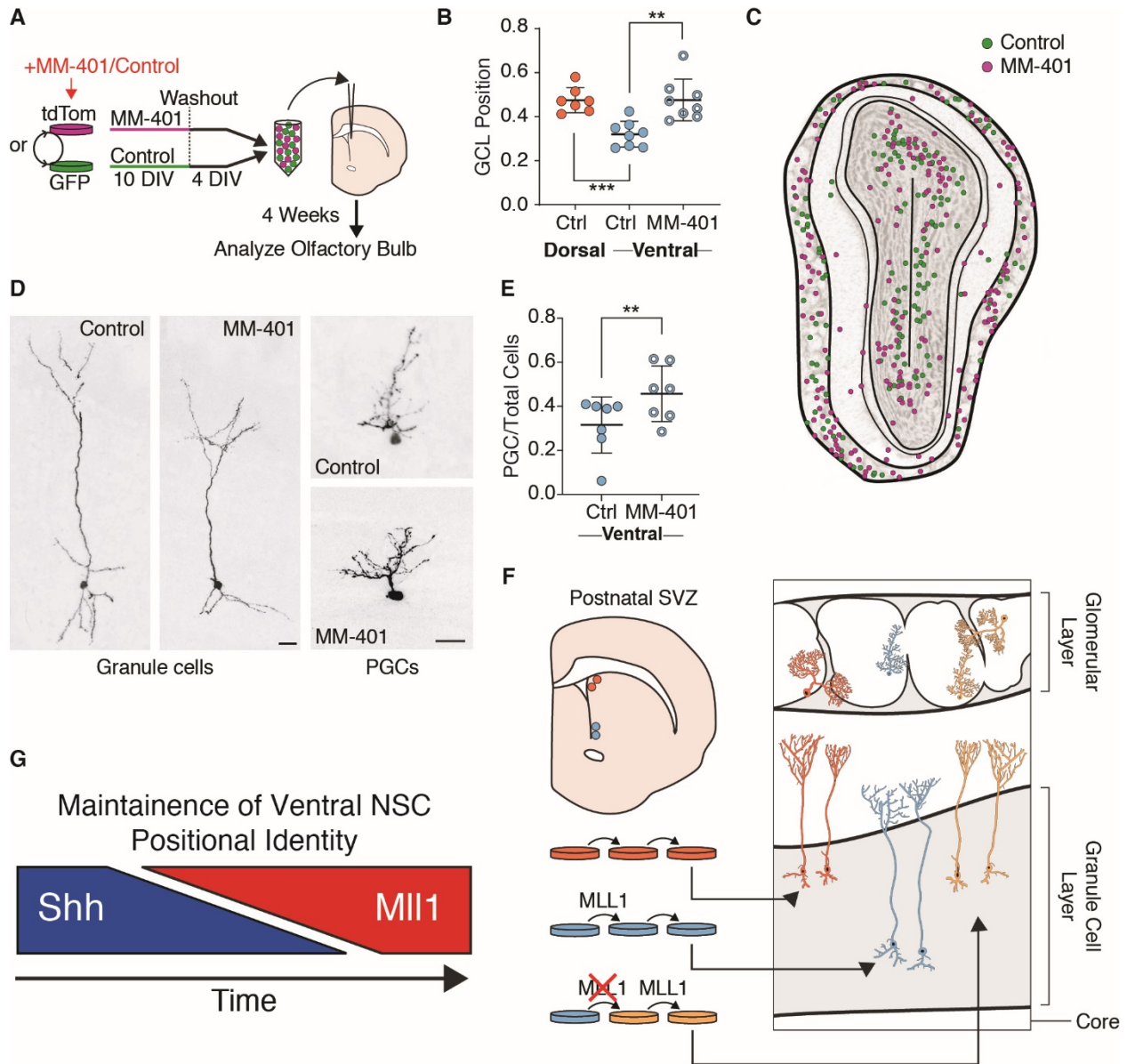


Fig. 2.11. Transient MLL1 inhibition alters NSC positional identity.

(A) Derivation and treatment of NSC cultures labeled with GFP or tdTomato for transplantation into adult V-SVZ. (B) Granule cell layer (GCL) position of transplant-derived olfactory bulb (OB) GC interneurons per animal (mean  $\pm$  SD,  $**P < 0.01$ ,  $***P < 0.001$ , two-tailed student's t test, three separate rounds of transplantation). Dorsal-derived cells, orange; ventral-derived cells, light blue; control-treated cells, solid circles; MM-401-treated cells, rings. (C) Map of ventral NSC transplant-derived neurons within OB, pooled from two animals. MM-401-treated cells (magenta) and control cells (green). (D) Representative GC and periglomerular (PGC) OB interneurons generated by transplanted ventral NSCs. Scale bars, 20  $\mu$ m. (E) Relative proportion of transplant-derived PGCs produced by control and MM-401-treated ventral NSCs

(mean  $\pm$  SD,  $**P < 0.01$ , two-tailed student's t test). (F) Schematized results of MM-401-mediated MLL1 inhibition followed by washout and transplantation. GC interneurons derived from transplanted NSCs are color coded to indicate positional identity: dorsal, orange; ventral, light blue; "dorsal-like," yellow. (G) Generalized model of the regulation of ventral NSC positional identity over the course of development, where Shh signaling is initially required but later shifts to a state of MLL1-dependence.

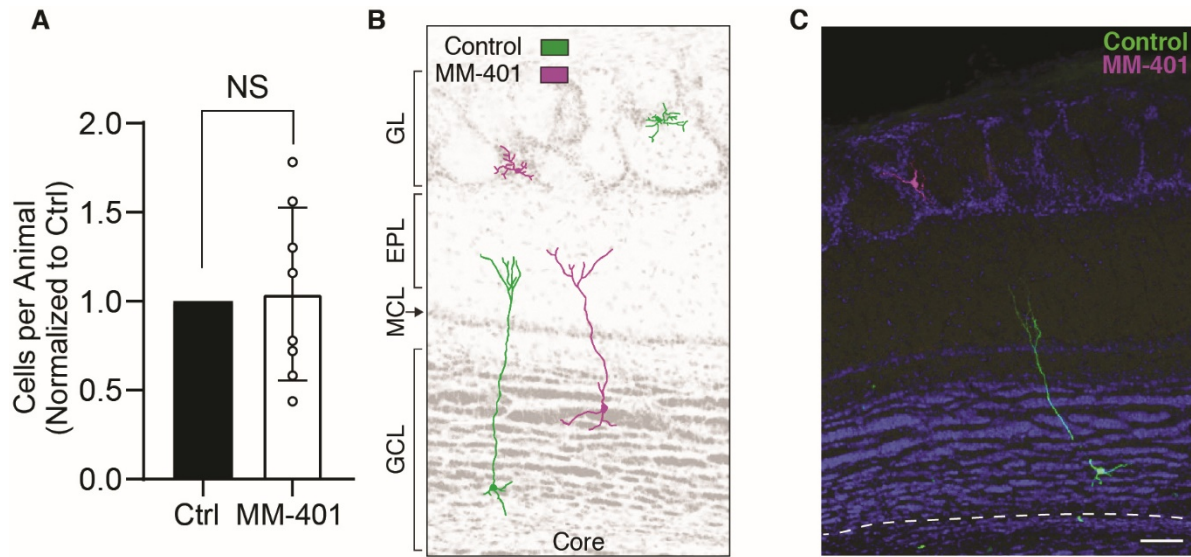


Fig. 2.12. MM-401 does not reduce transplanted cell numbers in the OB.

(A) Quantification of olfactory bulb (OB) interneurons derived from MM-401 and control-treated ventral NSC transplants (cultures established from mT/mG or UBI-GFP mice). Counts normalized within each transplanted animal to control group (mean  $\pm$  SD, two-tailed ratio paired t-test, NS= not significant). (B) Representative traces of control (green) and MM-401 (magenta) GCs and PGCs. GL, glomerular layer. EPL, external plexiform layer. MCL, mitral cell layer. GCL, granule cell layer. (C) Immunohistochemistry for tdTomato (MM-401-treated group) and GFP (control-treated group) in representative coronal OB sections from subjects that received ventral NSCs. Dotted white line demarcates the core of the OB. Scale bar, 75  $\mu$ m (C).

## **Chapter 3: Single-cell RNA-seq shows heterogeneous lineage commitment of NSCs in the V-SVZ**

### *The biological importance of stem cell diversity*

NSC heterogeneity is an important contributor to the diversity of neuron subtypes the brain requires to work properly (Arlotta & Pasca 2019). With the rapid expansion of single-cell RNA sequencing (scRNA-seq) technology, the sheer diversity of cell types in the brain has become increasingly apparent (Mu et al. 2019), but the connection of NSCs with their corresponding neuronal progeny has been harder to establish. Through transgenic expression of fluorescent markers, viral injection, and other fate-mapping experiments, it has been possible to link small subsets of NSCs with their neuronal progeny (Merkle et al. 2014, Obernier et al. 2018, Ma et al. 2018). Whether there are transcriptional links that carry through from the NSC stage through to the neuron stage is not known.

The general model in the field is that NSCs become more strongly committed to specific lineages as they advance to the intermediate progenitor stage, restricting the set of neurons and glia that they are able to produce (Desai & McConnell 2000). Yet, there is evidence that the transcriptional identity of even quiescent NSCs directly informs their progression along the lineage, and that lineage commitment may occur earlier than generally described. In the postnatal ventricular-subventricular zone (V-SVZ), a stem cell niche that lines the walls of the lateral ventricles, NSCs display striking commitment to their region-specific lineages.

### *Heterogeneity in the V-SVZ*

The V-SVZ is a domain of persistent neurogenesis in the postnatal and adult mouse, continuing to produce a broad repertoire of interneuron types for the olfactory bulb throughout the animal's life (Doetsch et al. 1999, Merkle et al. 2006, Young et al. 2007). It is home to a variety of cell types, including ependymal cells (E cells), quiescent and activated NSCs (B cells),

transit-amplifying intermediate progenitors (C cells), and young neuroblasts (A cells). The V-SVZ displays region-specific gene expression corresponding to distinct NSC domains laid out by morphogen signaling during embryogenesis (Fuentealba et al. 2015). Populations expressing regional markers in the V-SVZ are linked to different developmental fates in the olfactory bulb interneurons they produce (Fiorelli et al. 2015, Chaker et al. 2016).

The regional heterogeneity of B cells appears to be cell-intrinsic, with individual cells maintaining their identities for long periods of time. Even when removed from their original *in vivo* context, B cells produce interneurons characteristic of their original V-SVZ domain (Merkle et al. 2007, Delgado et al. 2020). However, beyond a small number of markers, little is known about what distinguishes B cells from one another. As an unbiased method of surveying gene expression in all cells of the niche, scRNA-seq holds the potential to reveal transcriptional links between B cells and their progeny.

#### *ScRNA-seq and V-SVZ lineage commitment*

While previous single-cell sequencing experiments in the SVZ have described the many broad classes of cells that reside in the niche, they have not been able to resolve regional differences among B cells in the lateral wall, nor the heterogeneity that leads to the generation of different neuronal subtypes. Transcriptional analyses after cell sorting have identified stages in the B-C-A cell lineage (Dulken et al. 2017), as well as populations of NSCs that appear to activate after injury (Llorens-Bobadilla et al. 2015). Profiling of the entire niche has highlighted differences between quiescent and activated B cells and revealed regional distinctions between the lateral and septal walls of the ventricle (Zywitzka et al. 2018, Mizrak et al. 2019), but have not found major differences between B cell populations committed to regionally distinct lineages.

By thoroughly profiling B, C, and A cells in the V-SVZ, we set out to find elements of neuronal identity that are carried all the way from nascent stem cell states through the entire lineage. Such understanding could help us predict B cell fate while revealing genes that produce



meaningful biological differences between lineage-committed B cell populations, essential to the production of neuronal diversity.

## Results

### *Generation of the whole-cell sequencing dataset*

For single-cell transcriptome analysis, we dissected the lateral wall of the lateral ventricle from hGFAP:GFP mice at postnatal day (P) 29-35 (n=8, Fig. 3.1A). To determine possible sex differences in downstream analyses, male and female samples (pooled in biological duplicate, n=4 samples) were dissociated and multiplexed by labeling each sample with MULTI-seq barcodes (McGinnis et al. 2019). Multiplexed samples were then pooled for the remainder of the single cell isolation protocol, and two technical replicates were loaded in separate wells of the Chromium Controller chip (10x Genomics) for single cell barcoding and downstream mRNA library preparation and sequencing. Cells carrying multiple barcodes or high number of mRNA reads (4,128 out of 35,025 cells, 11.7%) were considered doublets and were eliminated from our analysis, as were cells with <10% mitochondrial gene content. Technical replicates were batch-corrected using integration in Seurat v3 (Stuart et al. 2019). We then performed unbiased clustering of cell profiles. The clustering of lateral wall V-SVZ cells was not driven by sample, technical replicate, or sex (Fig. 3.1B). Cell identities were annotated based on the detection of known cell type markers. We identified 37 clusters corresponding to cell types within the V-SVZ, including B cells, C cells, A cells, parenchymal astrocytes, ependymal cells, neurons, oligodendroglia, microglia, pericytes, vascular smooth muscle cells, and endothelial cells (Fig. 3.1C).

The majority of cells analyzed were part of the neurogenic lineage, comprised of primary progenitors, intermediate progenitors, and young neurons (the B-C-A lineage). These neurogenic clusters are in the center of the UMAP plot and display a “bird-like” shape, with B cells (clusters 5, 14, 13, and 22) at the top in the head and neck, proliferating cells (clusters 8,

10, 16, and 17) including C cells (12) in the body and wing, and A cells (clusters 0, 1, 4, 6 and 15) in the tail (Fig. 3.2A and B). Consistent with previous studies, all B-cell clusters express *Gfap* and *S100a6*. We identified a subpopulation of B cells as quiescent (clusters 5, 14 and 22) based on high expression of *Thbs4*, low *Ascl1*, and no expression of *Egfr* (Fig. 3.2C). In contrast, cluster 13 (located in the neck region of the “bird”) corresponds to activated B cells with lower *Gfap* and *S100a6* expression but high *Ascl1* and *Egfr* (Codega et al. 2014) (Fig. 3.2C). Cluster 13 also expresses *Notum*, a marker recently associated with quiescent NSCs undergoing activation (Mizrak et al. 2019). Below cluster 13 is 12, identified as the C cell cluster by reduced expression of astrocytic markers *Gfap* and *GFP* and high expression of *Egfr* and *Ascl1*. The wing of the bird contains *mKi67+* and *Top2a*-expressing cells, indicating active proliferation (Fig. 3.2C). Using expression of specific cell cycle markers, we scored and classified cells into G2M, S, or G1 phase (Tirosh et al. 2016). We found that most of the cells in cluster 12 were in S phase, consistent with C cell identity (Fig. 3.2D).

A closer look at the clusters of cells in G2M phase (clusters 10, 16, 17, and 8) showed that their gene expression pattern mirrors the progression of non-dividing neurogenic lineage cells: Cluster 10 expresses markers of activated B cells, cluster 16 has markers of C cells, and cluster 8 expresses markers of A cells (Fig. 3.2E). This suggests that these clusters correspond to dividing B, C, and A cells, respectively, which have all been previously observed by electron and confocal microscopy *in vivo* (Doetsch et al. 1997). The largest contribution of cells in the neurogenic lineage came from neuroblasts and young neurons, or A cells, characterized by high *Dcx* expression in clusters 0, 1, 4, 6 and 15) (Fig. 3.2B). Clusters 6 and 15 contain *Dcx+* A cells expressing proliferative markers *mKi67* and *Top2a*, consistent with previous work showing that a subpopulation of newly generated neurons continue to divide (Menezes et al. 1995; Lois and Alvarez-Buylla 1993). The overall progression from B-C-A cells is supported by RNA-velocity lineage trajectory reconstruction (La Manno et al. 2018) (Fig. 3.2F).

Overall, our single-cell transcriptomic analysis recapitulates the known neurogenic lineage, starting from NSCs (B cells) in the head of the bird to young neurons (A cells) in the tail and transitioning through proliferative activated B cells and transit-amplifying C cells in the neck and wing. This analysis also reveals surprising heterogeneity among B, C, and A cells, explored below. Among C cells, clustering is largely driven by cell-cycle-related genes. But what else might drive heterogeneity in the neurogenic lineage of the V-SVZ? To investigate in more detail, we turned to single-nucleus RNA-seq.

#### *Generation of the single-nucleus sequencing dataset*

A prominent feature of the V-SVZ is the epithelial layer of B and ependymal cells that makes up the cerebral spinal fluid-brain barrier, making it difficult to isolate healthy single whole cells from the adult mouse brain. Incomplete dissociation may result in doublets that would confound downstream analysis, while too forceful a dissociation can kill sensitive cell types. Thus, we reasoned that isolating single nuclei for sequencing would allow us to faithfully capture the diversity of cell types in the V-SVZ. In addition to the whole-cell sequencing (wcSeq) dataset described above, we generated a single-nucleus sequencing (snSeq) dataset from 16 P30 CD1 mice (n=8 males, 8 females). To resolve regional differences, we isolated nuclei from four distinct microdissected quadrants of the V-SVZ: the anterior-dorsal (AD), posterior-dorsal (PD), anterior-ventral (AV), and posterior-ventral (PV) regions (Fig. 1D) (Mirzadeh et al. 2008; Redmond et al. 2019). All four V-SVZ regions were collected from each of the 16 mice, and all tissue from each region (e.g. AD) was pooled together prior to nucleus isolation. The four regions (AD, PD, AV, and PV samples) were then processed in parallel for single-nucleus RNA sequencing. Each region was loaded into a separate well of the same 10x Chromium Controller chip for single nucleus barcoding and downstream mRNA library preparation (Fig. 3.3A).

After quality control and filtering of doublets, the single nucleus dataset contained 45,820 cell profiles. Data from each sample were combined and integrated (Seurat v3 IntegrateData;

Stuart et al. 2019), then clustered as the wcSeq dataset above. Cell identities were annotated based on the detection of known cell type markers. We identified 42 clusters, including those corresponding to B cells, C cells, and A cells (Fig. 3.3B). We also identified a parenchymal astrocyte cluster, ependymal cells, striatal neurons, oligodendroglia, microglia, pericytes and vascular smooth muscle cells, endothelial cells, and leptomeningeal cells (Fig. 3.3B). While most single nucleus clusters include contributions from all four regions, some clusters were comprised of nuclei from only one to three regions (Fig. 3.3C). This may represent a persistent batch effect, region-specific cell type, or variability in tissue microdissection. We also compared the median numbers of UMIs and genes detected in the snSeq dataset with those in the wcSeq dataset and found that sequenced whole cells had three-fold more UMIs and 2.1-fold more genes detected per whole cell as compared to the nuclei (UMIs: 9,181wcSeq/3,062snSeq; genes: 3,549wcSeq/1,679snSeq).

A striking difference between the wcSeq and snSeq datasets are the proportions of neurogenic lineage cells compared to mature neurons. The wcSeq dataset is 60.4% B, C, and A cells (14,660/24,261 total cells), compared to 10.6% of the snSeq dataset (4,859/45,820 total nuclei). Conversely, only 1.6% of the wcSeq dataset is neurons (395 cells), compared to 61.5% of the snSeq dataset (28,185 nuclei). The wcSeq and snSeq datasets are 37.9% (9,206 cells) and 25.1% (11,480 nuclei) glial cells, respectively. The same glial subtypes are represented in both datasets. Trade-offs between cell type capture, sequencing depth, number of genes detected, and suitability for different tissue types (e.g. archival or fresh-frozen human tissue) can guide the selection of the most suitable single-cell sequencing method for a proposed experiment. Here our goal is to understand the molecular diversity of V-SVZ neurogenic lineage cells and their differential capacity to generate many types of olfactory bulb neurons. For its enrichment of neurogenic lineage cells, higher numbers of UMIs and genes detected per cell, and decreased presence of doublets as detected by MULTI-seq, we focused on the wcSeq

dataset, using information from regional microdissection of the snSeq dataset to inform our analysis.

### *B cell clusters correspond to regionally distinct domains*

B cells in our wcSeq dataset fell into three clusters: 5<sub>B</sub>, 14<sub>B</sub>, and 22<sub>B</sub> (Fig. 3.2B, 3.4A). To understand the molecular differences between these three B cell clusters, we conducted differential expression analysis to identify significantly upregulated genes in each. Upregulated genes were considered to be differentially expressed if the average log-fold change (logFC) was greater than 0.1 and the Student's t-test adjusted p-value was less than 0.05. Of all genes expressed by at least one of the three B cell clusters, 2,277 were significantly differentially expressed (Fig. 3.4B). We found that 840 genes were specifically upregulated in cluster 14<sub>B</sub>, 990 genes in cluster 22<sub>B</sub>, and 368 genes in cluster 5<sub>B</sub>. 79 genes were upregulated in more than one B cell cluster, and 20,678 genes were not significantly differentially expressed (Fig. 3.4B). To find specific marker genes for each cluster, as opposed to up-regulated genes present in multiple B cell clusters, we focused on differentially expressed genes that were present in the target cluster (e.g. 14<sub>B</sub>) but in no more than 20% of all other B cells combined (Fig. 3.4B, inset).

When we examined the top ten candidate markers for each cluster, we found that some genes correspond to known markers of dorsal and ventral B cell identity. For example, *Nkx6-2*, a transcription factor expressed in the ventral postnatal ventricular zone (Merkle et al. 2014), is enriched in cluster 14<sub>B</sub>, as are *Notum* and *Lmo1* (Fig. 3.4C). *Gsx2*, a marker of dorsal B cells, is a marker of cluster 5<sub>B</sub> (Fig. 3.4C). While none of the top 10 marker genes for 22<sub>B</sub> are known to be spatially organized in the V-SVZ, dorsal B cell markers such as *Emx1* are expressed in 22<sub>B</sub>. When we overlay the expression of these markers on the neurogenic lineage UMAP plot, we find that their expression is largely restricted to cells within a single B cell cluster, and in the case of *Gsx2*, is retained in C cells and early-stage A cells (Fig. 3.4D). Activated B cells located in cluster 13 also show the expression of these regional markers, but do not separate into

multiple clusters at this resolution (Fig. 3.2B). The clear regional signature that drives clustering in quiescent B cells appears diminished as these primary progenitors move into the activated state.

To determine if B cell clustering reflects spatial organization in the V-SVZ, we took advantage of the region-specific microdissection of the snSeq cells (Fig. 3.3A) and a recently developed technique to identify closely related groups of cells across datasets (Stuart et al. 2019). First, we subsetted quiescent B cells from both the wcSeq and snSeq datasets (5<sub>B</sub>, 14<sub>B</sub>, 22<sub>B</sub>, and snSeq cluster 7), then calculated sets of ‘anchoring’ genes that linked similar groups of whole cells and single nuclei, as determined by a nearest-neighbor graph (Stuart et al. 2019). This algorithm was developed to predict cell type identities between datasets. However, as our interest is in the potential spatial organization of B cell clusters, we instead calculated likelihood prediction scores for region (Dorsal or Ventral) for each wcSeq B cell. We found that cluster 14<sub>B</sub> had a higher average Ventral score than Dorsal score, while clusters 5<sub>B</sub> and 22<sub>B</sub> had higher Dorsal scores than Ventral scores (Fig. 3.4E). We then calculated the difference between Dorsal and Ventral scores for each wcSeq B cell. In the UMAP plot, we found that cells within each cluster were strongly Dorsal (green) or Ventral (purple), with relatively few B cells having similar Dorsal and Ventral prediction scores (gray) (Fig. 3.4F). This unsupervised, unbiased prediction of Region identity based on scSeq regional microdissection reinforces our observation that wcSeq B cells clusters have strong signatures of dorsal or ventral V-SVZ identity.

We then asked whether other differentially expressed genes in wcSeq B cell clusters were novel markers for dorsal or ventral B cells. We identified *Crystallin mu* (*Crym*) as a marker of putative ventral cluster 14<sub>B</sub>, and *Urah* (which encodes the enzyme 5-hydroxyisourate hydrolase) and *HOP homeobox* (*Hopx*) as markers of putative dorsal clusters 5<sub>B</sub> and 22<sub>B</sub> (Fig. 3.4G). To investigate if these markers defined regionally organized groups of B cells, we used RNAscope in combination with GFAP and DCX staining in P30 *hGFAP:GFP* mouse coronal

brain sections (Fig. 3.4H). *Crym* was detected in ventral and mid-V-SVZ B cells, while no expression was detected in the dorsal wedge of the V-SVZ. Interestingly, the *Crym*<sup>+</sup> domain decreased in size along the anterior-posterior axis. Consistent with our single cell data, A cells identified by DCX expression were *Crym*<sup>-</sup> in dorsal and ventral regions. Striatal neurons and astrocytes also expressed *Crym*, as previously described (Mizrak et al. 2019; Chai et al. 2017). To determine if *Crym* was regionally expressed at the protein level, we analyzed CRYM expression in *hGFAP:GFP* mice by antibody staining. Consistent with our RNAscope findings, ventral V-SVZ B cells were CRYM<sup>+</sup> while dorsal wedge B cells were negative (Fig. 3.4I). To better visualize anterior-posterior differences, we turned to whole mount preparations of the V-SVZ. Whole-mount analysis confirmed that the CRYM<sup>+</sup> domain corresponds to the ventral and mid-V-SVZ and decreases in size moving posterior (Fig. 3.4I).

#### *A cell heterogeneity is linked to regional identity*

As we observed in B cells, A cells also separated into multiple clusters, each enriched for a unique set of genes (Fig. 3.5 A). Using an approach similar to the B cell cluster analysis, we identified differentially expressed genes in each of the 5 clusters in order to characterize them. A cells were grouped in two main sets of transcriptionally-related clusters, with clusters 15<sub>A</sub> and 6<sub>A</sub> expressing genes associated with mitosis and cell cycle regulation including *Top2a* and *Mcm2* (Fig. 3.5B). Clusters 1<sub>A</sub>, 0<sub>A</sub>, and 4<sub>A</sub> were enriched in genes involved in cell migration and neuronal differentiation, such as *Dab1* and *Foxp2*. To investigate the identities of A cell clusters, we created gene sets based on gene ontology (GO) annotation, then scored cells for expression of genes in each set using AUCell (Aibar et al. 2017). In agreement with our identification of 15<sub>A</sub> and 6<sub>A</sub> as dividing, immature A cells, mitotic DNA Replication (GO:1902969) and mitosis DNA replication initiation (GO:1902975) are highly upregulated in clusters 15<sub>A</sub> and 6<sub>A</sub> (Fig. 3.5C). These clusters are also enriched in cells in S and G1M phases (Fig. 3.2D). Two of the overrepresented GO categories in clusters 1<sub>A</sub> and 0<sub>A</sub> were related to regional specification of

the brain: dorsoventral axonal guidance (GO:0033563) and cerebral cortex regionalization (GO:0021796) (Fig.3.5C). We decided to investigate which genes contribute to enrichment in these GO categories and found *Slit2* and *Pax6* highly expressed in clusters 1<sub>A</sub> and 0<sub>A</sub>, respectively. Recent findings suggest that the V-SVZ's dorsoventral axis can be identified by *Vax1* and *Pax6* expression (Coré et al. 2020). In our dataset, *Vax1* and *Pax6* were highly enriched in clusters 1<sub>A</sub> and 0<sub>A</sub>, respectively, consistent with the hypothesis that these clusters correspond to ventral and dorsal A cells (Fig. 3.5D).

When new neurons are born in the V-SVZ, they migrate dorsally and anteriorly via chain migration to join the RMS leading to the olfactory bulb (Alvarez-Buylla & García-Verdugo 2002). Based on this migration pattern, we can predict what types of A cells we will detect in regional dissections of the V-SVZ. A cells born in the dorsal V-SVZ primarily migrate anteriorly, so are unlikely to be found in the PV region. Cells born in the ventral V-SVZ are likely to be detected in both ventral and dorsal regions of the V-SVZ, as they migrate through dorsal-anterior domains. To test these predictions, we calculated sets of anchor genes between wcSeq and snSeq A cells (wcSeq clusters 0<sub>A</sub>, 1<sub>A</sub>, 4<sub>A</sub>, 6<sub>A</sub>, and 15<sub>A</sub>, snSeq clusters 12 and 29) and scored each wcSeq A cell for either Dorsal or Ventral predicted identity based on the cell's similarity to dorsally or ventrally dissected A cell nuclei. As with B cell predictions above, we then calculated and plotted the difference in Dorsal and Ventral prediction scores on a UMAP plot of wcSeq A cells (Fig. 3.5E). Dorsal-scoring cells are highly enriched in wcSeq cluster 0<sub>A</sub>, which contains relatively few highly Ventral-scoring cells. Cluster 1<sub>A</sub> contains both Ventral-scoring cells and Dorsal-scoring cells, suggesting that our dissection of the dorsal V-SVZ included both dorsal-born and ventral-born A cells migrating dorsal-anteriorly toward the RMS. Dividing immature neuroblast clusters 6<sub>A</sub> and 15<sub>A</sub> largely correspond to ventrally dissected A cells in the snSeq dataset, in line with the idea that A cells from the dorsal dissection are more mature and are entering the RMS. Overall, these findings support the conclusion that cluster 0<sub>A</sub> represents dorsally derived A cells, while cluster 1<sub>A</sub> represents ventrally derived A cells.



### *Specific markers define dorsal/ventral neurogenic lineages*

Regional specification is a main driver for gene expression heterogeneity in both B and A cells. Interestingly, expression of some of these domain-specific genes seem to be preserved along the neurogenic lineage (e.g., *Pax6*, *Slit2*). In order to determine if the dorsal and ventral domains have a specific signature that persists throughout the neurogenic lineage, we looked for ventral and dorsal markers that were present in both B and A cells. We determined differentially expressed genes between ventral cluster 14<sub>B</sub> and dorsal clusters 5<sub>B</sub>/22<sub>B</sub>, then overlapped region-specific markers with corresponding markers defining ventral cluster 1<sub>A</sub> compared to dorsal cluster 0<sub>A</sub> (Fig. 3.6A).

In total, we identified a set of 4 genes expressed throughout the dorsal lineage (*Rlbp1*, *Gm29260*, *Pax6*, and *Dcc*) and 5 genes expressed throughout the ventral lineage (*Adgrl3*, *Slit2*, *Ptprn2*, *Rbms1*, *Sntb1*, Fig. 3.6B). RNAscope confirmed that the putative dorsal lineage genes are highly enriched in the dorsal region of the ventricular-subventricular zone, with *Rlbp1* and *Pax6* being particularly enriched in the wedge region of the V-SVZ. Conversely, the putative ventral markers *Adgrl3* and *Slit2* had a higher expression in the ventral domain of the V-SVZ (Fig. 3.6C).

To understand what makes the dorsal and ventral lineages different from one another, we searched for more genes that followed patterns of region-specific expression throughout the neurogenic lineage. To do so, we used the dorsal and ventral gene sets we identified to rank cells for enrichment of a dorsal or ventral signature by AUCCell (Aibar et al. 2017). Based on their AUC score, cells were classified as dorsal or ventral (Fig. 3.6D), providing a tool to compare differences in gene expression between the entire putative dorsal and ventral neurogenic lineages. Differential expression analysis revealed 89 differentially expressed genes between the dorsal and ventral neurogenic lineage, 48 dorsal markers and 41 ventral markers (Fig. 3.6E). We then conducted GO analysis on markers of the dorsal and ventral lineages. Ventral

genes were enriched for terms associated with neurite outgrowth and neural development including regulation of neuron migration (GO:2001222), receptor localization to synapse (GO:0097120), and axon guidance (GO:0007411). In contrast, dorsal markers were enriched for neuronal and glial development (cerebral cortex development, GO:0021987; glial cell differentiation, GO:0010001) as well as terms associated with copper, zinc, and cadmium ion response and metabolism (GO:0071280, GO:0006882, GO:0071276), likely due to the regional expression of metallothioneins and ion transporters (Fig. 3.6F).

## Discussion

Together, our wcSeq and snSeq datasets provide a wealth of information about the diverse cells that populate the V-SVZ. Focusing on the neurogenic lineage, we successfully uncovered differences in B cell identity driven by regional patterns of gene expression, which previous single-cell analyses in the V-SVZ had not been able to resolve. We also found region-associated gene expression programs contributing to A cell identity and a subset of dorsal- and ventral-specific genes expressed through the entire putative dorsal and ventral neurogenic lineages. Using these persistent regional genes, we were able to identify a broader set of expression differences between the dorsal and ventral V-SVZ lineages, which has yielded some insight into what biological pathways or functions might distinguish them from one another.

Looking at GO analyses and annotations of individual markers, many ventral markers associate with axon guidance and neurite outgrowth. In contrast, dorsal markers are enriched for genes associated with gliogenic and cortical identity and, surprisingly, markers of ion metabolism, detoxification, and response. Metallothioneins are proteins that transport and detoxify metals and are expressed in the CNS, but their exact function is still not known. The *Mt* gene family may be neuroprotective, helping cells manage oxidative stress (West et al. 2008), but why we find them specifically enriched in the dorsal V-SVZ lineage is a topic for future investigation. In addition, we identified a handful of region-specific non-coding RNAs expressed

throughout the neurogenic lineage (Fig. 3.6E). The expression of long non-coding RNAs (lncRNAs) has been associated with active enhancers, recruitment of chromatin modifiers, and other gene-regulatory programs that could contribute to epigenetic maintenance of identity (Ntini & Marsico 2019).

In summary, we present the first large-scale single cell description of regional identity in the lateral wall of the V-SVZ. Not only do we recapitulate known divisions between dorsal and ventral B cells, but we identify novel regional B cell markers and uncover a regional gene expression program that remains active across transitions from B to C to A cells. These data form a strong basis for future investigation of NSC identity and lineage commitment, providing clues to help us understand how positional information is maintained in the V-SVZ.

## **Materials and Methods**

### *Mice*

Mice were housed on a 12h day-night cycle with free access to water and food in a specific pathogen-free facility in social cages (up to 5 mice/cage) and treated according to the guidelines from the UCSF. Institutional Animal Care and Use Committee (IACUC) and NIH. All mice used in this study were healthy and immuno-competent, and did not undergo previous procedures unrelated to the experiment. CD1-elite mice (Charles River Laboratories) and hGFAP::GFP (FVB/N-Tg(GFAPGFP)14Mes/J, The Jackson Laboratory (003257) (Zhuo et al. 1997) lines were used.

### *Single Whole Cell Sample Preparation and Multiplexing*

Mice received intraperitoneal administration of 2.5% Avertin followed by decapitation. Brains were extracted and 1 mm slices were obtained with an adult mouse brain slicer (Steel Brain Matrix - Coronal 0.5mm, Alto). Four samples were processed: G1:2 males P35, G2:2 males P35, G3: 2 females P29 and G4: 2 females P29. The lateral ventricle walls were

microdissected in L-15 medium and the tissue was transferred to Papain-EBSS (LK003150, Worthington). Tissue was digested during 30 mins at 37°C in the thermomixer at 900 RPM and mechanical dissociation was performed during 5 min. Incubation with DNAase/ovomucoid inhibitor. Cells were incubated in Red blood cell lysis buffer (420301, Biolegend) 3-4 min 4°C.

For Multi-seq barcoding, cells were suspended with 10x Anchor:Barcode (every sample labeled with a unique barcode) for 5 minutes at 4°C. A Co-Anchor solution was added and incubated for 5 minutes (McGinnis et al. 2019). Samples were combined and filtered with a FlowMi 40um filter (BAH136800040-50EA, Sigma). To remove myelin the cell suspension was incubated with Myelin Removal Beads (130-096-733, Miltenyi Biotec) (6µl/brain) 15 mins at 2-8°C. Cells were washed with 0.5% BSA-PBS and transferred to MACS columns (30-042-401 and QuadroMACS Separator 130-090-976, Miltenyi Biotec). The effluent was collected and cell density was counted. GFP expression of isolated cells was observed under light microscope.

#### *Whole Cell Sequencing Data Alignment & Processing*

We pooled the cDNA from each 10x Genomics Single Cell Controller well (technical replicates) and sequenced it on one lane of a NovaSeq 6000. Reads were aligned using Cell Ranger 3.0.2-v3.2.0 (10x Genomics) to a custom mouse reference genome that included the GFP gene (Supplementary table/file). We classified cells into sample groups and identified doublets using MULTI-seq barcode abundances (McGinnis et al. 2019). We used Seurat Integration (Seurat 3) Canonical correlation analysis (CCA) to reduce data dimensionality and capture the most correlated data features to align the data batches (Stuart et al. 2019).

#### *Single Nucleus Sample Preparation*

Brains were extracted and 1mm slices were obtained. We microdissected the anterior ventral, anterior-dorsal, posterior-ventral and dorsal V-SVZ regions of 16 P30 CD1 mice. We

processed tissue samples for nucleus isolation and snRNA-seq using the 10x Genomics droplet-based platform RNA library preparation & sequencing

We microdissected four regions of the lateral walls of the lateral ventricles. We extracted whole brains from sixteen one month old, male and female wildtype CD1 mice. We used a brain matrix to cut 1 mm thick coronal slabs of the mouse forebrain and used histological landmarks to identify each sampling area (e.g. anterior region landmarks: septum; posterior regions: hippocampus). Regions were dissected under a microscope to reduce the amount of underlying striatum in each sample. Each microdissected V-SVZ region was processed in parallel as a distinct sample. We generated a single nucleus suspension using a tissue douncer in nucleus isolation medium. Debris was removed via ultracentrifugation on a 1.8M sucrose cushion. We loaded approximately 12,000 nuclei from each sample into its own well of a 10x Genomics Chromium Single Cell Controller microfluidics instrument. Nuclei were sorted into droplets with one barcoded bead. We used the 10x Genomics Chromium Single Cell 3' Library & Gel Bead Kit v2 to generate cDNA libraries for sequencing. We measured cDNA library fragment size and concentration with a Bioanalyzer (Agilent Genomics).

#### *Single Nucleus Sequencing Data Alignment & Processing*

We pooled the cDNA from each single nucleus sample and sequenced it on one lane of an Illumina HiSeq4000. Reads were aligned using CellRanger 2.1.0-2.3.0 (AV, AD, PD samples); 3.0.2-v3.2.0 (PV sample) (10x Genomics) to a custom mouse reference genome that includes unspliced mRNA, which we expect to be present in cell nuclei.

#### *Single Cell Sequencing Data Normalization and Dimensionality Reduction*

We used Seurat 3 (Stuart et al. 2019) to analyze both the Whole Cell and Single Nucleus datasets: The data were normalized using regularized negative binomial regression (SCTransform package, Hafemeister et al. 2019). We calculated 100 principal components

(PCs) per dataset, and used 50 (whole cell) or 100 (single nuclei) to calculate cell cluster identities at five distinct resolutions (0.5, 0.8, 1.0, 1.5 and 2.0) and UMAP coordinates. The cell cluster identities presented in this manuscript correspond to resolution 1.5 (whole cell metadata column `integrated_snn_res.1.5`) or 2 (single nucleus metadata column `integrated_snn_res.2`), and were chosen based on visual correspondence with the expression of known neurogenic lineage markers.

### *Dual Fluorescent in situ Hybridization-Immunofluorescence*

Mouse brains were serially sectioned using a Leica cryostat (10  $\mu$ m-thick sections in Superfrost Plus slides). Sections were incubated 10 min with 4% PFA and washed 3x10 min with phosphate-buffered saline (PBS) to remove OCT. Slides were incubated with ACD hydrogen peroxide for 10 min, treated in 1x target retrieval buffer (ACD) for 5 min (at 96–100 °C) and rinsed in water and 100% ethanol. Samples were air dried at 60°C during 15 min and kept at room temperature overnight. The day after, samples were treated with Protease Plus for 30 min at 40 °C in the RNAscope oven. Hybridization of probes and amplification solutions was performed according to the manufacturer's instructions. Amplification and detection steps were performed using the RNAscope 2.5 HD Red Detection Kit reagents (ACD, 320497) for single-plex probes. RNAscope probes used: Mm-Lphn3 (317481), Mm-Rlbp1 (468161), Mm-Crym (466131), Mm-Pax6 (412821). DapB mRNA probe (310043) was used as negative and Mm-PPIB (313911) as positive controls.

RNAscope assay was directly followed by antibody staining for chicken anti-GFAP (Abcam) and rabbit anti-DCX (Cell signaling). Samples were blocked with TNB solution (0.1 M Tris-HCl, pH 7.5, 0.15 M NaCl, 0.5% PerkinElmer TSA blocking reagent) 30 min and incubated in primary antibodies overnight. Samples were washed with PBS-Tx0.1% and incubated with secondary antibodies Donkey anti-Chicken Alexa 647 and Donkey anti-Rabbit biotinylated in TNB buffer for 1.5 hrs. Samples were washed and incubated with Streptavidin HRP (1:200 in

TNB solution) for 30 min. Washed 3x5 min and incubated with Fluorescein Tyramide 5 min (1:50 in amplification diluent) rinsed and incubated with DAPI 10 min. media.

### *Immunohistochemistry*

Coronal Sections and whole mounts were incubated with Immunosaver (1:200; EMS, Fort Washington, PA) 20 min 60°C and 15 min RT and blocking solution (10% donkey serum and 0.2% Triton X-100 in 0.1 M PBS) 1hr. followed by overnight incubation at 4°C with the primary antibodies: mouse anti-Crym, rabbit anti-Bcatenin, Chicken anti-GFP. On the next day, sections were rinsed and incubated with Alexa Fluor secondary antibodies.

### *Differential Gene Expression Analysis*

We used Seurat 3 functions FindMarkers (two groups) or FindAllMarkers (more than two groups) to identify differentially expressed genes among groups of single cells. For both functions, default parameters were used with the following exceptions: min.FC = 0.1, test.use = "t" (Student's T-test), and only.pos = T (FindAllMarkers only). Selection of genes from the resulting lists for further analysis are described in the text.

### *Data & Code Availability*

Web-based, interactive versions of the datasets are available from the University of California Santa Cruz Cell Browser (<https://cells.ucsc.edu>):

Single Whole Cell Sequencing dataset: <https://cells-test.gi.ucsc.edu/?ds=svzneurogeniclineage>

## Figures

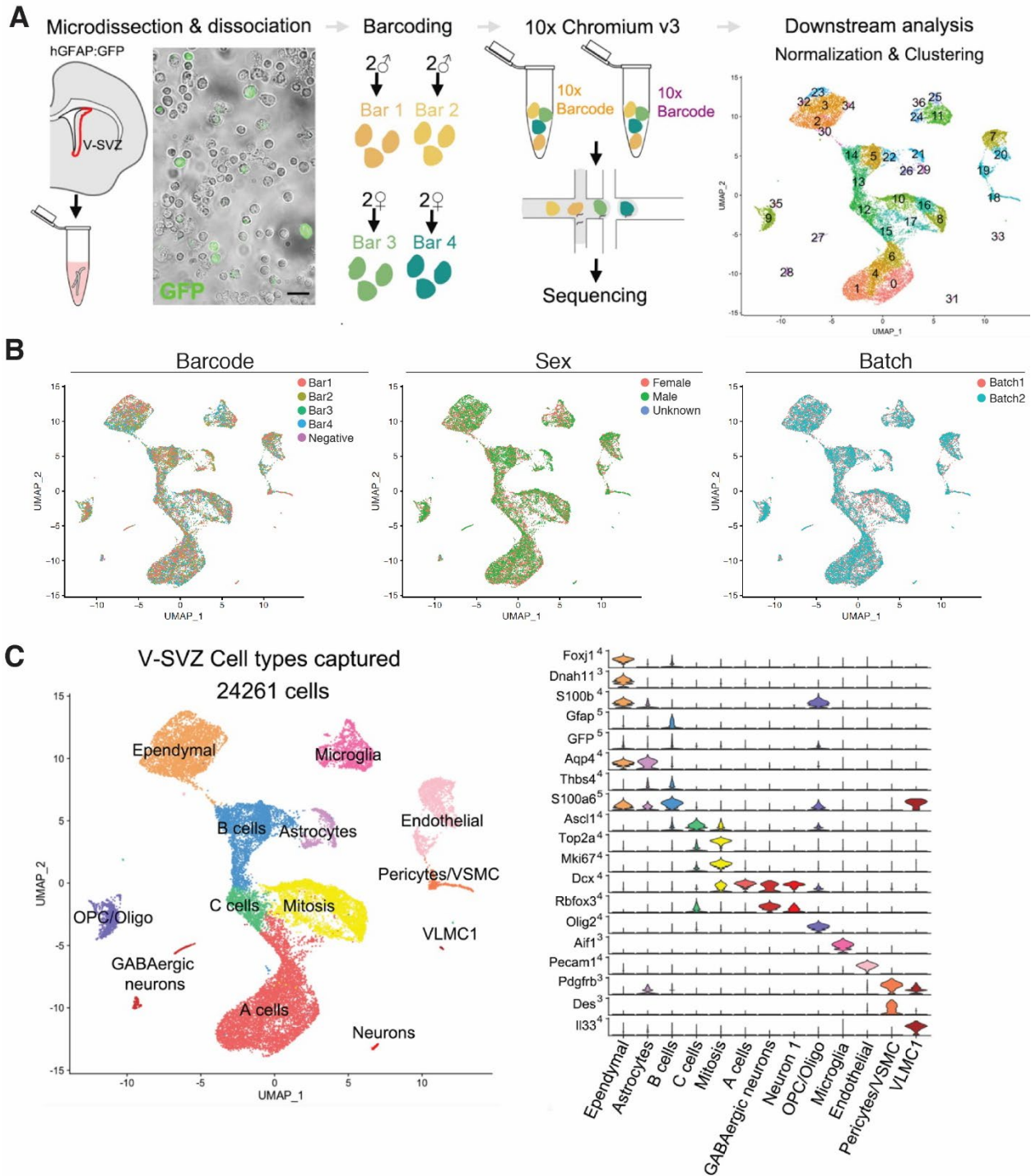


Fig. 3.1. Single-cell analysis of the V-SVZ recapitulates the cellular diversity of the region. (A) Schematic outlining the single-cell RNA-seq workflow. After dissection and debris removal, cells were checked for GFP expression, then barcoded with MULTI-seq barcodes. Samples



were combined into two wells of the 10X Chromium chip for library preparation and sequencing. (B) UMAP plots visualizing the distribution of MULTI-seq barcodes (left), sex (center), and well (right). (C) UMAP plot (left) with cell types color-coded and labeled based on marker expression, shown in the volcano plots on the right. Cell types identified include ependymal (E) cells, B cells, C cells, A cells, astrocytes, microglia, endothelial cells, pericytes and vascular smooth muscle cells (VSMC), vascular leptomeningeal cells (VLMC1), oligodendrocyte precursor cells (OPC) and oligodendrocytes, and multiple types of neurons.

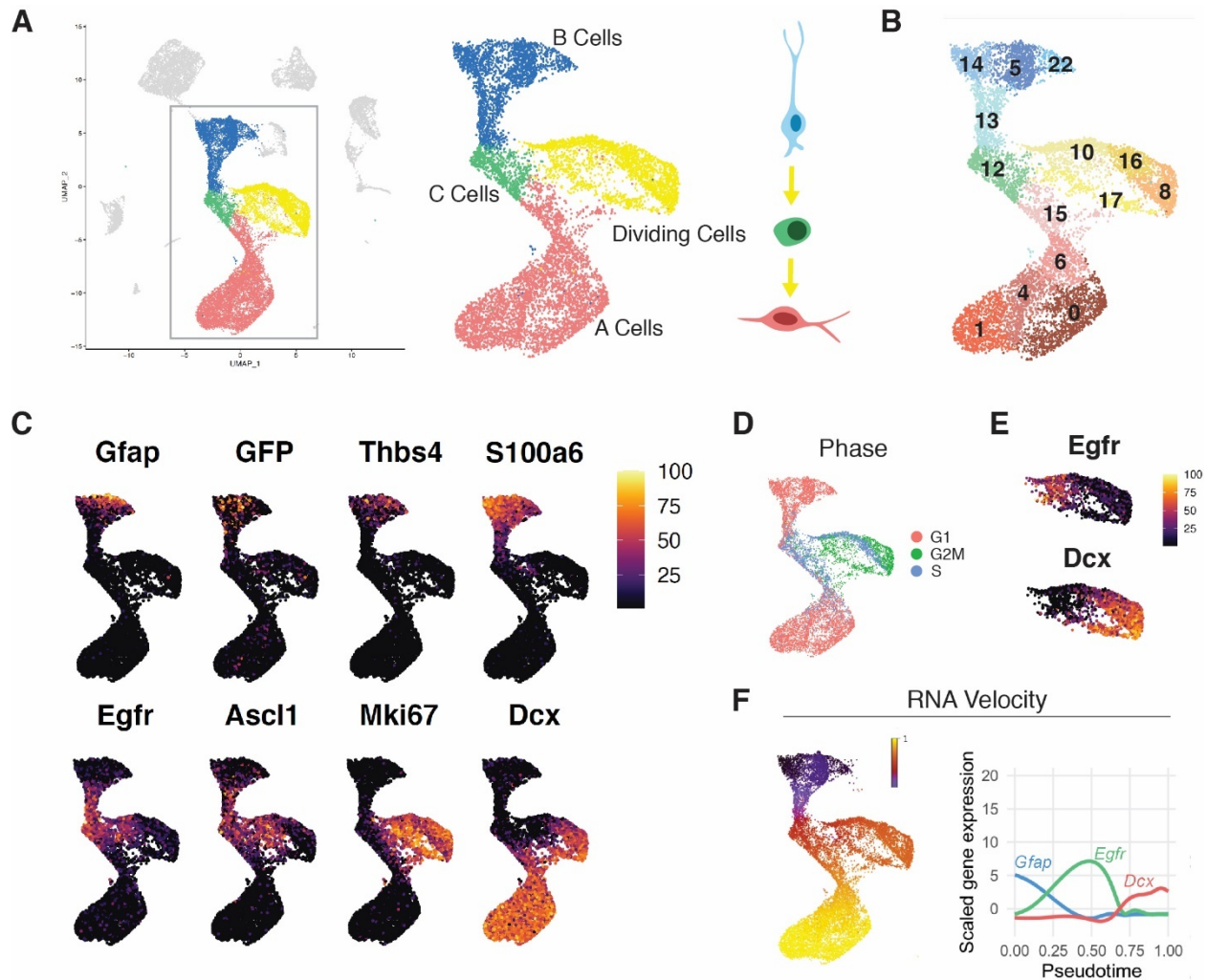


Fig. 3.2. Single-cell sequencing captures all stages of the neurogenic lineage.

(A) The neurogenic lineage has a “bird-like” shape, with B cells forming the head (blue), C cells in the body (green), dividing cells in the wing (yellow), and A cells in the tail (red). The lineage follows the trajectory of B cells to C cells to A cells (right). (B) The neurogenic lineage is made up of 14 clusters, including 4 B cell clusters, 1 C cell cluster, 4 clusters of dividing cells, and 5 A cell clusters. (C) Gene expression captures progression along the lineage, with canonical markers of each stage expressed in its corresponding region of the UMAP plot. (D) Scoring cells by phase of the cell cycle reveals cells in G2M and S phase occupying the wing of the bird. (E) Different compartments of mitotic cells express genes characteristic of activated B cells or neuroblasts. (F) Pseudotime calculated by RNA velocity recapitulates the B to C to A trajectory along the neurogenic lineage (left). Genes associated with B cells, activated B and C cells, and A cells peak in expression at corresponding stages in the lineage.

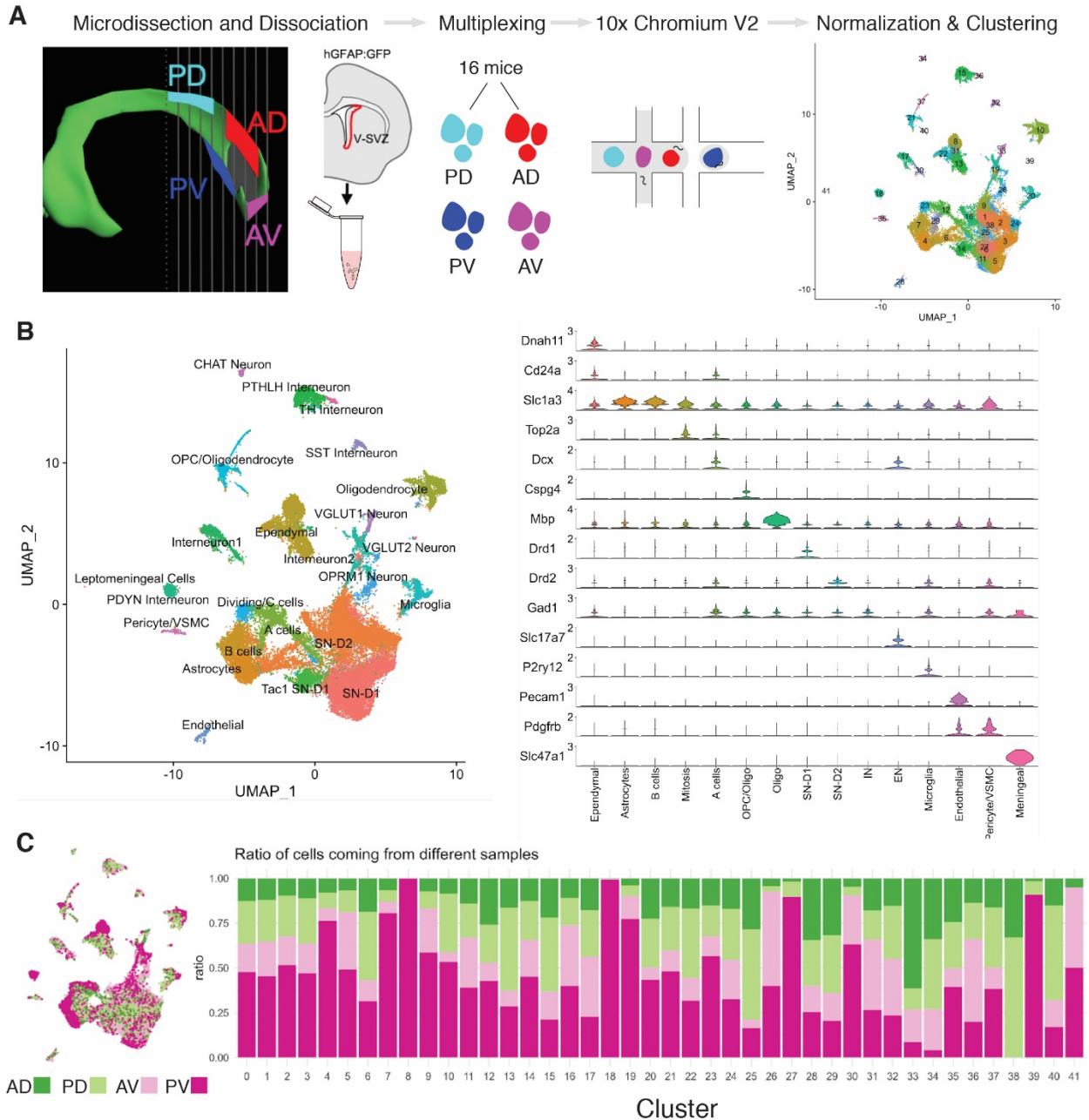


Fig. 3.3. Single-nucleus sequencing identifies cell types of the V-SVZ.

(A) Schematic illustrating microdissection of cells from posterior-dorsal (PD), anterior-dorsal (AD), posterior-ventral (PV), and anterior-ventral (AV) regions of the V-SVZ (left), followed by sample preparation for single-nucleus RNA-sequencing. (B) UMAP plot (left) with cell types color-coded and labeled based on marker expression, shown in volcano plots on the right. Cell types identified include ependymal (E) cells, B cells, C cells, A cells, astrocytes, microglia, endothelial cells, pericytes and vascular smooth muscle cells (VSMC), leptomeningeal cells, and oligodendrocyte precursor cells (OPC) and oligodendrocytes. We also identified several neuronal subtypes, including parathyroid hormone-like peptide (PTHLH) interneurons, cholinergic (CHAT) neurons, somatostatin (SST) interneurons, tyrosine hydroxylase (TH)

interneurons, 3 large populations of dopaminergic striatal neurons (Tac1 SN-D1, SN-D1, SN-D2), 2 groups of glutamatergic neurons (VGLUT1 & VGLUT2), and two miscellaneous interneuron clusters. (C) UMAP plot visualizing the contribution to each cluster by each microdissected region, with nuclei color-coded by region of origin (left), accompanied by a bar plot illustrating the relative contribution of each region to each cluster of the snSeq dataset (right).

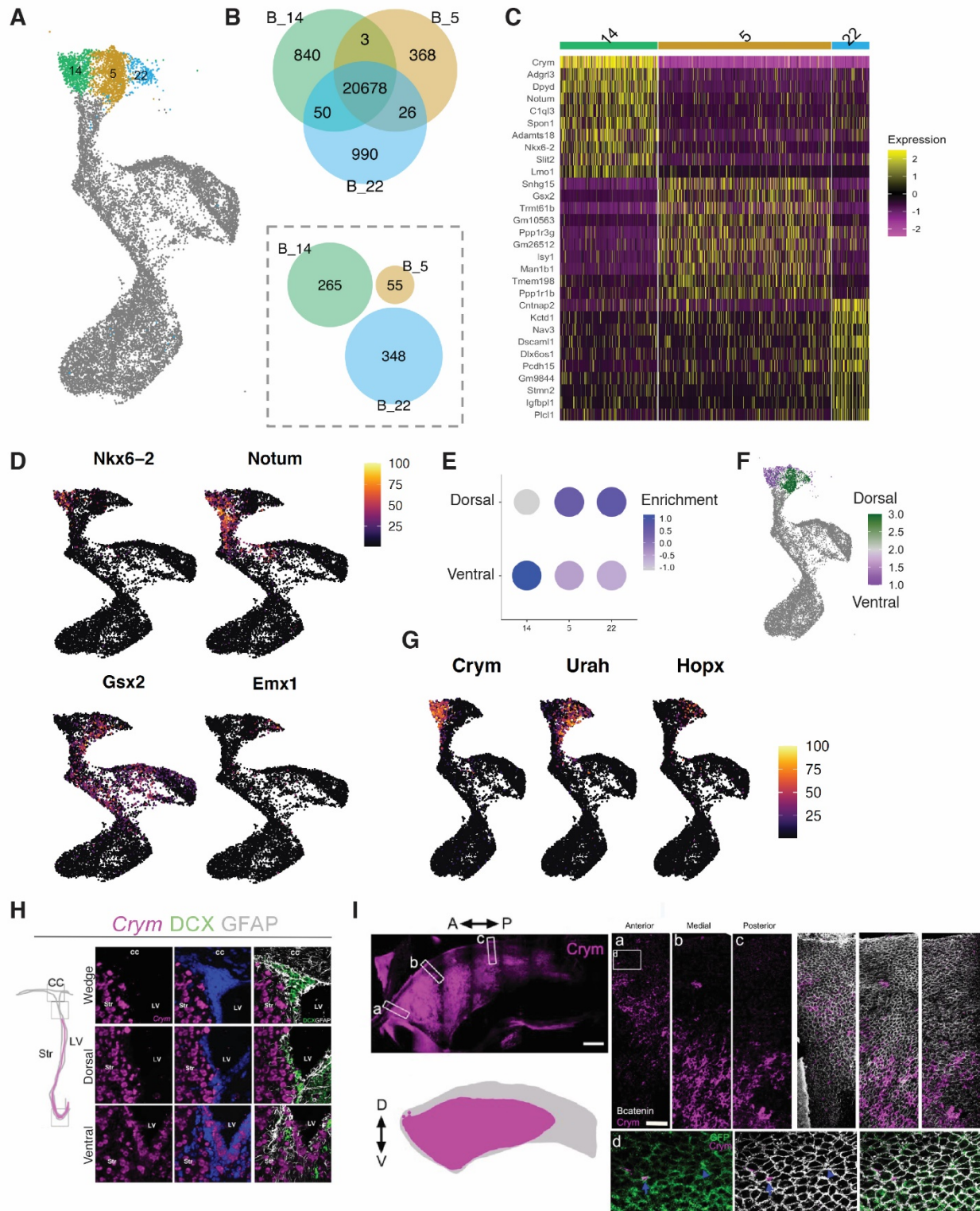


Fig. 3.4. B cell clustering is driven by regional identity.

(A) B cells fall into 3 clusters, 14<sub>B</sub>, 5<sub>B</sub>, and 22<sub>B</sub>. (B) The venn diagram depicts overlap between significantly enriched genes within and between the B cell clusters and reveal very little overlap between 14<sub>B</sub> and 5<sub>B</sub> (top). Fewer genes were present uniquely in one cluster and in no more

than 20% of all other B cells combined (bottom). (C) Heatmap depicting expression of the top 10 differentially expressed genes in each cluster. (D) Canonical markers of regional V-SVZ identity are enriched in each of the B cell clusters. (E) Clusters 5<sub>B</sub> and 22<sub>B</sub> are enriched for the dorsal signature generated by label transfer from the dorsally dissected B cells in the snSeq dataset, and cluster 14<sub>B</sub> is enriched for the signature generated from ventral B cells. (F) UMAP plot displaying dorsal (green) and ventral (purple) signatures generated from regional dissection. (G) UMAP plots showing expression of novel markers of ventral and dorsal B cell identity. (H) RNAscope and accompanying schematic of the V-SVZ showing expression of newly identified ventral marker *Crym*, with *Crym* RNA in magenta, DCX antibody stain in green, and GFAP antibody stain in white. LV: lateral ventricle, CC: corpus callosum, Str: striatum. (I) Immunostaining of a whole-mount preparation of the lateral wall of the V-SVZ, co-stained with  $\beta$ -catenin (white) and GFP (green). Bottom left schematic depicts the extent of the CRYM+ domain. A: anterior, P: posterior, D: dorsal, V: ventral.

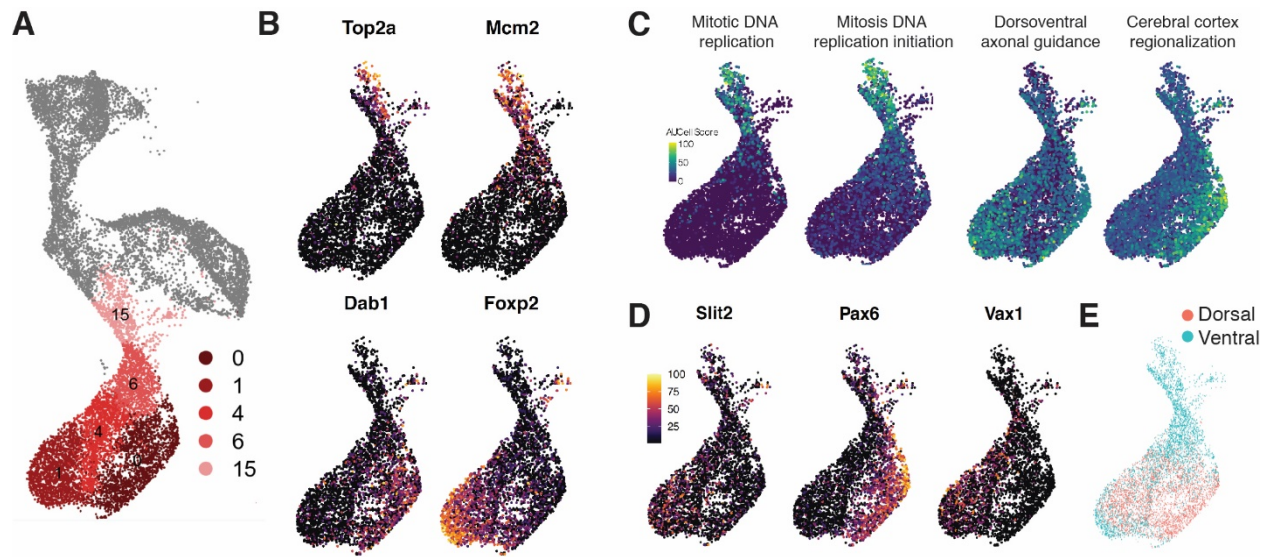


Fig. 3.5. A cells display signatures corresponding with their region of origin. (A) A cells fall into 5 clusters, 15<sub>A</sub>, 6<sub>A</sub>, 4<sub>A</sub>, 1<sub>A</sub>, and 0<sub>A</sub>. (B) Plot showing markers of cell division in clusters 15<sub>A</sub> and 6<sub>A</sub> (top) and markers of neuronal development and differentiation in clusters 0<sub>A</sub>, 1<sub>A</sub>, and 4<sub>A</sub> (bottom). (C) Gene ontology (GO) enrichment scores calculated using AUCell are mapped onto the UMAP plot of A cells. The two left plots confirm the enrichment of cell-cycle-associated genes in 15<sub>A</sub> and 6<sub>A</sub>. Regionalization-associated GO terms are enriched in clusters 0<sub>A</sub> and 1<sub>A</sub> (right). (D) Regionally expressed A cell genes are differentially enriched in clusters 1<sub>A</sub> and 0<sub>A</sub>, with 1<sub>A</sub> displaying ventral markers and 0<sub>A</sub> displaying dorsal markers (E) UMAP plot of A cells categorized by dorsal (red) and ventral (blue) signatures generated from regionally dissected A cells in the snSeq dataset. Cluster 0<sub>A</sub> is enriched for the dorsal signature and cluster 1<sub>A</sub> is enriched for A cell signatures from both ventral and dorsal dissections.

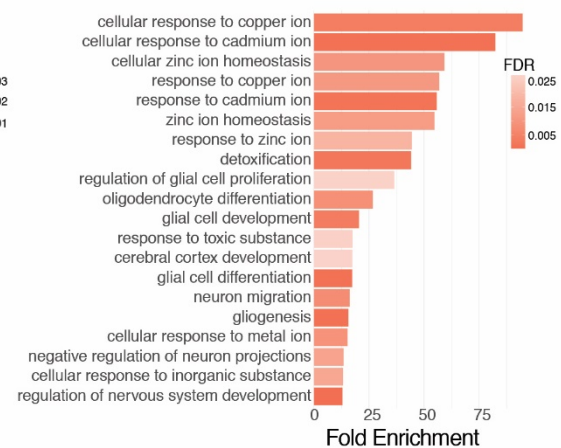
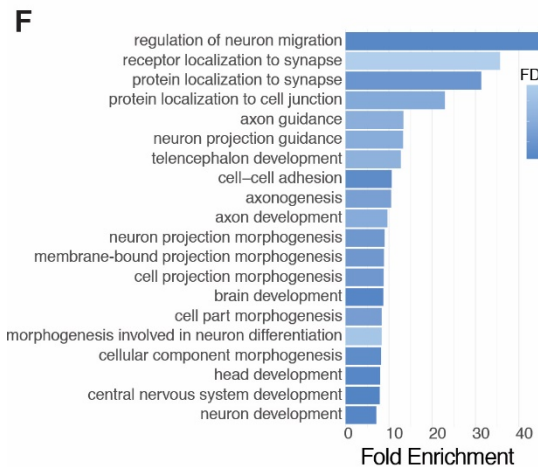
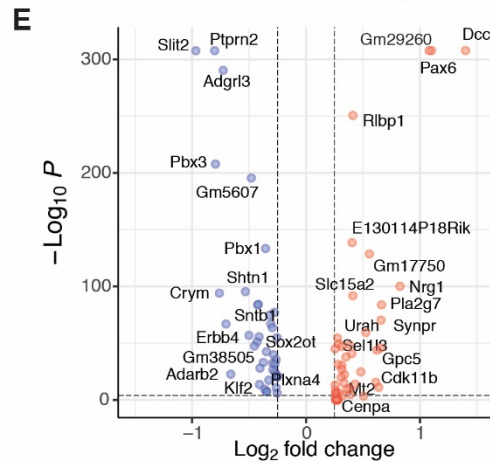
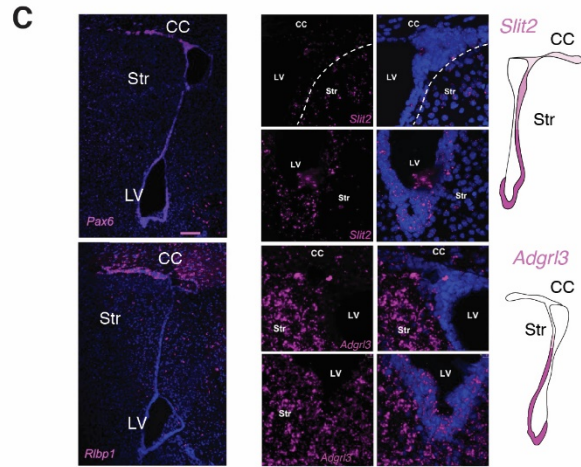
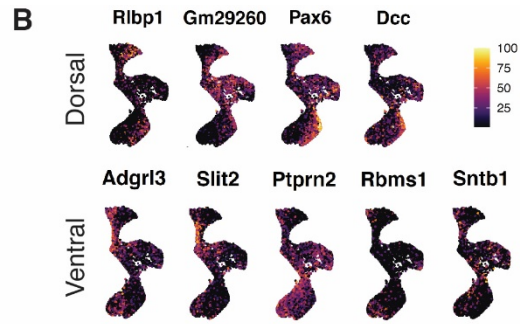
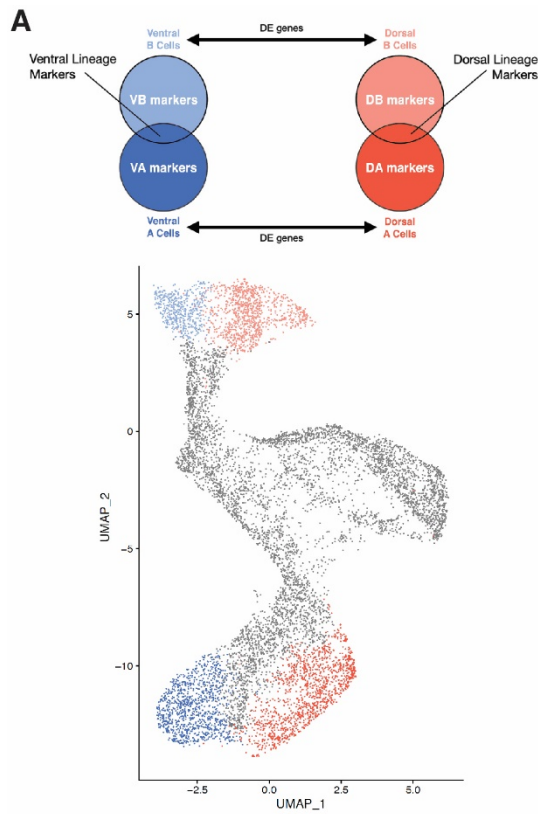




Fig. 3.6. Reconstructing the entire dorsal and ventral B-C-A lineage.

(A) Schematic illustrating our approach to identify genes that are differentially enriched in dorsal B and A and ventral B and A cells (top), with a UMAP plot depicting the clusters being compared ( $14_B$  to  $1_A$ ,  $5_B/22_B$  to  $0_A$ ) below. (B) Expression patterns of dorsal (top) and ventral markers identified as active throughout the B-C-A lineage. (C) RNAscope validation of dorsal lineage markers *Pax6* and *Rbp1* (left) and ventral markers *Slit2* and *Adgrl3*. CC: corpus callosum, Str: striatum, LV: lateral ventricle. (D) AUCell scoring and classification of dorsal (red) and ventral (blue) cells based on genes expressed through the entire B-C-A lineage. (E) Volcano plot depicting 89 differentially expressed genes between the dorsal and ventral lineages. (F) Significantly enriched GO terms among markers of the dorsal and ventral lineages.

## Chapter 4: Discussion and Concluding Remarks

### *Overview*

NSCs in the developing and postnatal brain are heterogeneous, taking on unique transcriptional identities during development based on their location in the tissue. This heterogeneity is essential to generate the enormous diversity of neurons and glia that compose the mammalian brain. Contrary to predominant models in the field, my findings indicate that positional identities established during development can be maintained by epigenetic memory programs independent of their initializing morphogen. In addition, regional lineage commitment may occur earlier than anticipated in the course of differentiation. NSC commitment may be traced through transcription linking quiescent NSCs to corresponding populations of neuroblasts, though follow-up experiments will be needed to confirm this finding. These persistent transcriptional programs may too be perpetuated by epigenetic mechanisms. However, several broad mechanistic questions remain.

### *How does MLL1 maintain positional identity?*

While MLL1 has a role in maintaining ventral identity in the V-SVZ, how exactly it acts is still unknown. As discussed in Chapter 1, trithorax response elements (TREs) have not been found in the mammalian genome. Such binding sites have been difficult to find using techniques like genome-wide chromatin immunoprecipitation analysis due to a dearth of reliable MLL1-ChIP antibodies. It has been proposed that MLL1 may recognize and bind to CpG islands, stretches of GC-rich DNA that are persistently methylated. These have also been proposed as binding sites for PcG proteins, suggesting that MLL1 might competitively occupy loci and prevent PcG from silencing them (Bina et al. 2013, Rickels et al. 2016, Almouzni & Cedar 2016). However, I do not observe a stable increase in PcG-associated mark H3K27me3 after MLL1 inhibition, nor significant changes in chromatin accessibility by ATAC-seq. I was not able to find significant

changes in recruitment to the nuclear lamina using LaminB CUT&RUN. Lastly, MLL1 inhibition does not appear to persistently reduce H3K4me3, the active chromatin mark often associated with TrxG activity.

We do have several important pieces of evidence that help us build a model for how MLL1 might be maintaining ventral NSC identity. Although MLL1 has primarily been described as a histone methyltransferase, it may also facilitate gene activation by other means. Mutations to its methyltransferase domain do not appear to affect MLL1's activity in differentiation of the hematopoietic lineage (Mishra et al. 2014). MLL1 has also been described to recruit transcriptional coactivator CREB (Ernst et al. 2001) and interact with CREB binding protein (De Guzman et al. 2006). I found that transient inhibition of MLL1 causes a persistent loss of enhancer mark H3K4me1 and active enhancer/promoter mark H3K27ac across the genome, suggesting that MLL1 may play a role in maintaining active enhancers associated with a ventral transcriptional program.

Enhancer recruitment is dynamic and cell-type specific, and thus a strong candidate for maintaining regional information. However, enhancer maintenance across cell division requires some heritable signal upstream (Bulger & Groudine 2011, Nord et al. 2013, Pattabiraman et al. 2014, Ypsilanti & Rubenstein 2016, Markenscoff-Papadimitriou et al. 2020). It is possible that MLL1 may serve as that signal. When I prevented NSCs from cycling, loss of *Nkx2-1* expression (and thus, ventral identity) was attenuated. Previous work has found MLL1 complexed to the chromatin through mitosis, suggesting that it might “bookmark” loci for enhancer recruitment and rapid reactivation after division is complete (Blobel et al. 2009, Petruk et al. 2012). It has also been found to localize to the nucleolus, perhaps indicating a role in regulating chromatin structure by anchoring or regulation of nucleolus-associated domains (Karole et al. 2018).

Together, evidence from the literature and new findings described here support a model by which MLL1 recognizes a subset of regional NSC genes during embryonic development and maintains their expression by complexing with the genome, re-establishing active transcription

potentially through enhancer recruitment. Future experiments using genetically tagged versions of the MLL1 protein, improved MLL1 antibodies, and chromatin conformation analysis may provide more insight into how MLL1 selects sites for maintenance and how exactly the chromatin is altered in its absence. In the meantime, several questions remain. When exactly does the hand-off from Shh-mediated maintenance of *Nkx2-1* occur? Are MLL1-inhibited NSCs made vulnerable to re-specification to another lineage? What exactly is the role of morphogen signaling in the postnatal niche? And how generalizable is the epigenetic maintenance of positional identity?

#### *What distinguishes B cell populations from one another?*

Beyond the *Nkx2-1* lineage, our single-cell analysis of the V-SVZ has revealed broad distinctions between ventral and dorsal B cell lineages. Certain region-specific gene expression programs appear to persist throughout these lineages even across transitions from B to C to A cells (Fig. 3.6). In addition to genes known to be related to regional identity, many other differentially expressed genes contribute to differences between B cell populations in the V-SVZ. Within B cells, cluster 22<sub>B</sub> expresses not only dorsal markers, but also pallial and oligodendroglial markers like *Emx1* and *Pcdh15*, in contrast to neighboring dorsal cluster 5<sub>B</sub>. The expression of oligodendroglial and pallial markers in cluster 22<sub>B</sub>, along with its location in the UMAP nearest to parenchymal astrocyte clusters (Fig. 3.2A and B, Fig. 3.3A-D), suggest that it may represent a group of B cells at the upper margin of the dorsal wedge that are primed to generate oligodendrocytes for the corpus callosum (Menn et al. 2006).

Surprisingly, I identified genes associated with ion metabolism as enriched in the dorsal V-SVZ lineage, particularly the metallothionein family *Mt1* through *Mt4*. Metallothioneins have been studied largely in the context of oxidative stress in human disease, including neurodegenerative disorders, epilepsy, and brain injury (West et al. 2008, Juárez-Rebollar et al. 2017). Animal studies have provided some evidence that metallothioneins serve not only a

neuroprotective function, but also facilitate neurite outgrowth and axon regeneration after injury (Santos et al. 2012). The regional enrichment of these genes in the dorsal lineage could hint at a differential metabolic requirement, potentially related to the specific function and circuit activity of the neurons each region of the V-SVZ produces.

I also found a small number of lncRNAs among the differentially expressed genes detected between the dorsal and ventral lineages. The profound cell-type specificity of lncRNAs relative to protein-coding genes might help us understand region-specific differences between cells of the V-SVZ neurogenic lineage (Liu et al. 2017). Of 6 lncRNAs that emerged as regional markers in our analysis, 5 overlap putative enhancer loci annotated by ENCODE (Siggens & Ekwall 2014). lncRNA expression correlates with local enhancer activity, and non-coding transcripts may regulate enhancer stability and recruitment (Ntini & Marsico 2019), raising the possibility that differentially expressed lncRNAs indicate region-specific enhancer function. Ventral lncRNA *Gm26871* is transcribed from the same site as mir-137, a microRNA described to regulate neuronal maturation and differentiation (Smrt et al. 2010). Additionally, 3 of the 6 regional non-coding transcripts overlap or are adjacent to coding genes *Sox2* and *Sox1*. Although neither of these Sox genes were detected in our dataset, they both play important roles in regulating NSC pluripotency and proliferation (Venere et al. 2012, Zhang & Cui 2014). The regional specificity of these lncRNAs provides several intriguing clues to what distinguishes dorsal and ventral NSC lineages from one another, and what mechanisms may preserve these regional transcriptional programs throughout transitions from B through A cells.

While MLL1 maintains ventral NSC identity in the V-SVZ, it does not appear to have a role in maintaining dorsal identity. It remains unknown how other persistent regional expression patterns in the V-SVZ are propagated across cellular generations. Given that we find TrxG and PcG transcripts expressed in all cells of the neurogenic lineage, it is possible that distinct populations of B cells use other chromatin modifiers to retain gene expression patterns. Future experiments could use dorsally microdissected V-SVZ cultures to explore other chromatin

modifiers that might maintain dorsal identity. That being said, there may still be populations of B cells in the V-SVZ that remain morphogen sensitive for longer periods of time. After disruption of Shh signaling in P7 ventral V-SVZ cultures, *Nkx6-2* is downregulated, although it is the only non-Shh-pathway regional gene I find responding to morphogens in this way (Delgado et al. 2020).

### *Cellular memory systems and NSC identity*

The mammalian brain is composed of extraordinarily complex structures and circuits that are assembled from hundreds of types of neurons and glia (Erö et al. 2018). These cell types have unique transcriptional signatures, morphologies, and functions essential for brain activity, and all are derived from NSCs during development (Arlotta & Pasca 2019, Khakh & Sofroniew 2015, Miterko et al. 2018). Proper brain development requires finely coordinated regulation of NSC positional identity, which is necessary to produce the proper types of cells for the correct brain regions. I present evidence for a new model of neural development in which information about NSC positional identity may be passed from extrinsic morphogen signaling to a cell-intrinsic epigenetic memory system, which will maintain region-specific programs of gene expression across cell divisions and potentially even through differentiation.

Impaired neuronal differentiation can lead to developmental disorders, including intellectual disability, epilepsy, and autism spectrum disorder (Parenti et al. 2020). Mutations in epigenetic regulators are associated with developmental disorders and intellectual disabilities, like *Mll1* and Wiedemann-Steiner syndrome (Jones et al. 2012, Kleefstra et al. 2014, Iwase et al. 2017). By uncovering the role of epigenetic regulators in maintenance of NSC diversity, we improve our understanding of development and the ways it can go wrong. Additional knowledge of the factors guiding cell fate may help us generate specific neuroglial subtypes for use in cell therapy and regenerative medicine. Perhaps most importantly, this work brings us a step closer to understanding how an organ as intricate as the mammalian brain comes to be.

## References

- Aibar, S., González-blas, C. B., Moerman, T., Huynh-thu, V. A., Imrichova, H., Hulselmans, G., ... Atak, Z. K. (2017). AUCell: Identifying cells with active gene sets. *Nature Methods*.  
<https://doi.org/10.1038/nmeth.4463>
- Akam, M. (1987). The molecular basis for metamerism in the *Drosophila* embryo. *Development*, 101(1), 1–22. <https://doi.org/citeulike-article-id:10064978>
- Almouzni, G., & Cedar, H. (2016). Maintenance of epigenetic information. *Cold Spring Harbor Perspectives in Biology*. <https://doi.org/10.1101/cshperspect.a019372>
- Alvarez-Buylla, A., Kohwi, M., Nguyen, T. M., & Merkle, F. T. (2008). The heterogeneity of adult neural stem cells and the emerging complexity of their niche. *Cold Spring Harbor Symposia on Quantitative Biology*. <https://doi.org/10.1101/sqb.2008.73.019>
- Alvarez-Buylla, A., & García-Verdugo, J. M. (2002). Neurogenesis in adult subventricular zone. *Journal of Neuroscience*. <https://doi.org/10.1523/jneurosci.22-03-00629.2002>
- Arlotta, P., & Paşca, S. P. (2019). Cell diversity in the human cerebral cortex: from the embryo to brain organoids. *Current Opinion in Neurobiology*.  
<https://doi.org/10.1016/j.conb.2019.03.001>
- Ashe, H. L., & Briscoe, J. (2006). The interpretation of morphogen gradients. *Development* (Cambridge, England), 133(3), 385–394. <https://doi.org/10.1242/dev.02238>
- Bier, E., & De Robertis, E. M. (2015). BMP gradients: A paradigm for morphogen-mediated developmental patterning. *Science*. <https://doi.org/10.1126/science.aaa5838>
- Bina, M., Wyss, P., Novorolsky, E., Zulkelfi, N., Xue, J., Price, R., ... Wang, D. (2013). Discovery of MLL1 binding units, their localization to CpG Islands, and their potential function in mitotic chromatin. *BMC Genomics*. <https://doi.org/10.1186/1471-2164-14-927>
- Blobel, G. A., Kadauke, S., Wang, E., Lau, A. W., Zuber, J., Chou, M. M., & Vakoc, C. R. (2009). A Reconfigured Pattern of MLL Occupancy within Mitotic Chromatin Promotes

- Rapid Transcriptional Reactivation Following Mitotic Exit. *Molecular Cell*, 36(6), 970–983. <https://doi.org/10.1016/j.molcel.2009.12.001>
- Blobel, G. A., Kadauke, S., Wang, E., Lau, A. W., Zuber, J., Chou, M. M., & Vakoc, C. R. (2009). A Reconfigured Pattern of MLL Occupancy within Mitotic Chromatin Promotes Rapid Transcriptional Reactivation Following Mitotic Exit. *Molecular Cell*. <https://doi.org/10.1016/j.molcel.2009.12.001>
- Bond, A. M., Bhalala, O. G., & Kessler, J. A. (2012). The dynamic role of bone morphogenetic proteins in neural stem cell fate and maturation. *Developmental Neurobiology*. <https://doi.org/10.1002/dneu.22022>
- Bonzano, S., Bovetti, S., Gendusa, C., Peretto, P., & De Marchis, S. (2016). Adult born olfactory bulb dopaminergic interneurons: Molecular determinants and experience-dependent plasticity. *Frontiers in Neuroscience*. <https://doi.org/10.3389/fnins.2016.00189>
- Bray, N. L., Pimentel, H., Melsted, P., & Pachter, L. (2016). Near-optimal probabilistic RNA-seq quantification. *Nature Biotechnology*. <https://doi.org/10.1038/nbt.3519>
- Britto, J., Tannahill, D., & Keynes, R. (2002). A critical role for sonic hedgehog signaling in the early expansion of the developing brain. *Nature Neuroscience*, 5(stage 27), 103–110. <https://doi.org/10.1038/nn797>
- Bulger, M., & Groudine, M. (2011). Functional and mechanistic diversity of distal transcription enhancers. *Cell*. <https://doi.org/10.1016/j.cell.2011.01.024>
- Cao, F., Townsend, E. C., Karatas, H., Xu, J., Li, L., Lee, S., ... Dou, Y. (2014). Targeting MLL1 H3K4 Methyltransferase Activity in Mixed-Lineage Leukemia. *Molecular Cell*, 53(2), 247–261. <https://doi.org/10.1016/j.molcel.2013.12.001>
- Cao, R., & Zhang, Y. (2004). The functions of E(Z)/EZH2-mediated methylation of lysine 27 in histone H3. *Current Opinion in Genetics and Development*. <https://doi.org/10.1016/j.gde.2004.02.001>



- Chaker, Z., Codega, P., & Doetsch, F. (2016). A mosaic world : puzzles revealed by adult neural stem cell heterogeneity. *Developmental Biology*. <https://doi.org/10.1002/wdev.248>
- Chambers, S. M., Qi, Y., Mica, Y., Lee, G., Zhang, X. J., Niu, L., ... Studer, L. (2012). Combined small-molecule inhibition accelerates developmental timing and converts human pluripotent stem cells into nociceptors. *Nature Biotechnology*.  
<https://doi.org/10.1038/nbt.2249>
- Codega, P., Silva-Vargas, V., Paul, A., Maldonado-Soto, A. R., DeLeo, A. M., Pastrana, E., & Doetsch, F. (2014). Prospective Identification and Purification of Quiescent Adult Neural Stem Cells from Their In Vivo Niche. *Neuron*.  
<https://doi.org/10.1016/j.neuron.2014.02.039>
- Coré, N., Erni, A., Hoffmann, H. M., Mellon, P. L., Saurin, A. J., Beclin, C., & Cremer, H. (2020). Stem cell regionalization during olfactory bulb neurogenesis depends on regulatory interactions between *Vax1* and *Pax6*. *ELife*. <https://doi.org/10.7554/eLife.58215>
- Cosgrove, M. S., & Patel, A. (2010). Mixed lineage leukemia: A structure-function perspective of the MLL1 protein. *FEBS Journal*. <https://doi.org/10.1111/j.1742-4658.2010.07609.x>
- Crews, S. T., & Pearson, J. C. (2009). Transcriptional autoregulation in development. *Current Biology*. <https://doi.org/10.1016/j.cub.2009.01.015>
- Cuny, G. D., Yu, P. B., Laha, J. K., Xing, X., Liu, J. F., Lai, C. S., ... Peterson, R. T. (2008). Structure-activity relationship study of bone morphogenetic protein (BMP) signaling inhibitors. *Bioorganic and Medicinal Chemistry Letters*.  
<https://doi.org/10.1016/j.bmcl.2008.06.052>
- Das, A., Acharya, S., Gottipati, K. R., Mcknight, J. B., Chandru, H., Alcorn, J. L., & Boggaram, V. (2011). Thyroid transcription factor-1 (TTF-1) gene: Identification of ZBP-89, Sp1, and TTF-1 sites in the promoter and regulation by TNF- $\alpha$  in lung epithelial cells. *American Journal of Physiology - Lung Cellular and Molecular Physiology*.  
<https://doi.org/10.1152/ajplung.00090.2011>

- De Guzman, R. N., Goto, N. K., Dyson, H. J., & Wright, P. E. (2006). Structural basis for cooperative transcription factor binding to the CBP coactivator. *Journal of Molecular Biology*. <https://doi.org/10.1016/j.jmb.2005.09.059>
- Desai, A. R., & McConnell, S. K. (2000). Progressive restriction in fate potential by neural progenitors during cerebral cortical development. *Development*.
- Delgado, R. N., & Lim, D. A. (2017). Maintenance of positional identity of neural progenitors in the embryonic and postnatal telencephalon. *Frontiers in Molecular Neuroscience*. <https://doi.org/10.3389/fnmol.2017.00373>
- Delgado, R. N., & Lim, D. A. (2015). Embryonic Nkx2.1-expressing neural precursor cells contribute to the regional heterogeneity of adult V-SVZ neural stem cells. *Developmental Biology*, 407(2), 265–274. <https://doi.org/10.1016/j.ydbio.2015.09.008>
- Delgado, R. N., Mansky, B., Ahanger, S. H., Lu, C., Andersen, R. E., Dou, Y., ... Lim, D. A. (2020). Maintenance of neural stem cell positional identity by mixed-lineage leukemia 1. *Science*. <https://doi.org/10.1126/science.aba5960>
- Doetsch, F., Caille, I., Lim, D. A., Garcia-Verdugo, J. M., & Alvarez-Buylla, A. (1999). Subventricular zone astrocytes are neural stem cells in the adult mammalian brain. *Cell*, 97(6), 703–716. [https://doi.org/10.1016/S0092-8674\(00\)80783-7](https://doi.org/10.1016/S0092-8674(00)80783-7)
- Doetsch, F., García-Verdugo, J. M., & Alvarez-Buylla, A. (1997). Cellular composition and three-dimensional organization of the subventricular germinal zone in the adult mammalian brain. *Journal of Neuroscience*. <https://doi.org/10.1523/jneurosci.17-13-05046.1997>
- Dou, Y., Milne, T. A., Ruthenburg, A. J., Lee, S., Lee, J. W., Verdine, G. L., ... Roeder, R. G. (2006). Regulation of MLL1 H3K4 methyltransferase activity by its core components. *Nature Structural and Molecular Biology*. <https://doi.org/10.1038/nsmb1128>
- Dulken, B. W., Leeman, D. S., Phane, S., Boutet, C., Hebestreit, K., Brunet Correspondence, A., & Brunet, A. (2017). Single-Cell Transcriptomic Analysis Defines Heterogeneity and

- Transcriptional Dynamics in the Adult Neural Stem Cell Lineage. *Cell Reports*, 18, 777–790. <https://doi.org/10.1016/j.celrep.2016.12.060>
- Ericson, J., Briscoe, J., Rashbass, P., Van Heyningen, V., & Jessell, T. M. (1997). Graded sonic hedgehog signaling and the specification of cell fate in the ventral neural tube. *Cold Spring Harbor Symposia on Quantitative Biology*.  
<https://doi.org/10.1101/sqb.1997.062.01.053>
- Ericson, J., Muhr, J., Placzek, M., Lints, T., Jessel, T. M., & Edlund, T. (1995). Sonic hedgehog induces the differentiation of ventral forebrain neurons: A common signal for ventral patterning within the neural tube. *Cell*. [https://doi.org/10.1016/0092-8674\(95\)90536-7](https://doi.org/10.1016/0092-8674(95)90536-7)
- Ernst, P., Wang, J., Huang, M., Goodman, R. H., & Korsmeyer, S. J. (2001). MLL and CREB Bind Cooperatively to the Nuclear Coactivator CREB-Binding Protein. *Molecular and Cellular Biology*. <https://doi.org/10.1128/mcb.21.7.2249-2258.2001>
- Erö, C., Gewaltig, M. O., Keller, D., & Markram, H. (2018). A cell atlas for the mouse brain. *Frontiers in Neuroinformatics*. <https://doi.org/10.3389/fninf.2018.00084>
- Fiorelli, R., Azim, K., Fischer, B., & Raineteau, O. (2015). Adding a spatial dimension to postnatal ventricular-subventricular zone neurogenesis. *Development (Cambridge)*.  
<https://doi.org/10.1242/dev.119966>
- Flames, N., Pla, R., Gelman, D. M., Rubenstein, J. L. R., Puelles, L., & Marín, O. (2007). Delineation of multiple subpallial progenitor domains by the combinatorial expression of transcriptional codes. *Journal of Neuroscience*.  
<https://doi.org/10.1523/JNEUROSCI.2750-07.2007>
- Flames, N., Pla, R., Gelman, D. M., Rubenstein, J. L. R., Puelles, L., & Marín, O. (2007). Delineation of multiple subpallial progenitor domains by the combinatorial expression of transcriptional codes. *Journal of Neuroscience*.  
<https://doi.org/10.1523/JNEUROSCI.2750-07.2007>

- Flandin, P., Zhao, Y., Vogt, D., Jeong, J., Long, J., Potter, G., ... Rubenstein, J. L. R. (2011). Lhx6 and Lhx8 Coordinately Induce Neuronal Expression of Shh that Controls the Generation of Interneuron Progenitors. *Neuron*, 70(5), 939–950.  
<https://doi.org/10.1016/j.neuron.2011.04.020>
- Fuccillo, M., Joyner, A. L., & Fishell, G. (2006). Morphogen to mitogen: The multiple roles of hedgehog signalling in vertebrate neural development. *Nature Reviews Neuroscience*.  
<https://doi.org/10.1038/nrn1990>
- Fuccillo, M., Rallu, M., McMahon, A. P., & Fishell, G. (2004). Temporal requirement for hedgehog signaling in ventral telencephalic patterning. *Development*.  
<https://doi.org/10.1242/dev.01349>
- Fuentealba, L. C., Rompani, S. B., Parraguez, J. I., Obernier, K., Romero, R., Cepko, C. L., & Alvarez-Buylla, A. (2015). Embryonic Origin of Postnatal Neural Stem Cells. *Cell*, 161(7), 1644–1655. <https://doi.org/10.1016/j.cell.2015.05.041>
- Furuta, Y., Piston, D. W., & Hogan, B. L. M. (1997). Bone morphogenetic proteins (BMPs) as regulators of dorsal forebrain development. *Development*.
- Geisler, S. J., & Paro, R. (2015). Trithorax and polycomb group-dependent regulation: A tale of opposing activities. *Development (Cambridge)*. <https://doi.org/10.1242/dev.120030>
- Gould, A. (1997). Functions of mammalian Polycomb group and trithorax group related genes. *Current Opinion in Genetics and Development*, Vol. 7, pp. 488–494.  
[https://doi.org/10.1016/S0959-437X\(97\)80075-5](https://doi.org/10.1016/S0959-437X(97)80075-5)
- Hafemeister, C., & Satija, R. (2019). Normalization and variance stabilization of single-cell RNA-seq data using regularized negative binomial regression. *Genome Biology*.  
<https://doi.org/10.1186/s13059-019-1874-1>
- Hanson, R. D., Hess, J. L., Yu, B. D., Ernst, P., Van Lohuizen, M., Berns, A., ... Korsmeyer, S. J. (1999). Mammalian Trithorax and Polycomb-group homologues are antagonistic

- regulators of homeotic development. *Proceedings of the National Academy of Sciences of the United States of America*. <https://doi.org/10.1073/pnas.96.25.14372>
- Hillman, N., Sherman, M. I., & Graham, C. (1972). The effect of spatial arrangement on cell determination during mouse development. *Embryol. Exp. Morph*, 28(2), 263–278.
- Hochstim, C., Deneen, B., Lukaszewicz, A., Zhou, Q., & Anderson, D. J. (2008). Identification of Positionally Distinct Astrocyte Subtypes whose Identities Are Specified by a Homeodomain Code. *Cell*, 133(3), 510–522. <https://doi.org/10.1016/j.cell.2008.02.046>
- Iwase, S., Bérubé, N. G., Zhou, Z., Kasri, N. N., Battaglioli, E., Scandaglia, M., & Barco, A. (2017). Epigenetic etiology of intellectual disability. *Journal of Neuroscience*. <https://doi.org/10.1523/JNEUROSCI.1840-17.2017>
- Jones, W. D., Dafou, D., McEntagart, M., Woollard, W. J., Elmslie, F. V., Holder-Espinasse, M., ... Simpson, M. A. (2012). De novo mutations in MLL cause Wiedemann-Steiner syndrome. *American Journal of Human Genetics*. <https://doi.org/10.1016/j.ajhg.2012.06.008>
- Juárez-Rebollar, D., Rios, C., Nava-Ruiz, C., & Méndez-Armenta, M. (2017). Metallothionein in Brain Disorders. *Oxidative Medicine and Cellular Longevity*. <https://doi.org/10.1155/2017/5828056>
- Jude, C. D., Climer, L., Xu, D., Artinger, E., Fisher, J. K., & Ernst, P. (2007). Unique and Independent Roles for MLL in Adult Hematopoietic Stem Cells and Progenitors. *Cell Stem Cell*. <https://doi.org/10.1016/j.stem.2007.05.019>
- Karole, A. M., Chodisetty, S., Ali, A., Kumari, N., & Tyagi, S. (2018). Novel sub-cellular localizations and intra-molecular interactions may define new functions of Mixed Lineage Leukemia protein. *Cell Cycle*. <https://doi.org/10.1080/15384101.2018.1553338>
- Khakh, B. S., & Sofroniew, M. V. (2015). Diversity of astrocyte functions and phenotypes in neural circuits. *Nature Neuroscience*. <https://doi.org/10.1038/nn.4043>

- Kleefstra, T., Schenck, A., Kramer, J. M., & Van Bokhoven, H. (2014). The genetics of cognitive epigenetics. *Neuropharmacology*. <https://doi.org/10.1016/j.neuropharm.2013.12.025>
- Kosaka, T., & Kosaka, K. (2010). Heterogeneity of calbindin-containing neurons in the mouse main olfactory bulb: I. General description. *Neuroscience Research*.  
<https://doi.org/10.1016/j.neures.2010.04.009>
- Kouzarides, T. (2007). Chromatin Modifications and Their Function. *Cell*, Vol. 128, pp. 693–705.  
<https://doi.org/10.1016/j.cell.2007.02.005>
- Kriegstein, A., & Alvarez-Buylla, A. (2009). The glial nature of embryonic and adult neural stem cells. *Annual Review of Neuroscience*, 32, 149–184.  
<https://doi.org/10.1146/annurev.neuro.051508.135600>
- Lakso, M., Pichel, J. G., Gorman, J. R., Sauer, B., Okamoto, Y., Lee, E., ... Westphal, H. (1996). Efficient in vivo manipulation of mouse genomic sequences at the zygote stage. *Proceedings of the National Academy of Sciences of the United States of America*.  
<https://doi.org/10.1073/pnas.93.12.5860>
- Langmead, B., & Salzberg, S. L. (2012). Fast gapped-read alignment with Bowtie 2. *Nature Methods*. <https://doi.org/10.1038/nmeth.1923>
- Lewis, E. B. (1978). A gene complex controlling segmentation in *Drosophila*. *Nature*, 276(5688), 565–570. <https://doi.org/10.1126/AAC.03728-14>
- Leyva-Díaz, E., & Hobert, O. (2019). Transcription factor autoregulation is required for acquisition and maintenance of neuronal identity. *Development (Cambridge)*.  
<https://doi.org/10.1242/dev.177378>
- Lim, D. A., & Alvarez-Buylla, A. (2016). The adult ventricular/subventricular zone (V-SVZ) and olfactory bulb (OB) neurogenesis. *Cold Spring Harbor Perspectives in Biology*, 8(5).  
<https://doi.org/10.1101/cshperspect.a018820>
- Lim, D. A., Huang, Y.-C., Swigut, T., Mirick, A. L., Garcia-Verdugo, J. M., Wysocka, J., ... Alvarez-Buylla, A. (2009). Chromatin remodelling factor Mll1 is essential for

- neurogenesis from postnatal neural stem cells. *Nature*, 458(7237), 529–533.  
<https://doi.org/10.1038/nature07726>
- Liu, S. J., Horlbeck, M. A., Cho, S. W., Birk, H. S., Malatesta, M., He, D., ... Lim, D. A. (2017). CRISPRi-based genome-scale identification of functional long noncoding RNA loci in human cells. *Science*. <https://doi.org/10.1126/science.aah7111>
- Lledo, P. M., Merkle, F. T., & Alvarez-Buylla, A. (2008). Origin and function of olfactory bulb interneuron diversity. *Trends in Neurosciences*, Vol. 31, pp. 392–400.  
<https://doi.org/10.1016/j.tins.2008.05.006>
- Llorens-Bobadilla, E., Zhao, S., Baser, A., Saiz-Castro, G., Zwadlo, K., & Martin-Villalba, A. (2015). Single-Cell Transcriptomics Reveals a Population of Dormant Neural Stem Cells that Become Activated upon Brain Injury. *Cell Stem Cell*.  
<https://doi.org/10.1016/j.stem.2015.07.002>
- Lois, C., & Alvarez-Buylla, A. (1993). Proliferating subventricular zone cells in the adult mammalian forebrain can differentiate into neurons and glia. *Proceedings of the National Academy of Sciences of the United States of America*.  
<https://doi.org/10.1073/pnas.90.5.2074>
- Long, F., Zhang, X. M., Karp, S., Yang, Y., & McMahon, A. P. (2001). Genetic manipulation of hedgehog signaling in the endochondral skeleton reveals a direct role in the regulation of chondrocyte proliferation. *Development*.
- Ntini, E., & Marsico, A. (2019). Functional impacts of non-coding RNA processing on enhancer activity and target gene expression. *Journal of Molecular Cell Biology*.  
<https://doi.org/10.1093/jmcb/mjz047>
- Ma, J., Shen, Z., Yu, Y. C., & Shi, S. H. (2018). Neural lineage tracing in the mammalian brain. *Current Opinion in Neurobiology*. <https://doi.org/10.1016/j.conb.2017.10.013>

- Madisen, L., Zwingman, T. A., Sunkin, S. M., Oh, S. W., Zariwala, H. A., Gu, H., ... Zeng, H. (2010). A robust and high-throughput Cre reporting and characterization system for the whole mouse brain. *Nature Neuroscience*. <https://doi.org/10.1038/nn.2467>
- Mahmoudi, T., & Verrijzer, C. P. (2001). Chromatin silencing and activation by Polycomb and trithorax group proteins. *Oncogene*, 20(24), 3055–3066. <https://doi.org/10.1038/sj.onc.1204330>
- Mallo, M., & Alonso, C. R. (2013). The regulation of Hox gene expression during animal development. *Development (Cambridge)*. <https://doi.org/10.1242/dev.068346>
- Markenscoff-Papadimitriou, E., Whalen, S., Przytycki, P., Thomas, R., Binyameen, F., Nowakowski, T. J., ... Rubenstein, J. L. (2020). A Chromatin Accessibility Atlas of the Developing Human Telencephalon. *Cell*. <https://doi.org/10.1016/j.cell.2020.06.002>
- Martí, E., & Bovolenta, P. (2002). Sonic hedgehog in CNS development: One signal, multiple outputs. *Trends in Neurosciences*, Vol. 25, pp. 89–96. [https://doi.org/10.1016/S0166-2236\(02\)02062-3](https://doi.org/10.1016/S0166-2236(02)02062-3)
- Mattout, A., Cabianca, D. S., & Gasser, S. M. (2015). Chromatin states and nuclear organization in development - a view from the nuclear lamina. *Genome Biology*. <https://doi.org/10.1186/s13059-015-0747-5>
- McGinnis, C. S., Patterson, D. M., Winkler, J., Conrad, D. N., Hein, M. Y., Srivastava, V., ... Gartner, Z. J. (2019). MULTI-seq: sample multiplexing for single-cell RNA sequencing using lipid-tagged indices. *Nature Methods*. <https://doi.org/10.1038/s41592-019-0433-8>
- Menezes, J. R. L., Smith, C. M., Nelson, K. C., & Luskin, M. B. (1995). The division of neuronal progenitor cells during migration in the neonatal mammalian forebrain. *Molecular and Cellular Neurosciences*. <https://doi.org/10.1006/mcne.1995.0002>
- Merkle, F. T., Fuentealba, L. C., Sanders, T. A., Magno, L., Kessar, N., & Alvarez-Buylla, A. (2014). Adult neural stem cells in distinct microdomains generate previously unknown



- interneuron types. *Nature Neuroscience*, 17(2), 207–214.  
<https://doi.org/10.1038/nn.3610>
- Merkle, F. T., & Alvarez-Buylla, A. (2006). Neural stem cells in mammalian development. *Current Opinion in Cell Biology*, 18(6), 704–709.  
<https://doi.org/10.1016/j.ceb.2006.09.008>
- Merkle, F. T., Tramontin, A. D., García-Verdugo, J. M., & Alvarez-Buylla, A. (2004). Radial glia give rise to adult neural stem cells in the subventricular zone. *Proceedings of the National Academy of Sciences of the United States of America*.  
<https://doi.org/10.1073/pnas.0407893101>
- Merkle, F. T., Mirzadeh, Z., & Alvarez-Buylla, A. (2007). Mosaic organization of neural stem cells in the adult brain. *Science (New York, N.Y.)*, 317(5836), 381–384.  
<https://doi.org/10.1126/science.1144914>
- Miller, F. D., & Gauthier, A. S. (2007). Timing Is Everything: Making Neurons versus Glia in the Developing Cortex. *Neuron*. <https://doi.org/10.1016/j.neuron.2007.04.019>
- Milne, T. A., Briggs, S. D., Brock, H. W., Martin, M. E., Gibbs, D., Allis, C. D., & Hess, J. L. (2002). MLL targets SET domain methyltransferase activity to Hox gene promoters. *Molecular Cell*. [https://doi.org/10.1016/S1097-2765\(02\)00741-4](https://doi.org/10.1016/S1097-2765(02)00741-4)
- Milne, T. A., Briggs, S. D., Brock, H. W., Martin, M. E., Gibbs, D., Allis, C. D., & Hess, J. L. (2002). MLL targets SET domain methyltransferase activity to Hox gene promoters. *Molecular Cell*. [https://doi.org/10.1016/S1097-2765\(02\)00741-4](https://doi.org/10.1016/S1097-2765(02)00741-4)
- Mishra, B. P., Zaffuto, K. M., Artinger, E. L., Org, T., Mikkola, H. K. A., Cheng, C., ... Ernst, P. (2014). The histone methyltransferase activity of MLL1 is dispensable for hematopoiesis and leukemogenesis. *Cell Reports*. <https://doi.org/10.1016/j.celrep.2014.04.015>
- Miterko, L. N., Lackey, E. P., Heck, D. H., & Sillitoe, R. V. (2018). Shaping Diversity Into the Brain's Form and Function. *Frontiers in Neural Circuits*.  
<https://doi.org/10.3389/fncir.2018.00083>

- Mizrak, D., Levitin, H. M., Delgado, A. C., Crotet, V., Yuan, J., Chaker, Z., ... Doetsch, F. (2019). Single-Cell Analysis of Regional Differences in Adult V-SVZ Neural Stem Cell Lineages. *Cell Reports*. <https://doi.org/10.1016/j.celrep.2018.12.044>
- Moazed, D. (2011). Mechanisms for the inheritance of chromatin states. *Cell*. <https://doi.org/10.1016/j.cell.2011.07.013>
- Mu, Q., Chen, Y., & Wang, J. (2019). Deciphering Brain Complexity Using Single-cell Sequencing. *Genomics, Proteomics and Bioinformatics*. <https://doi.org/10.1016/j.gpb.2018.07.007>
- Mu, Q., Chen, Y., & Wang, J. (2019). Deciphering Brain Complexity Using Single-cell Sequencing. *Genomics, Proteomics and Bioinformatics*. <https://doi.org/10.1016/j.gpb.2018.07.007>
- Muzumdar, M. D., Tasic, B., Miyamichi, K., Li, N., & Luo, L. (2007). A global double-fluorescent cre reporter mouse. *Genesis*. <https://doi.org/10.1002/dvg.20335>
- Nord, A. S., Blow, M. J., Attanasio, C., Akiyama, J. A., Holt, A., Hosseini, R., ... Visel, A. (2013). Rapid and pervasive changes in genome-wide enhancer usage during mammalian development. *Cell*, 155(7), 1521–1531. <https://doi.org/10.1016/j.cell.2013.11.033>
- Nüsslein-Volhard, C., & Wieschaus, E. (1980). Mutations affecting segment number and polarity in *Drosophila*. *Nature*, 287(5785), 795–801. <https://doi.org/10.1038/287795a0>
- Obernier, K., Cebrian-Silla, A., Thomson, M., Parraguez, J. I., Anderson, R., Guinto, C., ... Alvarez-Buylla, A. (2018). Adult Neurogenesis Is Sustained by Symmetric Self-Renewal and Differentiation. *Cell Stem Cell*. <https://doi.org/10.1016/j.stem.2018.01.003>
- Obernier, K., Tong, C. K., & Alvarez-Buylla, A. (2014). Restricted nature of adult neural stem cells: Re-evaluation of their potential for brain repair. *Frontiers in Neuroscience*. <https://doi.org/10.3389/fnins.2014.00162>

- Oguchi, H., & Kimura, S. (1998). Multiple transcripts encoded by the thyroid-specific enhancer-binding protein (T/EBP)/thyroid-specific transcription factor-1 (TTF-1) gene: Evidence of autoregulation. *Endocrinology*. <https://doi.org/10.1210/endo.139.4.5933>
- Okano, H., & Temple, S. (2009). Cell types to order: temporal specification of CNS stem cells. *Current Opinion in Neurobiology*. <https://doi.org/10.1016/j.conb.2009.04.003>
- Papp, B., & Müller, J. (2006). Histone trimethylation and the maintenance of transcriptional ON and OFF states by trxG and PcG proteins. *Genes and Development*. <https://doi.org/10.1101/gad.388706>
- Parenti, I., Rabaneda, L. G., Schoen, H., & Novarino, G. (2020). Neurodevelopmental Disorders: From Genetics to Functional Pathways. *Trends in Neurosciences*. <https://doi.org/10.1016/j.tins.2020.05.004>
- Patel, A., Dharmarajan, V., Vought, V. E., & Cosgrove, M. S. (2009). On the mechanism of multiple lysine methylation by the human mixed lineage leukemia protein-1 (MLL1) core complex. *Journal of Biological Chemistry*. <https://doi.org/10.1074/jbc.M109.014498>
- Pattabiraman, K., Golonzhka, O., Lindtner, S., Nord, A. S., Taher, L., Hoch, R., ... Rubenstein, J. L. R. (2014). Transcriptional regulation of enhancers active in protodomains of the developing cerebral cortex. *Neuron*. <https://doi.org/10.1016/j.neuron.2014.04.014>
- Petruk, S., Sedkov, Y., Johnston, D. M., Hodgson, J. W., Black, K. L., Kovermann, S. K., ... Mazo, A. (2012). TrxG and PcG proteins but not methylated histones remain associated with DNA through replication. *Cell*, 150(5), 922–933. <https://doi.org/10.1016/j.cell.2012.06.046>
- Pimentel, H., Bray, N. L., Puente, S., Melsted, P., & Pachter, L. (2017). Differential analysis of RNA-seq incorporating quantification uncertainty. *Nature Methods*. <https://doi.org/10.1038/nmeth.4324>
- Quinlan, A. R., & Hall, I. M. (2010). BEDTools: A flexible suite of utilities for comparing genomic features. *Bioinformatics*. <https://doi.org/10.1093/bioinformatics/btq033>

- Raccaud, M., & Suter, D. M. (2018). Transcription factor retention on mitotic chromosomes: regulatory mechanisms and impact on cell fate decisions. *FEBS Letters*.  
<https://doi.org/10.1002/1873-3468.12828>
- Rickels, R., Hu, D., Collings, C. K., Woodfin, A. R., Piunti, A., Mohan, M., ... Shilatifard, A. (2016). An Evolutionary Conserved Epigenetic Mark of Polycomb Response Elements Implemented by Trx/MLL/COMPASS. *Molecular Cell*, 63(2), 318–328.  
<https://doi.org/10.1016/j.molcel.2016.06.018>
- Ringrose, L., & Paro, R. (2007). Polycomb/Trithorax response elements and epigenetic memory of cell identity. *Development (Cambridge, England)*, 134(2), 223–232.  
<https://doi.org/10.1242/dev.02723>
- Ruzankina, Y., Pinzon-Guzman, C., Asare, A., Ong, T., Pontano, L., Cotsarelis, G., ... Brown, E. J. (2007). Deletion of the Developmentally Essential Gene ATR in Adult Mice Leads to Age-Related Phenotypes and Stem Cell Loss. *Cell Stem Cell*.  
<https://doi.org/10.1016/j.stem.2007.03.002>
- Santos, C. R. A., Martinho, A., Quintela, T., & Gonçalves, I. (2012). Neuroprotective and neuroregenerative properties of metallothioneins. *IUBMB Life*.  
<https://doi.org/10.1002/iub.585>
- Schaefer, B. C., Schaefer, M. L., Kappler, J. W., Marrack, P., & Kiedl, R. M. (2001). Observation of antigen-dependent CD8+ T-cell/dendritic cell interactions in vivo. *Cellular Immunology*. <https://doi.org/10.1006/cimm.2001.1895>
- Schindelin, J., Arganda-Carreras, I., Frise, E., Kaynig, V., Longair, M., Pietzsch, T., ... Cardona, A. (2012). Fiji: An open-source platform for biological-image analysis. *Nature Methods*.  
<https://doi.org/10.1038/nmeth.2019>
- Schindelin, J., Arganda-Carreras, I., Frise, E., Kaynig, V., Longair, M., Pietzsch, T., ... Cardona, A. (2012). Fiji: An open-source platform for biological-image analysis. *Nature Methods*.  
<https://doi.org/10.1038/nmeth.2019>

- Schoenfelder, S., Sugar, R., Dimond, A., Javierre, B. M., Armstrong, H., Mifsud, B., ... Elderkin, S. (2015). Polycomb repressive complex PRC1 spatially constrains the mouse embryonic stem cell genome. *Nature Genetics*. <https://doi.org/10.1038/ng.3393>
- Schuettengruber, B., Bourbon, H. M., Di Croce, L., & Cavalli, G. (2017). Genome Regulation by Polycomb and Trithorax: 70 Years and Counting. *Cell*. <https://doi.org/10.1016/j.cell.2017.08.002>
- Schuettengruber, B., Chourrout, D., Vervoort, M., Leblanc, B., & Cavalli, G. (2007). Genome Regulation by Polycomb and Trithorax Proteins. *Cell*. <https://doi.org/10.1016/j.cell.2007.02.009>
- Schuettengruber, B., Martinez, A.-M., Iovino, N., & Cavalli, G. (2011). Trithorax group proteins: switching genes on and keeping them active. *Nature Reviews Molecular Cell Biology*, 12(12), 799–814. <https://doi.org/10.1038/nrm3230>
- Sedkov, Y., Tillib, S., Mizrokhi, L., & Mazo, A. (1994). The bithorax complex is regulated by trithorax earlier during *Drosophila* embryogenesis than is the Antennapedia complex, correlating with a bithorax-like expression pattern of distinct early trithorax transcripts. *Development*.
- Shen, L., Shao, N. Y., Liu, X., Maze, I., Feng, J., & Nestler, E. J. (2013). diffReps: Detecting Differential Chromatin Modification Sites from ChIP-seq Data with Biological Replicates. *PLoS ONE*. <https://doi.org/10.1371/journal.pone.0065598>
- Shimamura, K., Hartigan, D. J., Martinez, S., Puellas, L., & Rubenstein, J. L. R. (1995). Longitudinal organization of the anterior neural plate and neural tube. *Development*.
- Shimamura, K., & Rubenstein, J. L. R. (1997). Inductive interactions direct early regionalization of the mouse forebrain. *Development*.
- Siggens, L., & Ekwall, K. (2014). Epigenetics, chromatin and genome organization: Recent advances from the ENCODE project. *Journal of Internal Medicine*. <https://doi.org/10.1111/joim.12231>

- Skene, P. J., & Henikoff, S. (2017). An efficient targeted nuclease strategy for high-resolution mapping of DNA binding sites. *ELife*. <https://doi.org/10.7554/eLife.21856>
- Smrt, R. D., Szulwach, K. E., Pfeiffer, R. L., Li, X., Guo, W., Pathania, M., ... Zhao, X. (2010). MicroRNA miR-137 regulates neuronal maturation by targeting ubiquitin ligase mind bomb-1. *Stem Cells (Dayton, Ohio)*. <https://doi.org/10.1002/stem.431>
- Steffen, P. a, & Ringrose, L. (2014). What are memories made of? How Polycomb and Trithorax proteins mediate epigenetic memory. *Nature Reviews. Molecular Cell Biology*, 15(5), 340–356. <https://doi.org/10.1038/nrm3789>
- Strom, S. P., Lozano, R., Lee, H., Dorrani, N., Mann, J., O'Lague, P. F., ... Quintero-Rivera, F. (2014). De Novo variants in the KMT2A (MLL) gene causing atypical Wiedemann-Steiner syndrome in two unrelated individuals identified by clinical exome sequencing. *BMC Medical Genetics*. <https://doi.org/10.1186/1471-2350-15-49>
- Stuart, T., Butler, A., Hoffman, P., Hafemeister, C., Papalexi, E., Mauck, W. M., ... Satija, R. (2019). Comprehensive Integration of Single-Cell Data. *Cell*. <https://doi.org/10.1016/j.cell.2019.05.031>
- Sultan, K. T., Liu, W. A., Li, Z. L., Shen, Z., Li, Z., Zhang, X. J., ... Shi, S. H. (2018). Progressive divisions of multipotent neural progenitors generate late-born chandelier cells in the neocortex. *Nature Communications*. <https://doi.org/10.1038/s41467-018-07055-7>
- Sur, M., & Rubenstein, J. L. R. (2005). Patterning and plasticity of the cerebral cortex. *Science*. <https://doi.org/10.1126/science.1112070>
- Sussel, L., Marin, O., Kimura, S., & Rubenstein, J. L. (1999). Loss of Nkx2.1 homeobox gene function results in a ventral to dorsal molecular respecification within the basal telencephalon: evidence for a transformation of the pallidum into the striatum. *Development*, 126(15), 3359–3370. <https://doi.org/10393115>

- Taniguchi, H., He, M., Wu, P., Kim, S., Paik, R., Sugino, K., ... Huang, Z. J. (2011). A Resource of Cre Driver Lines for Genetic Targeting of GABAergic Neurons in Cerebral Cortex. *Neuron*. <https://doi.org/10.1016/j.neuron.2011.07.026>
- Terranova, R., Agherbi, H., Boned, A., Meresse, S., & Djabali, M. (2006). Histone and DNA methylation defects at Hox genes in mice expressing a SET domain-truncated form of Mll. *Proceedings of the National Academy of Sciences of the United States of America*. <https://doi.org/10.1073/pnas.0507425103>
- Tirosh, I., Izar, B., Prakadan, S. M., Wadsworth, M. H., Treacy, D., Trombetta, J. J., ... Garraway, L. A. (2016). Dissecting the multicellular ecosystem of metastatic melanoma by single-cell RNA-seq. *Science*. <https://doi.org/10.1126/science.aad0501>
- van Steensel, B., & Belmont, A. S. (2017). Lamina-Associated Domains: Links with Chromosome Architecture, Heterochromatin, and Gene Repression. *Cell*. <https://doi.org/10.1016/j.cell.2017.04.022>
- Venere, M., Han, Y. G., Bell, R., Song, J. S., Alvarez-Buylla, A., & Blelloch, R. (2012). Sox1 marks an activated neural stem/progenitor cell in the hippocampus. *Development (Cambridge)*. <https://doi.org/10.1242/dev.081133>
- Ventura, A., Meissner, A., Dillon, C. P., McManus, M., Sharp, P. A., Van Parijs, L., ... Jacks, T. (2004). Cre-lox-regulated conditional RNA interference from transgenes. *Proceedings of the National Academy of Sciences of the United States of America*.
- West, A. K., Hidalgo, J., Eddins, D., Levin, E. D., & Aschner, M. (2008). Metallothionein in the central nervous system: Roles in protection, regeneration and cognition. *NeuroToxicology*. <https://doi.org/10.1016/j.neuro.2007.12.006>  
<https://doi.org/10.1073/pnas.0403954101>
- Wolpert, L. (1969). Positional information and the spatial pattern of cellular differentiation. *Journal of Theoretical Biology*, 25(1), 1–47. [https://doi.org/10.1016/S0022-5193\(69\)80016-0](https://doi.org/10.1016/S0022-5193(69)80016-0)

- Wonders, C. P., & Anderson, S. A. (2006). The origin and specification of cortical interneurons. *Nature Reviews Neuroscience*, 7(9), 687–696. <https://doi.org/10.1038/nrn1954>
- Xu, Q. (2004). Origins of Cortical Interneuron Subtypes. *Journal of Neuroscience*, 24(11), 2612–2622. <https://doi.org/10.1523/JNEUROSCI.5667-03.2004>
- Xu, Q., Tam, M., & Anderson, S. A. (2008). Fate mapping Nkx2.1-lineage cells in the mouse telencephalon. *Journal of Comparative Neurology*. <https://doi.org/10.1002/cne.21529>
- Xu, Q., Wonders, C. P., & Anderson, S. A. (2005). Sonic hedgehog maintains the identity of cortical interneuron progenitors in the ventral telencephalon. *Development*. <https://doi.org/10.1242/dev.02090>
- Young, K. M., Fogarty, M., Kessar, N., & Richardson, W. D. (2007). Subventricular zone stem cells are heterogeneous with respect to their embryonic origins and neurogenic fates in the adult olfactory bulb. *Journal of Neuroscience*. <https://doi.org/10.1523/JNEUROSCI.0476-07.2007>
- Ypsilanti, A. R., & Rubenstein, J. L. R. (2016). Transcriptional and epigenetic mechanisms of early cortical development – an examination of how Pax6 coordinates cortical development. *J Comp Neurol*, 8(5), 583–592. <https://doi.org/10.1002/aur.1474.Replication>
- Yu, B. D., Hanson, R. D., Hess, J. L., Horning, S. E., & Korsmeyer, S. J. (1998). MLL, a mammalian trithorax-group gene, functions as a transcriptional maintenance factor in morphogenesis. *Proceedings of the National Academy of Sciences of the United States of America*, 95(18), 10632–10636. <https://doi.org/10.1073/pnas.95.18.10632>
- Yu, B. D., Hess, J. L., Horning, S. E., Brown, G. A. J., & Korsmeyer, S. J. (1995). Altered Hox expression and segmental identity in Mll-mutant mice. *Nature*. <https://doi.org/10.1038/378505a0>
- Zhang, S. (2014). Sox2, a key factor in the regulation of pluripotency and neural differentiation. *World Journal of Stem Cells*. <https://doi.org/10.4252/wjsc.v6.i3.305>



Zhang, S. (2014). Sox2, a key factor in the regulation of pluripotency and neural differentiation.

World Journal of Stem Cells. <https://doi.org/10.4252/wjsc.v6.i3.305>

Zhang, Y., Liu, T., Meyer, C. A., Eeckhoute, J., Johnson, D. S., Bernstein, B. E., ... Shirley, X.

S. (2008). Model-based analysis of ChIP-Seq (MACS). *Genome Biology*.

<https://doi.org/10.1186/gb-2008-9-9-r137>

Zywitzka, V., Misios, A., Bunatyan, L., Willnow, T. E., & Rajewsky, N. (2018). Single-Cell

Transcriptomics Characterizes Cell Types in the Subventricular Zone and Uncovers

Molecular Defects Impairing Adult Neurogenesis. *Cell Reports*.

<https://doi.org/10.1016/j.celrep.2018.11.003>

## Publishing Agreement

It is the policy of the University to encourage open access and broad distribution of all theses, dissertations, and manuscripts. The Graduate Division will facilitate the distribution of UCSF theses, dissertations, and manuscripts to the UCSF Library for open access and distribution. UCSF will make such theses, dissertations, and manuscripts accessible to the public and will take reasonable steps to preserve these works in perpetuity.

I hereby grant the non-exclusive, perpetual right to The Regents of the University of California to reproduce, publicly display, distribute, preserve, and publish copies of my thesis, dissertation, or manuscript in any form or media, now existing or later derived, including access online for teaching, research, and public service purposes.

DocuSigned by:  
  
1266F627275C48C... Author Signature

11/27/2020  
Date